Hugo Ferreira Anselmo

Licenciado em Ciências da Engenharia Química e Bioquímica

Preparation of Encapsulated Add-Value Bioactive Phenolic Compounds by Supercritical CO_2-Assisted Spray Drying

Dissertação para obtenção do Grau de Mestre em

Engenharia Química e Bioquímica

Orientador: Doutora Ana Isabel Aguiar Ricardo, Professora Catedrática, FCT/UNL

Coorientador: Doutora Teresa Alves Casimiro, Professora Auxiliar, FCT/UNL

Júri:

Presidente: Doutor Rui Manuel Freitas Oliveira,
Professor Associado com Agregação, FCT/UNL

Arguente: Doutora Maria Madalena Alves Dionísio,
Professor Associado com Agregação, FCT/UNL

Vogal: Doutora Ana Isabel Aguiar Ricardo,
Professora Catedrática, FCT/UNL

Novembro 2020

FACULDADE DE CIÊNCIAS E TECNOLOGIA
UNIVERSIDADE NOVA DE LISBOA

Hugo Ferreira Anselmo

Licenciado em Ciências da Engenharia Química e Bioquímica

Preparation of Encapsulated Add-Value Bioactive Phenolic Compounds by Supercritical CO_2-Assisted Spray Drying

Dissertação para obtenção do Grau de Mestre em

Engenharia Química e Bioquímica

Orientador: Doutora Ana Isabel Aguiar Ricardo, Professora Catedrática, FCT/UNL

Coorientador: Doutora Teresa Alves Casimiro, Professora Auxiliar, FCT/UNL

Preparation of Encapsulated Add-Value Bioactive Phenolic Compounds by Supercritical CO_2-Assisted Spray Drying

It always seems impossible until it's done.

– *Nelson Mandela*

Acknowledgements

A realização deste trabalho com sucesso só foi possível graças ao envolvimento de várias pessoas ao longo desta jornada. Este trabalho foi o culminar de muitas emoções e fruto de muito esforço e dedicação.

Em primeiro lugar, devo agradecer às minhas orientadoras, à Prof.ª Dr.ª Ana Isabel Ricardo e à Prof.ª Dr.ª Teresa Casimiro, pela oportunidade de realizar a minha dissertação de mestrado nos seus laboratórios e pela bolsa que me foi concebida neste projeto, bem como por toda a orientação, conhecimento e confiança transmitidos.

Um agradecimento especial à Clarinda Costa, pois foi sem dúvida uma colega e uma amiga que me acompanhou desde início, por toda a ajuda com o SASD, e não só. Obrigado por toda a atenção, pelas dicas e conhecimentos transmitidos, foi uma pessoa excecional. Queria também agradecer às colegas de laboratório do Grupo 510 com quem convivi e sempre se disponibilizaram a ajudar e pelos conselhos dados, nomeadamente, à Ana Furtado e à Raquel Viveiros. Obrigado também à Rita Ferro, por me ter ajudado e acompanhado nos ensaios.

Queria agradecer de certa forma a todos os envolvidos nos ensaios de caraterização. Ao Nuno Costa (Laboratório de Análises, LAQV) pelos ensaios de XRPD, BET e HPLC e por toda a disponibilidade, simpatia e esclarecimentos. À Prof.ª Madalena Dionísio por me permitir realizar os testes de DSC no seu laboratório e pela sua disponibilidade e conhecimentos na área. À Prof.ª Luísa Ferreira, por me permitir usar o ATR-FTIR do seu laboratório. À Prof.ª Ana Pereiro, por me permitir realizar os testes de KF no seu laboratório. À Prof.ª Ana Sofia Matos (DEMI/FCT) pela ajuda na análise estatística dos resultados. À Dr.ª Isabel Nogueira (IST) pelos ensaios de SEM. À D.ª Maria José, D.ª Palminha e D.ª Idalina por toda a sua generosidade e assistência.

Obrigado aos amigos de sempre, minha segunda família nestes anos, Artur, Catarina e Rute, com o qual convivi e partilhei os melhores momentos de faculdade. À minha querida amiga Andreia, por toda a boa disposição e estar sempre disponível para me ajudar e ouvir. Obrigado aos meus amigos mais próximos que também estiveram sempre a torcer por mim.

Por fim, isto não seria possível sem as pessoas mais importantes da minha vida. A toda a minha família, aos meus pais, Teresa e Delfim, e à minha irmã, Márcia, porque sempre acreditaram em mim, me apoiaram e nunca me deixaram baixar os braços. À minha namorada, Inês, por toda a paciência que sempre teve para mim, mas sobretudo por me ter feito ver sempre o lado positivo, por toda a força e nunca me deixar desistir de mim. Obrigado a todos pelo vosso amor incondicional.

Este trabalho contou com o apoio do Laboratório Associado de Química Verde-LAQV, o qual é financiado com fundos nacionais da FCT/MCTES (UIDB/50006/2020 e UIDP/50006/2020) e do projeto PTDC/BIIBIO/30884/2017.

Abstract

Every year the vine-pruning activity produces a large amount of residues of which 90% correspond to vine shoot residues. These are a rich source of natural antioxidants, mostly phenolic compounds, which, when properly extracted, can give rise to add-value products. The phenolic compounds have typically very low bioavailability, due to their poor solubility in aqueous media and high susceptibility to thermal and oxidative degradation with consequent loss of bioactivity.

The encapsulation of these compounds in suitable excipients can have a positive impact in their bioavailability and bioactivity. Previous data on vine shoot extraction have identified gallic acid (GA) and resveratrol (RSV) as main phenolic compounds in the extracts. GA is found in high concentrations and RSV has wide therapeutic and cosmetic applications. In this work, model dry powder formulations (DPFs) of GA and RSV using hydroxypropyl cellulose (HPC) as excipient were developed using a green atomization technology, Supercritical CO_2-Assisted Spray Drying (SASD). The content of solids (maintaining constant the percentage of bioactive compound) and ethanol volume in the solution to be atomized, were studied using a 3^2 full factorial Design of Experiments (DoE) approach concerning the process yield, particle size, span and encapsulation efficiency. The DPFs were also characterized in terms of particle morphology, specific surface area, crystallinity and moisture content. Antioxidant activity tests as well as *in vitro* release studies were also performed to the DPFs.

Amorphous powders were obtained in yields above 60% and encapsulation efficiencies up to 100%, showing a good performance of the process. The SASD has proven to be an efficient encapsulation technique for the phenolic compounds being able to preserve their antioxidant activity with average EC_{50} values of 22.8 μg/mL for GA-DPFs and 149.4 μg/mL for RSV-DPFs assessed by the scavenging capacity for the DPPH radical.

Keywords: circular bioeconomy; vine shoots; phenolic compounds; antioxidants; encapsulation; Design of Experiments; Supercritical-CO_2 Assisted Spray Drying.

Resumo

Todos os anos, a atividade da poda produz um grande volume de resíduos dos quais 90% são de poda de videira. Estes são uma fonte rica em antioxidantes naturais, maioritariamente compostos fenólicos que, quando devidamente extraídos, podem dar origem a produtos de valor acrescido. Estes compostos têm, tipicamente, biodisponibilidade muito reduzida, devido à sua fraca solubilidade em meios aquosos e elevada suscetibilidade de degradação térmica e oxidativa com consequente perda de bioatividade.

A encapsulação destes compostos em excipientes adequados pode ter um impacto positivo na sua biodisponibilidade e bioatividade. O ácido gálico (GA) e o resveratrol (RSV) são identificados como os principais compostos fenólicos presentes nos extratos de poda de videira, tendo ambos vastas aplicações terapêuticas e cosméticas. Neste trabalho, formulações modelo de pó seco (DPFs) de GA e RSV usando a hidroxipropilcelulose (HPC) como excipiente foram produzidos através de uma tecnologia de atomização verde, Secagem Assistida por CO_2 Supercrítico (SASD). O teor de sólidos (mantendo constante a percentagem de composto bioativo) e o volume de etanol na solução a ser atomizada, foram estudados através de um Desenho de Experiências (DoE) com fatorial completo 3^2 relativamente ao rendimento do processo, tamanho de partícula, amplitude da distribuição de tamanhos e eficiência de encapsulação do composto bioativo na matriz polimérica. As DPFs foram caracterizadas em termos de tamanho de partícula, morfologia, área superficial, cristalinidade e teor de água. A atividade antioxidante e a libertação *in vitro* das DPFs foram também estudadas.

Formulações amorfas com rendimentos acima de 60% e eficiências de encapsulação próximas de 100%, demonstraram um bom desempenho do processo. O SASD provou ser eficiente na encapsulação dos compostos fenólicos, permitindo preservar as suas atividades antioxidantes com valores médios de concentração efetiva (EC_{50}) de 22,8 µg/mL para GA-DPFs e 149,4 µg/mL para RSV-DPFs, através da capacidade de eliminação do radical DPPH.

Palavras-chave: bioeconomia circular; poda de videira; compostos fenólicos; antioxidantes; encapsulação; Desenho de Experiências; Secagem Assistida por CO_2 Supercrítico.

Table of Contents

List of Figures

List of Tables

List of Abbreviations

ACI	Andersen Cascade Impactor
ANOVA	ANalysis Of VAriance
API	Active Pharmaceutical Ingredient
ASDs	Amorphous Solid Dispersions
CE	Conventional Extraction
CO_2	Carbon Dioxide
DDS	Drug Delivery Systems
DSC	Differential Scanning Calorimetry
DoE	Design of Experiments
DPF	Dry Powder Formulation
DPPH	2,2-Diphenyl-1-picrylhydrazyl
D_v	Particle Mean Volumetric Diameter
D_n	Particle Mean Nominal Diameter
EC_{50}	Effective Concentration
EE	Encapsulation Efficiency
FDA	Food and Drugs Administration
FPF	Fine Particle Fraction
ATR-FTIR	Attenuated Total Reflection Fourier Transform Infra-Red
GA	Gallic Acid
GRAS	Generally Recognized As Safe
GSD	Geometric Standard Deviation
HPLC	High Performance Liquid Chromatography
HPC	Hydroxypropyl Cellulose
MMAD	Mass Median Aerodynamic Diameter
OIV	International Organisation of Vine and Wine
PBS	Phosphate-Buffered Saline
PM	Physical Mixture
PS	Particle Size
PSD	Particle Size Distribution
QdD	Quality-by-Design

RESS	Rapid Expansion of Supercritical Solution
RH	Relative Humidity
RSV	Resveratrol
SAS	Supercritical Antisolvent
SASD	Supercritical CO_2-Assisted Spray Drying
SEM	Scanning Electron Microscopy
SEDS	Solution Enhanced Dispersion by Supercritical Fluids
$scCO_2$	Supercritical CO_2
SCF	Supercritical Fluid
T_g	Glass Transition Temperature
TR	Tinta Roriz
TN	Touriga Nacional
VLE	Vapor Liquid Equilibria
VPR	Vine-Pruning Residues
XRPD	X-Ray Powder Diffraction

1. Introduction

1.1. Circular Bioeconomy

The agri-food industry is considered a sector with great economic importance worldwide. Besides that, this is a sector that generates a considerable amount of organic residues and by-product every year. These residues constitute a significant part of the overall annual production of biomass residues and are a vital source of energy both for domestic additionally as industrial purposes. Generally, the biomass produced is composed by lignocellulosic materials, rich in chemicals, like proteins, vitamins, minerals, pigments, and antioxidants that end up being lost. In most cases, residues create a negative environmental impact by disposal, spread or burnt in the field, or eventually used to feed animals, that do not always meet their nutritional needs [1,2]. The recovery and reuse of organic waste allows not only to reduce the disposal costs but also to minimize the environmental impact. The Directive 2008/98/EC [3] stated by the European Union says that "waste prevention should be the first priority of waste management, and that re-use and material recycling should be preferred to energy recovery from waste".

A sustainable conversi2on of these natural resources and agri-food wastes can give rise to value added products for applications in the area of pharmaceuticals, cosmetics, and food additives, and therefore, to which the concept of "Circular Bioeconomy" is associated to (Figure 1.1).

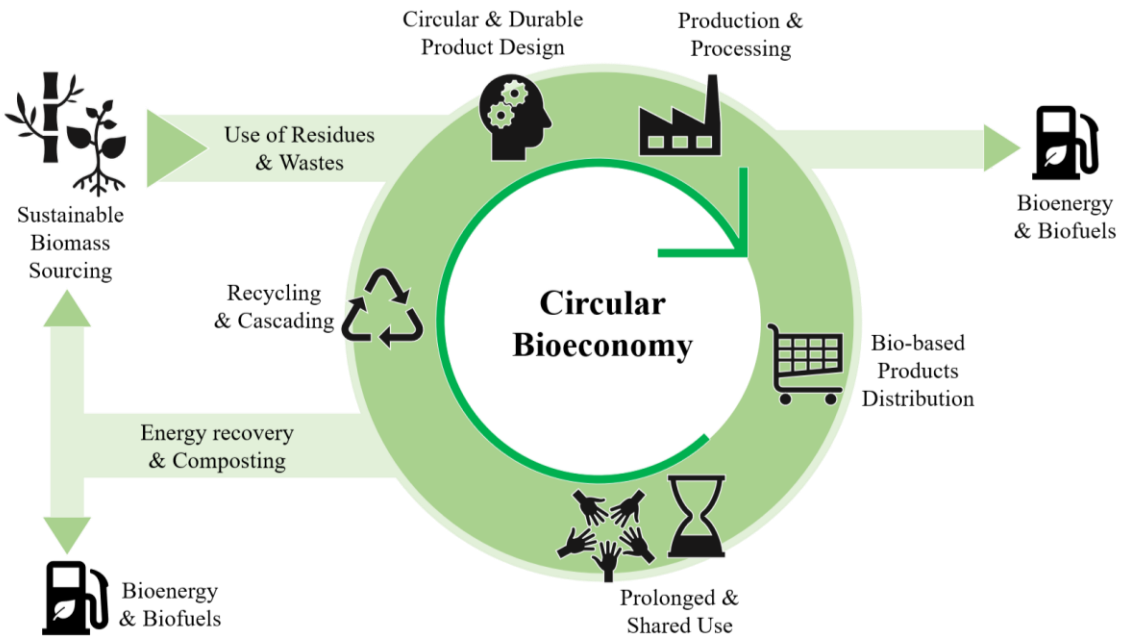

Figure 1.1 – Circular Bioeconomy and its overarching principles. Adapted from [4].

The Circular Bioeconomy is interconnected with some aspects of both the Circular Economy and Bioeconomy. While the Circular Economy focuses only on "maintaining the value of products, materials and resources in the economy for as long as possible, minimizing the generation of waste" and increasing the eco-efficiency of processes [5], the Circular Bioeconomy goes beyond these objectives. A Circular Bioeconomy encompasses the use of biomass from agriculture, forestry, and the marine environment including wastes and by-products, processing it to bioenergy/biofuels, food/feed, chemicals/materials to finally originate bio-based products. Beyond this biomass flow, the use of the bio-based products in cascading should be encouraged after the end of a lifetime, to avoid the use of high amounts of fresh biomass. The real challenge is to keep the value of these bio-based products along in this Circular Bioeconomy cycle [6].

1.2. Viticulture

Viticulture is considered one of the most important worldwide economic activities, namely in European Mediterranean countries [2,7]. According to the most recent annual report of the International Organisation of Vine and Wine (OIV) [8], the global area of grape cultivation in 2018 was about 7.5 million hectares. Additionally, Portugal is one of the ten countries with the largest registered area in the same year, with approximately 192 thousand hectares, being Tinta Roriz (TR) the commonly cultivated grape variety *Vitis vinifera* L. (Table 1.1) [9,10].

Table 1.1 – Most planted vine grape varieties of *V. vinifera* L. in Portugal and respective surface area (ha) in 2017. Adapted from [11].

Grape variety	Color	Surface area (ha)
Tinta Roriz	Red	18 000
Touriga Franca	Red	15 000
Castelão	Red	13 000
Fernão Pires	White	13 000
Touriga Nacional	Red	12 000
Trincadeira	Red	11 000
Baga	Red	7 000
Síria	White	7 000
Arinto	White	6 000
Syrah	Red	6 000
Other varieties	-	91 000

Although grape cultivation activities may consist either in the production of grapes for wine production or simply for raw consumption (table grapes), the cycle of cultivation of this fruit is the same (Figure 1.2). Every year, grape processing for winemaking gives rise to many organic by-products during grape harvest seasons, such as grape pomace residues, which include skins, seeds, pulp, stalks, and leaves. However, with the arrival of autumn and with the reduction of favorable conditions, such as temperature, the life cycle of grapevine enters a period of vegetative rest where the leaves fall. Consequently, it is when this period arrives that vines are pruned, called the vine-pruning season [12].

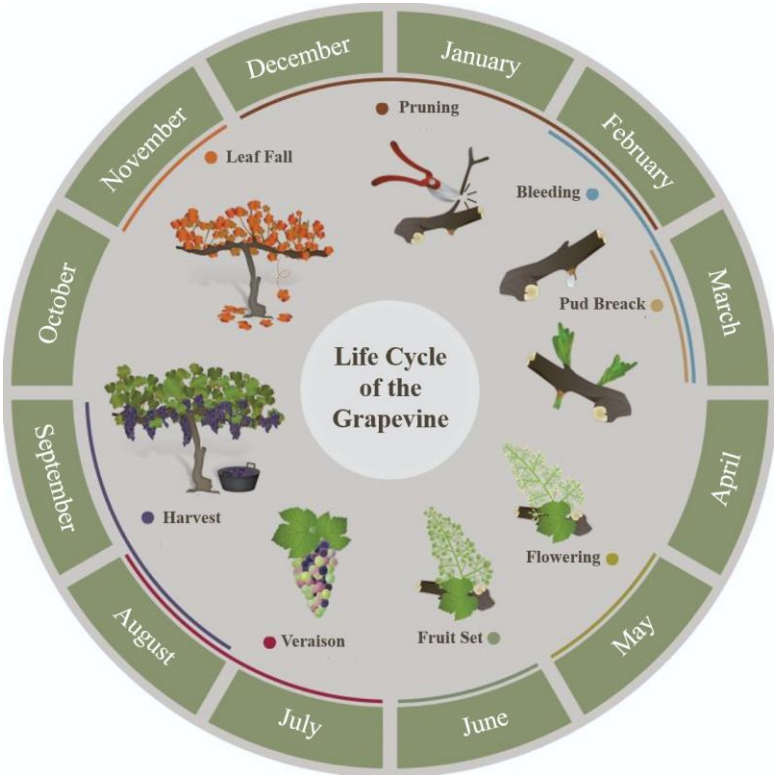

Figure 1.2 – Different seasons of the life cycle of a grapevine. Adapted from [13].

Vine pruning generates on average 1.5 tons per hectare of vine-pruning residues (VPR) worldwide each year, thus estimating the production of around 290,000 tons of VPR per year in Portugal [2,14]. Among VPR, the most abundant are the vine shoots (or vine canes) [15], representing more than 90 % of the total waste obtained from viticulture [16]. Mostly, this woody material ends up being lost in the environment, deposited in the agricultural soil for later incorporation, or burned because it no longer has economic value. These typical actions also have negative impacts on the environment and their decomposition may be a means of contamination of diseases to the whole culture [17].

VPR are a lignocellulose biomass enriched in natural bioactive compounds with potential to be converted into bio-based products by selective fractionation of the main components: lignin, cellulose and hemicellulose. Lignin constitutes about 20-39 % dry weight and is an important constituent of the cell wall of woody plants known for its structural properties. This is a macromolecular polymer with an amorphous three-dimensional structure built by oxidative radical coupling of the three monolignol units: *p*-coumaryl, coniferyl and sinapyl alcohols. It is in this major substructures where can be found the extractives and nonstructural components [18]. By hydrolysis, low molecular weight and valuable compounds can be released from the lignin structures, such as phenolic aldehydes, ketones, acids, and phenols. Therefore, VPR are a proposed source to obtain phenolic compounds for application in healthcare and wellness formulations as bioactive ingredients [14,18,19]. Despite that the phenolic compounds percentage is around 20 % of the dry weight of the vine shoots, their chemical composition may also depend on other factors, of which the cultivated vine variety, the growth conditions and the post-pruning storage time and conditions [15].

1.3. Phenolic Compounds

Polyphenols are known for their beneficial effects and protective action on human health and as naturally-occurring antioxidants broadly present in many parts of medicinal and woody plants, fruits and vegetables, including their peels, pulps and seeds [20]. Although, the distribution of polyphenols in plant materials is not uniform and its beneficial potential depends on the right minimum dosage and its bioavailability [21]. Polyphenols are secondary plant metabolites, resulting from its natural development and reproduction, and biogenetically induced from the shikimate or acetate pathways, as a way to adapt to their ecosystem [22,23]. Besides this, phenolic compounds expression is promoted as a defense tool under biotic (wounding, pathogen infections) or abiotic (ultraviolet radiation, deficit or excess of nutrients) plant stress conditions [22,24]. Apart from vine shoots, other vine by-products contain high concentrations of phenolic compounds such as stems, leaves and grape pomace [25].

1.3.1. Phenolic Classes in VPR Extracts

Phenolic compounds comprise a class of chemical substances with a very common structure, consisting by, at least, one aromatic ring, to which one (phenol) or more (polyphenol) hydroxyl functional groups are linked. Depending on the number of rings of the structure, as well as the bounding that is made between one ring to another through hydroxyl groups, phenolic compounds can be classified into different groups [26]. According to the literature, the most common classes found in VPR extracts are phenolic acids, flavonoids and stilbenes [9,14,27–31].

Phenolic acids are the simplest phenols structured by one aromatic ring and one carboxylic acid group. This class include the derivatives of benzoic acid (C6–C1, Figure 1.3a) and cinnamic acid (C6–C3, Figure 1.3b). These may occur in the free or conjugated form [24]. Gallic, protocatechuic, 4-hydroxyphenylacetic, 4-hydroxybenzoic, 4-hydroxybenzaldehyde, vanillic, syringic and ellagic acid are the most common hydroxybenzoic acids whereas the hydroxycinnamic acids are chlorogenic, caffeic, rosmarinic, *p*-coumaric, *o*-coumaric, ferulic, sinapic, cinnamic acid, caftaric and *p*-coutaric acids.

Flavonoids are the largest group of phenols in plant-derived materials characterized by a chemical structure that allows diversification into 13 different classes composed of two aromatic rings connected by a unit of three atoms (Figure 1.3c). So far, the presence of flavanols (catechin, epicatechin), flavanones (naringin, naringenin, pinocembrin, hesperidin), and flavonols (rutin, quercetin-3-*O*-glucopyranoside, myricetin, kaempferol-3-*O*-glucoside, kaempferol-3-*O*-rutinoside, quercetin, tiliroside, kaempferol) has been identified in VPR extracts.

Stilbenes are a small but important class of phenolic compounds whose structure consists in two aromatic rings connected by an ethene bridge (Figure 1.3d) [32]. Stilbenes are considered phytoalexins, that is, a toxin produced by plants as a mechanism of defense against *Botrytis cinerea* or *Plasmopora viticolaor* fungic infection or through UV radiation and heavy metal catalysis, for example [32]. The main stilbenes present in vine shoots are resveratrol and their glucosides (piceids), piceatannol and resveratrol dimers (viniferins) [31,33].

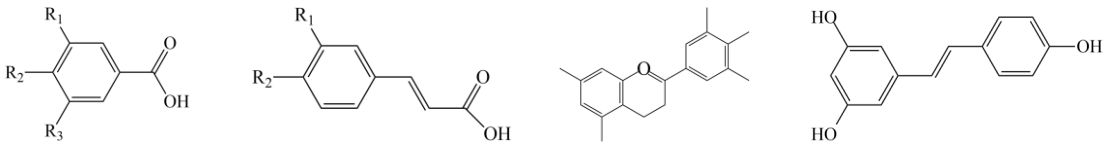

(a) (b) (c) (d)

Figure 1.3 – Chemical structure of (a) hydroxybenzoic acids, (b) hydroxycinnamic acids, (c) flavonoids and (d) stilbenes.

Over the past few years, various extraction techniques have been successfully applied for the recovery of phenolic compounds from different vine shoot varieties, among them, TR and TN portuguese varieties [9,19,27–29,34–36]. The techniques performed in the previous literature include conventional liquid-solid extractions, with the use of organic solvents, but also emerging extraction technologies, such as ultrasound-assisted extraction (UAE), microwave-assisted extraction (MAE) or subcritical water extraction (SWE). However, the different technologies and extraction procedures applied have direct implications on the total phenolic content and phenolic distribution in the extracts.

Regarding the latest extraction studies on VPR from TN and TR Portuguese varieties (Figure 1.4) [9,28], the class of phenolic acids is the major fraction present in the extracts obtained by SWE and MAE extraction methods mainly due to gallic acid (GA) content, which varies between 26–78 %w/w. In SWE, the higher the extraction temperature, the higher the GA content extracted. The stilbenes content in VPR extracts is mostly resveratrol (RSV). This compound is identified in greater quantity only in the TR and TN extracts obtained by the UAE, MAE and CE methods, whose contents vary between 6–27 %w/w. In the case of flavonoid classes present in the extracts, there are also other compounds that are highlighted, such as catechin (flavanol) or myricetin (flavonol). The maximum amount of catechin is obtained in SWE at 150 ºC whereas the myricetin is obtained with MAE at 100 ºC, for both varieties. These phenolic content variances reflect the influence of the application of different extraction techniques or process conditions.

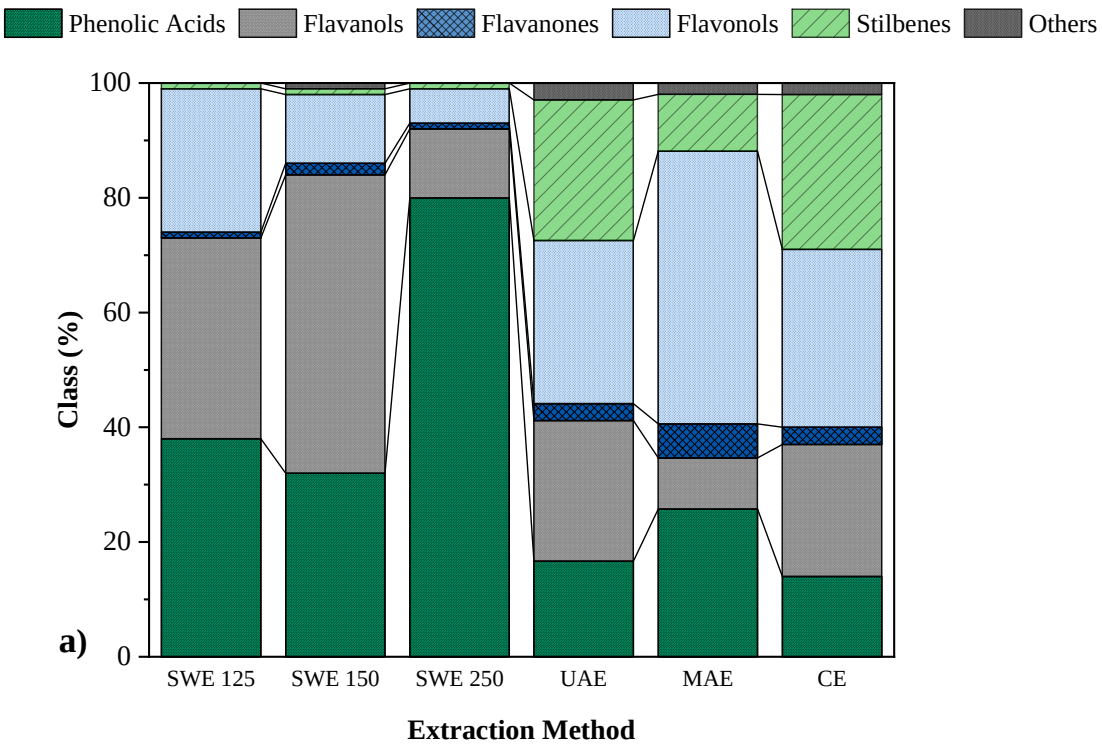

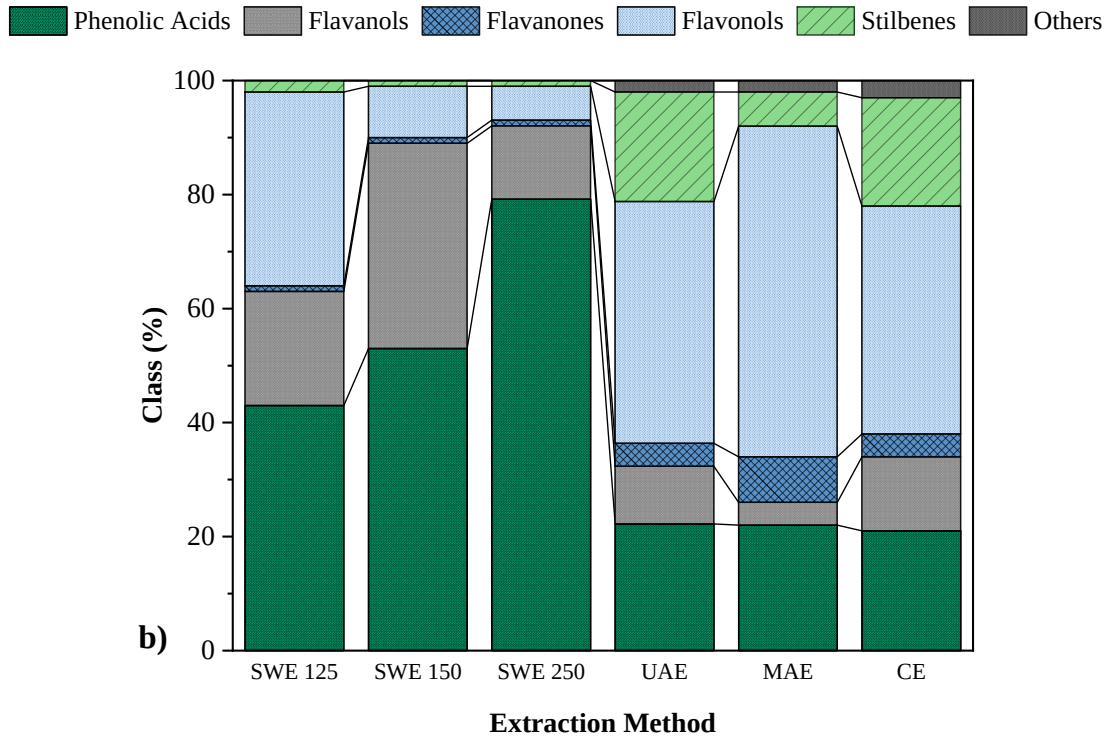

Figure 1.4 – Phenolic classes content in a) Tinta Roriz (TR) and b) Touriga Nacional (TN) extracts, expressed in %w/w (mg compound per 100 g dry weight), obtained from different extraction methods: SWE 125: Subcritical Water Extraction at 125 ºC, SWE 250: Subcritical Water Extraction at 250 ºC, UAE: Ultrasound-Assisted Extraction [28] and SWE 150: Subcritical Water Extraction at 150 ºC, MAE: Microwave-Assisted Extraction, CE: Conventional Extraction [9].

1.3.2. Resveratrol

Resveratrol (RSV, 3,5,4′-trihydroxystilbene) is the most abundant and well-known stilbene in vine shoots [37]. Its presence in these woody materials increases with the age of vines, post-pruning storage time to which they are subject, and also their storage conditions, such as temperature and humidity [15,38–40]. *trans*-Resveratrol is the most active form of resveratrol in the stilbene fraction of vine shoots, while only a few traces of its *cis*-isomer are present [32,41]. Apart from vine shoots, resveratrol continues to be the leading stilbene in other vine materials such as buds, roots, cluster stem, berry skin and seeds, although in lower quantities [42,43].

Cocoa, dry fruits (peanuts, walnuts, hazelnuts, almonds), bush berries (redcurrant, blackberries, strawberries, cranberries) and plants are among other resveratrol-rich natural sources [44,45]. Nevertheless, the protective or biological effects of this polyphenol are unlikely at normal nutritional intakes, since they are in very low amounts in the diet and this compound is oftenly more present in skin and seeds, which are not normally consumed [26].

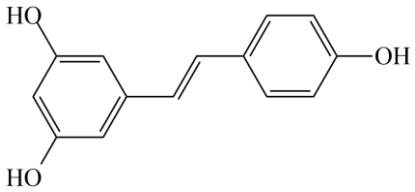

Figure 1.5 - Chemical structure of resveratrol ($C_{14}H_{12}O_3$, MW = 228.24 g/mol).

Trans-resveratrol is the one that has attracted large interest as an active ingredient for cosmetic, nutraceutical, and pharmaceutical formulations due to its potential human health benefits, strongly associated with its antioxidant capacity [46]. Resveratrol plays a key role in preventing certain diseases, including cardiovascular diseases, counteracting oxidative stress by directly scavenging for free radicals, decreasing reactive oxygen species (ROS) generation or even improving endogenous antioxidants [47]. As a chemopreventive agent in cancer treatment, resveratrol may inhibit the pathways that contribute to cell proliferation [48]. Its anti-inflammatory and immunomodulatory properties have shown improvements in liver diseases, diabetes, obesity and neurodegenerative disorders, like Parkinson's and Alzheimer's diseases [47].

From a cosmetic point of view, resveratrol also exhibits potential function on antiaging treatment and in solar skin protection against UV radiation. Its antiproliferative and chemopreventive properties combat skin carcinogenesis [49]. Resveratrol is considered a natural estrogen (or phytoestrogen) that may be incorporated in creams slowing down the aging process of the skin in postmenopausal women, due to its similarities to other synthetic estrogens (diethylstilbestrol) [49]. Resveratrol has also been proposed as an inhibitor of MITF (Microphthalmia-associated transcription factor) and tyrosinase promoting activities and therefore can be used as an additive for skin whitening products [50].

1.3.1. Gallic Acid

Gallic acid (GA, 3,4,5-trihydroxybenzoic acid) is found in appreciable concentrations in vine shoots aqueous extracts. This is a reference hydroxybenzoic acid not only in this material of the vine but in all other by-products obtained from grape processing, such as grape pomace (skins, seeds, and stems) [23]. It can be found in many vegetables and fruit plants, nuts and is usually found, abundantly, in tea extracts [51]. One of the reasons why gallic acid is so important is due to its role as a precursor of hydrolyzable tannins [27].

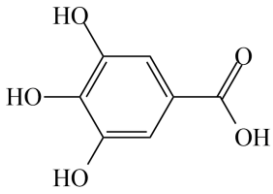

Figure 1.6 - Chemical structure of gallic acid ($C_7H_6O_5$, MW = 170.12 g/mol).

Other reason why gallic acid is so important is related to its potential as antioxidant for functional food, pharmaceutical and cosmetic industries, derived also to its low toxicity [52,53]. Gallic acid is seen as a phytochemical with good prospects mostly for cosmetic formulations, replacing synthetic compounds and making applications less invasive to the skin [54]. Its free radical scavenging capacity prevents skin cells from lipid peroxidation and trans-epidermal water loss. This way, gallic acid reveals to have good anti-aging properties against premature skin photo-aging [54]. Besides, this component can have some benefits in the treatment of skin hyper-pigmentation problems or help in wound healing and may be used for the formulation of antibacterial agents [54].

In the medicinal field, gallic acid can provide antibacterial effects against a wide range of pathogens, as well as anti-allergy, anti-inflammatory and antioxidant stress properties [36,53]. From another point of view, this compound can act as a prooxidant, concerning its activity in the regulation of oxidative stress and modification of the oxidoreductive status of cancer cells, giving gallic acid anti-cancer and apoptosis-inducing properties [53]. Its antioxidant activity also plays a role in the protection against cardiovascular disease and neurodegenerative disorders (Alzheimer's and Parkinson's diseases) [53].

1.4. Microencapsulation of Phenolic Compounds

1.4.1. Importance of Protecting Phenolic Compounds

Protection of bioactive compounds, like polyphenolics, is an important approach to expand its applications in the referred industries, however its use is limited by some relevant aspects. They have low aqueous solubility and are sensitive and unstable compounds under some conditions. When exposed to high temperatures, oxygen, pH variations, or ultraviolet light, natural phenolic compounds are prone to thermal and oxidative degradation causing the deactivation of their antioxidant activity during the different stages of processing or storage [55–57]. As the loss of activity increases, their appearance also begins to change in terms of color (brownish) and with unpleasant tastes and odors [58].

In the case of resveratrol, exposing it to ultraviolet light and high temperatures makes it a very sensitive and unstable molecule, promoting acceleration of isomerization to *cis*-resveratrol, its inactive form, and eventually suffering chemical degradation [46,59,60]. On the other hand, since it has a considerably short half-life (about 30–45 min) and its metabolism is relatively extensive in the liver and intestine, the bioavailability of oral administration becomes very low. Also, resveratrol has poor solubility in water (0,030 mg/mL), which affects its dispersibility in the aqueous medium of the human body, just as it is rapidly metabolized and eliminated [60,61]. This way, the therapeutic effects can be quite limited either by systemic or topical application. However, resveratrol is considered, according to the Biopharmaceutical Drug Classification (BCS), as a class-II component, since it has high membrane permeability [60–62]. Gallic acid is also a phenolic compound and because it has unsaturated bonds in its structure, it is also susceptible to degradation by light, heat, pH and water [63]. The oral administration of gallic acid is often limited due to low systemic and tissue bioavailability caused by the poor solubility in water (11 mg/mL) [54].

One of the most effective and promising ways to protect the bioactivity and grant a long lasting stability for a better life span of these natural phenols is through encapsulation methods [58]. Additionally, the encapsulated compound integrates the industrial circuit more economically and quickly, avoiding cold chain requirements, for example.

1.4.2. Encapsulation Material

Usually, encapsulation requires an excipient (coating material) that acts as a carrier and inhibits crystallization in both the dosage form and *in vivo*, so that the bioactive compound (core material) is protected in the matrix until reaching the desired target. The coating also gives robustness and a more uniform and spherical shape in the particle's morphology, although they can acquire irregular shapes [64].

The particle morphology may depend on the characteristics of the selected material as an excipient or even the encapsulation technique used [59]. Thus, different particle morphologies can also affect the performance of the powder during its storage and delivery [65]. The particles do not always compose a microcapsule with the core entirely coated (Figure 1.7a), as ideally would be intended. Instead, a microsphere can be formed, in which the bioactive compound can be at multiple capsules enclosed within the excipient (Figure 1.7b) or it can be homogeneously dispersed into the excipient (Figure 1.7c) [64]. Besides, other microparticles can be formed combining the previous morphologies, such as mononuclear with multiple shells, clusters of

microcapsules or even a coated insoluble matrix [64,65]. Encapsulation can include microcapsules with the core material either in solid, liquid or gas form [64].

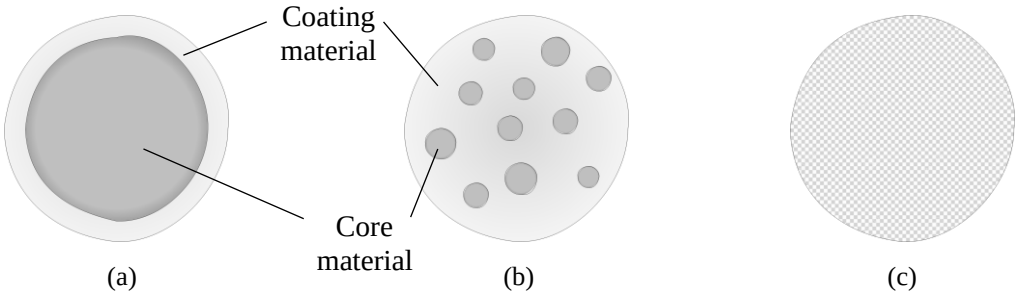

Figure 1.7 – Main particle morphologies: (a) mononuclear, (b) polynuclear and (c) matrix. Adapted from [65].

Typically, the excipient is insoluble and non-reactive with the core material and is applied as liquid solution or suspension, or as molten material to wrap the bioactive compound [65]. Many of the polymers used can be natural, semi-synthetic or synthetic polymers, or even gums or sugars [66]. Among these, natural polymers or biopolymers are gaining significantly more interest in the research field, for drug delivery through the skin, in cosmetic applications. These end up having a greater advantage over others because they are non-toxic and non-reactive when in contact with the human tissues and are easily metabolized and removed from the body [59].

The selection of the polymer requires special attention to some factors regarding its performance in the atomization step. Glass transition temperature (T_g) is a key factor: a high enough T_g of the polymer reduces the molecular mobility and decreases the crystallization tendency of the active compound. The molecular mobility is related to the macromolecular properties (e.g. viscosity) and determines the physical stability and reactivity quantified in terms of mean relaxation time; it is also viewed as an antiplasticizing of the drug by the polymer. Furthermore, polymer molecular weight is directly related to its T_g: high molecular weight polymers have a high T_g, thus favoring its use as a stabilizing agent. Hygroscopicity of the polymers can also negatively affect the T_g of amorphous solids: the increasing capacity of a material to absorb moisture from surroundings ambient increases the free volume between polymer chains and enhances structural mobility; moisture also accelerates chemical degradation and crystallization. The material must have a high degradation temperature (T_{deg}) so that the thermal stability of the polymer does not become an operational constraint, that is, process temperature below T_{deg}. The dissolution profile in organic solvents and the optimal solubilization of the active compound in the amorphous solid dispersions (ASDs) should also be considered [67,68].

1.4.2.1. Cellulose-based polymers

Cellulose is one of the most abundant biopolymers in the world, a raw material almost inexhaustible, that is mostly synthesized by plants, and composes the main structure of the cell walls [69]. This polysaccharide consists in a high molecular weight polymer with linear unbranched chains [69,70]. Unfortunately, its native form is not soluble in water due to its strong hydrogen bonds between the individual chains and its crystalline structure [69]. Therefore, to overcome this constrain, cellulose is chemically converted to water-soluble ester or ether derivatives [69].

Cellulose ethers are a result of alkylation wherein hydrogen atoms of the three –OH group on the anhydroglucose repeating unit is replaced by alkyl and mixed alkyl groups [69]. They are semi-synthetic polymers commonly used as excipients and stabilizers of the ASD formulations in combination with the active compound, due to its versatile properties such as rheology, enhanced viscosity, aqueous and organic solubility, and water retention ability [71]. However, their properties depend on the type of substituents, the degree of substitution and the distribution of the substituents along the polymer chain [72].

Hydroxypropyl cellulose (HPC) and hydroxypropylmethyl cellulose (HPMC, or abbreviated hypromellose) are the most commonly used cellulose-based polymers as excipients. Besides these, there are many others known and already investigated to improve the solubility of poorly water-soluble drugs such as methyl cellulose (MC), ethyl cellulose (EC), hydroxyethyl cellulose (HEC), hypromellose acetate succinate (HMPCAS), carboxymethyl cellulose acetate butyrate (CMCAB), carboxymethyl cellulose (CMC) or sodium carboxymethyl cellulose (NaCMC) [69,71].

HPC is a cellulose ether widely used as an excipient in many food, pharmaceutical and cosmetic formulations. It is Generally Recognized As Safe (GRAS) and also part of the Inactive Ingredients Database approved by Food and Drugs Administration (FDA) for both topical and oral formulations [73]. The structure of HPC (Figure 1.8) is a result of the reaction of alkali cellulose – obtained by the reaction of cellulose with sodium hydroxide and chemically more reactive than its native form – with propylene oxide at high pressures and temperatures. For each of the anhydroglucose units (AGU) in the cellulose chain, there are three reactive hydroxyls from which propylene oxide can be substituted via ether linkages [74]. Aqueous systems with HPC characterizes a strong electron–donor interaction through hydrogen bonds [75].

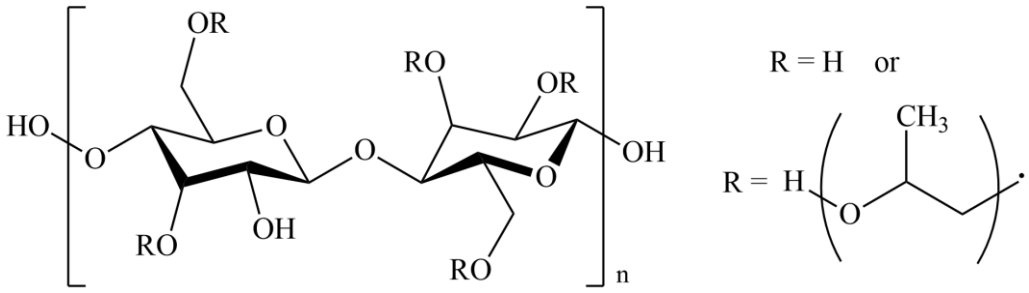

Figure 1.8 – Chemical structure of Hydroxypropyl Cellulose (HPC) and its possible R groups.

HPC exists in a wide range of molecular weights, from 40,000 to 1,150,000 Da, as well as in different viscosity solution grades [74]. HPC is a biocompatible, non-ionic, and semi-crystalline polymer with low crystallinity and a high degree of amorphous domains of relatively low T_g (in the range of -25 to 0 ºC), thus suggesting a high degree of molecular mobility and plasticity [76,77]. Systems based in HPC depicts great interest due to its good solubility in water and organic solvents [78]. However, the presence of both hydrophilic and hydrophobic groups makes the HPC a thermosensitive polymer, so that becomes insoluble in aqueous solutions when the temperature rises above its lower critical solution temperature (LCST) of 40–45 ºC [76,79]. When the temperature is below LCST, hydrophilic bonds are stronger than the hydrophobics, but when the temperature exceeds the LCST, its affinity with water decreases and leads to a formation of two phases – an aqueous and a polymer-rich phase –, affecting the polymer's structure through gelling [79]. HPC can also form liquid crystals and many mesophases upon its concentration in water: isotropic, anisotropic, nematic and cholesteric [76,78].

In some microencapsulation processes, HPC can be used as a thickening and coating agent to increase the bioavailability of heat-sensitive drugs in aqueous and acid systems at high temperatures [80]. In oral products, HPC can be used in tablets as a binder, film-coating or extended-release-matrix former, whereas in topical formulations it can be used in transdermal patches and ophthalmic preparations (retains moisture, stabilizes the tear film and lubricates the eye). In cosmetic and food products it can act as a stabilizer and emulsifier agent [74]. Cellulose ethers were successfully used previously to encapsulate bioactive compounds [68].

Since the natural form of cellulose has limited solubility in water and in other common solvents, modified celluloses have enhanced their functionality and so they are considered as a suitable coating material [81].

1.4.3. Encapsulation Methods

The classification of the encapsulation methods can be subdivided into three classes: physical, physicochemical and chemical methods [58]. Some of the most known to encapsulate polyphenolics are listed in the Figure 1.9.

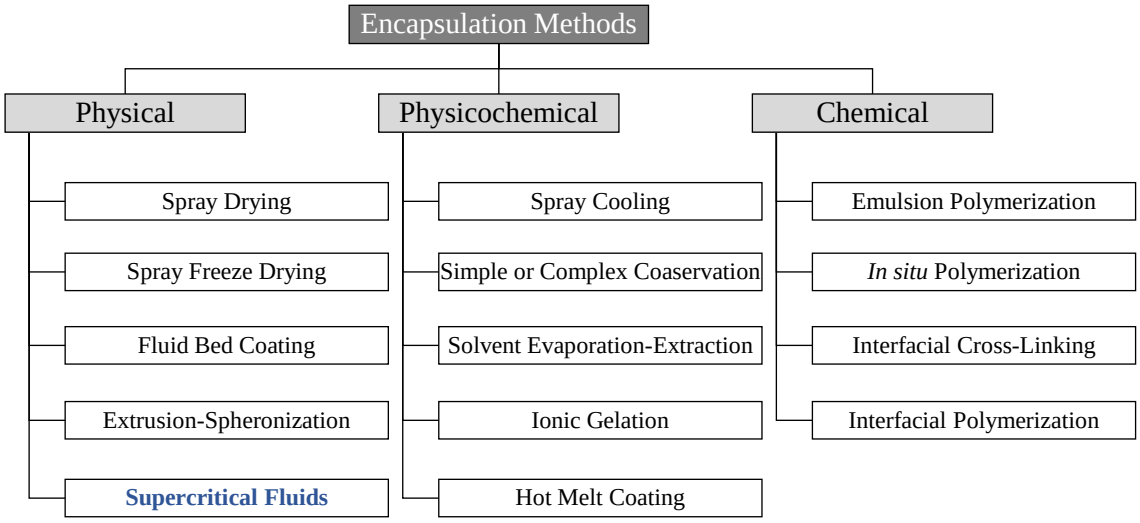

Figure 1.9 – Classification of encapsulation methods [58,82].

A few methods applied to encapsulate phenolic compounds are based on drying processes as they are often present in aqueous extracts and which, in turn, give rise to dry powder formulations (DPFs) [83]. Spray drying is probably the conventional method with the greatest reference when it comes to obtaining DPFs [81]. This technique involves the dissolution of both bioactive compounds and excipient in an appropriate solvent, usually, water or organic solvents; it can be done separately in case the active compound is hydrophobic.

Spray drying is a single-step continuous process, rapid and economically attractive, that allows the use of a wide variety of encapsulation materials. This process have a good flexibility for the industrial scale [84]. Small particle size powders (up to less than 10 μm) can be produced with good encapsulation efficiencies (10–90%) and residual moisture content [85].

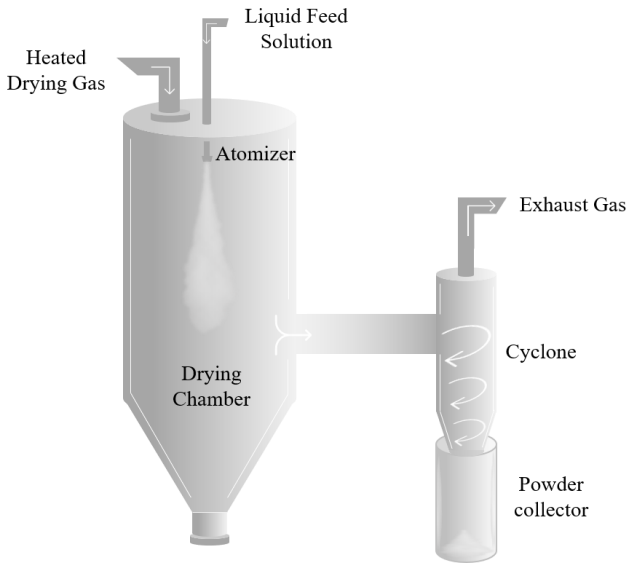

Figure 1.10 – Simplified schematic representation of the spray drying process.

In the spray drying process (Figure 1.10), the liquid solution is fed and then atomized through a nozzle orifice to a precipitation chamber. Simultaneously, an inlet hot gas stream allows the evaporation of the solvents from the atomized droplets and consequently to the formation of dry particles. The particles follow to a cyclone, where the gases and the particles are separated, allowing the final recovery of dry powder. Despite the typical operating temperatures in the range of 100–150 ºC, the exposure time with thermolabile compounds, such as antioxidants, is low (seconds or milliseconds) enough to avoid significant levels of oxidative degradation [86]. On the other hand, the outlet temperature, which is directly related with the inlet temperature of the gas stream, may also affect the bioactivity of the compounds. The powder being produced can be subjected to these temperatures until the end of the process batch and until the collection bottle has cooled [86]. For this reason, it is also expected that the final DPF contains the active compound embedded and protected by the coating material. Spray drying limits the particle's size control due to the rapid evaporation of the solvent, producing particles with a wide range of sizes with irregular shapes or aggregates [86].

Spray freeze-drying is an improvement on the encapsulation technique by freeze-drying (or lyophilization) to produce DPFs from a liquid sample [87]. The droplets are atomized and solidified in contact with liquid nitrogen to form microspheres and then dried under conditions of low temperature and pressure for a few hours [87]. Thus, it is a suitable technique for both hydrophobic and heat-sensitive compounds. This technique produces powders with high quality, although with higher hygroscopicity [65,88]. In contrast, this process requires much more time and energy consumption than spray drying [88].

Several studies available in the literature have shown the application of the previous conventional techniques to encapsulate phenolic compounds present in different natural extracts obtained from grape by-products of the *V*. vinifera L. varieties [89,90,99–102,91–98]. Recently, Da Rocha and Noreña [101] have successfully applied both spray drying and freeze drying techniques to produce DPFs using a grape pomace aqueous extract obtained by MAE with a combination of whey protein, arabic gum, and pectin as coating materials. Also, Escobar-Avello et al. [99] assessed the use of spray drying to encapsulate phenolic compounds from a grape cane extract along with β-cyclodextrins. In other cases, the use of spray and freeze-drying to encapsulate resveratrol or gallic acid alone has also been successfully applied. Li et al. [103] used three cellulose derivatives to form ASDs with resveratrol by spray drying, using an acetone/ethanol (1:4 v/v) system as a solvent solution and different weight resveratrol/polymer ratios (1/9, 1/3 and 1/1). Recently, Cardoso et al. [104] studied in his final academic work the encapsulation of resveratrol using gum arabic as encapsulating agent. The DPFs obtained had encapsulation efficiencies of up to 87 % with the highest studied concentration of 20 %w/v of gum arabic in the solution, for a final core/coating material ratio of 1:50 (w/w).

1.4.4. Supercritical Fluid Technologies

Supercritical fluids-based technologies have attracted great attention in the particle engineering field due to the possible combination of the advantageous properties of gases and liquids for the formulation of DPF, as it is possible with the supercritical fluids (SCFs). SCFs are characterized as high-pressure compressible fluids above their critical points and under the pressure for solidification to occur. Above critical point (CP), SCFs feature a liquid-like density promoting the mass transfer and whenever they act as solvents, their solvation power is approximately proportional to its density. On the other hand, they also feature gas-like viscosities that allows high diffusivities [105]. These thermophysical properties easily change with small manipulations of pressure or temperature, thus quickly reaching the system supersaturation and achieving small particle sizes [106,107].

Table 1.2 – Physicochemical properties of gases, liquids, and SCFs. Adapted from [105].

Property	**Gas**	**SCF**	**Liquid**
Density (g/cm^3)	10^{-3}	0.3	1
Viscosity (Pa s)	10^{-5}	10^{-4}	10^{-3}
Diffusivity (cm^2/s)	0.1	10^{-3}	5×10^{-6}

Supercritical carbon dioxide ($scCO_2$) is by far the SCF most used and easy to operate at mild conditions due to its relatively low critical point: T_c = 304 K and p_c = 7.38 MPa (Figure 1.11), what makes it suitable for thermal sensitivity compounds. According to the FDA, CO_2 has GRAS status, providing a more eco-friendly approach for the process since it can be recycled at the end of the process and minimize the atmosphere emissions [108,109]. CO_2 is also known as an inert solvent, non-flammable, non-toxic, inexpensive, and readily available in high purity [110,111]. The main drawback of $scCO_2$ is its limited solvating power, more specifically with polar substances, unless when used as an anti-solvent. Nevertheless, volatile compounds such as ethanol can be added as a cosolvent to overcome this constraint and increase the polarity of the medium through the formation of H-H bonds [112].

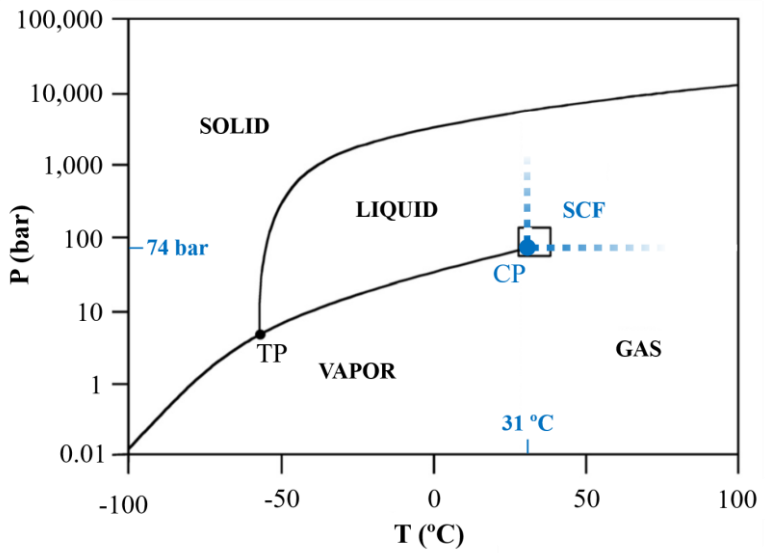

Figure 1.11 – The phase diagram of CO_2. CP: Critical Point; TP: Triple Point. Adapted from [105].

The use of $scCO_2$ in drying processes promote the absence or reduced use of organic solvents and the formation of an inert atmosphere at the process that prevents unstable compounds from degradation [113]. Besides that, the use of $scCO_2$ also decreases the temperature required to the solvent's evaporation, what also eliminates the need for additional steps, saving time and economizing energy [114]. As CO_2 is a gas at ambient temperature and atmospheric pressure, by the simple depressurization of the system, it expands from within the particles produced [115].

Supercritical fluid-based technologies differ from each other by the $scCO_2$ equilibrium behavior with the solute or in the binary system CO_2/solvent [113]. The interaction between $scCO_2$ with the biopolymer/active ingredient is also a key factor when it comes to the selection of the supercritical process to be used [116]. Thus, $scCO_2$ can take advantage as a solvent, antisolvent, plasticizer and atomization-aid/co-solute (Figure 1.12) [117].

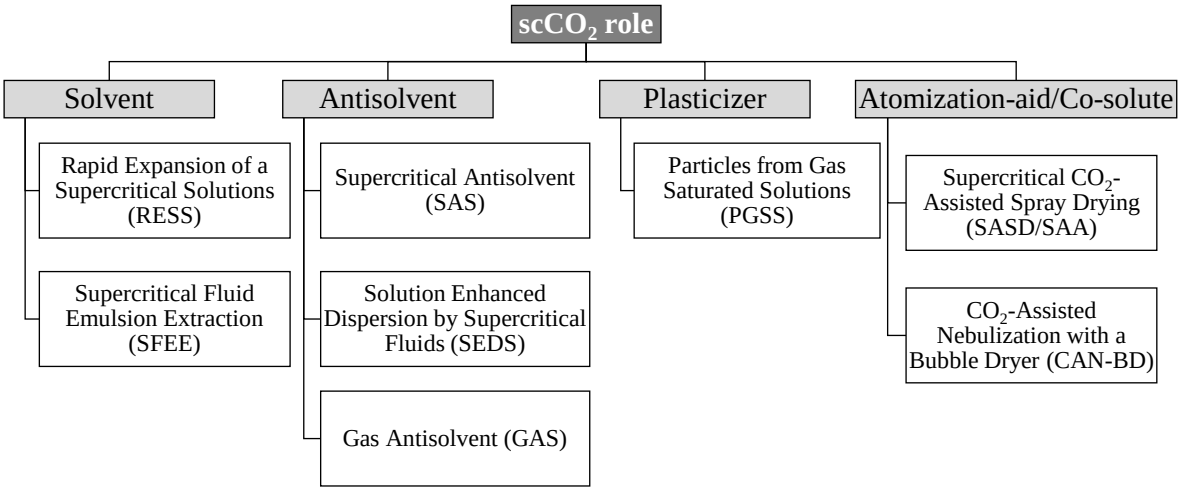

Figure 1.12 – Main supercritical fluid-based processes according to the role of $scCO_2$.

RESS (Figure 1.13a) is a relatively simple process where the solute is firstly dissolved in saturated $scCO_2$ and, then, rapidly expanded by sudden depressurization to the atmospheric pressure vessel through the nozzle. This fast depressurization makes the solvating power and the density of the $scCO_2$ decrease drastically, leading to the solute supersaturation and consequent formation of small particles [118,119]. This process is suitable for substances that are relatively soluble in $scCO_2$ [120] and for thermolabile compounds due to the use of moderated temperatures typically below 80 ºC [121]. The scale-up flexibility is hindered by the formation of particulate aggregates and nozzle clogging due to rapid expansion cooling, known as the Joule-Thompson effect [113]. RESS modified processes, such as Rapid Expansion of a Supercritical Solution with a Non-solvent (RESS-N) and Rapid Expansion of a Supercritical Solution into a Liquid Solvent (RESOLV), have emerged to overcome some of these limitations, in which organic solvents are used [119].

SAS and SEDS (Figure 1.13b) are the most studied antisolvent techniques and are usually used to process solutes with poor solubility in $scCO_2$. In this process, the solute is dissolved in a suitable organic solvent and subsequently sprayed inside a high-pressure vessel where a supercritical atmosphere was created. An enhancement of mass transfer takes place when droplets are formed after the solution spray. The antisolvent effect occurs when the SCF, in contact with the organic phase, saturates the liquid, resulting in the precipitation of the solute. Then, small particles with a narrow size distribution are obtained [119,122]. The SEDS process comes up as an improvement of the SAS process. In this method, the liquid solution and the SCF are simultaneously sprayed through a two or three coaxial passages nozzle. The high velocity of the co-current $scCO_2$ flow, in contact with the organic phase, decreases the solubility of the solute and then, the high supersaturation of the solute is quickly achieved [117,119].

PGSS (Figure 1.13c) is a versatile and continuous process that uses $scCO_2$ as a plasticizer, dissolved in a solution or melt drug in a stirred high-pressure reactor. The presence of the SCF creates a saturated mixture, leading to a decrease in both the melting point of the solute and the solution viscosity, aiding the subsequent atomization to the precipitator through the nozzle. The atmospheric depressurization combined with the rapid expansion cooling allows the solidification of the molten droplets to solid small particles. PGSS-drying is an adaptation of the PGSS process where CO_2 is used to extract and drag the solvent at temperatures suitable for evaporation [123].

SASD (Figure 1.13d) and CAN-BD are the two most known techniques where $scCO_2$ is used as an atomization-aid/co-solute. Both processes involve the mixing of the $scCO_2$ and an aqueous/organic drug solution for a short period. The solution is further atomized through a restrictor/nozzle inside an atmospheric pressure drying chamber and simultaneously dried with a co-current flow of a hot inert gas [117]. The main differences between these two processes are the mixing region (low volume tee and saturator, respectively for CAN-BD and SASD) and the extent of solubilization of $scCO_2$ in the liquid solution [118].

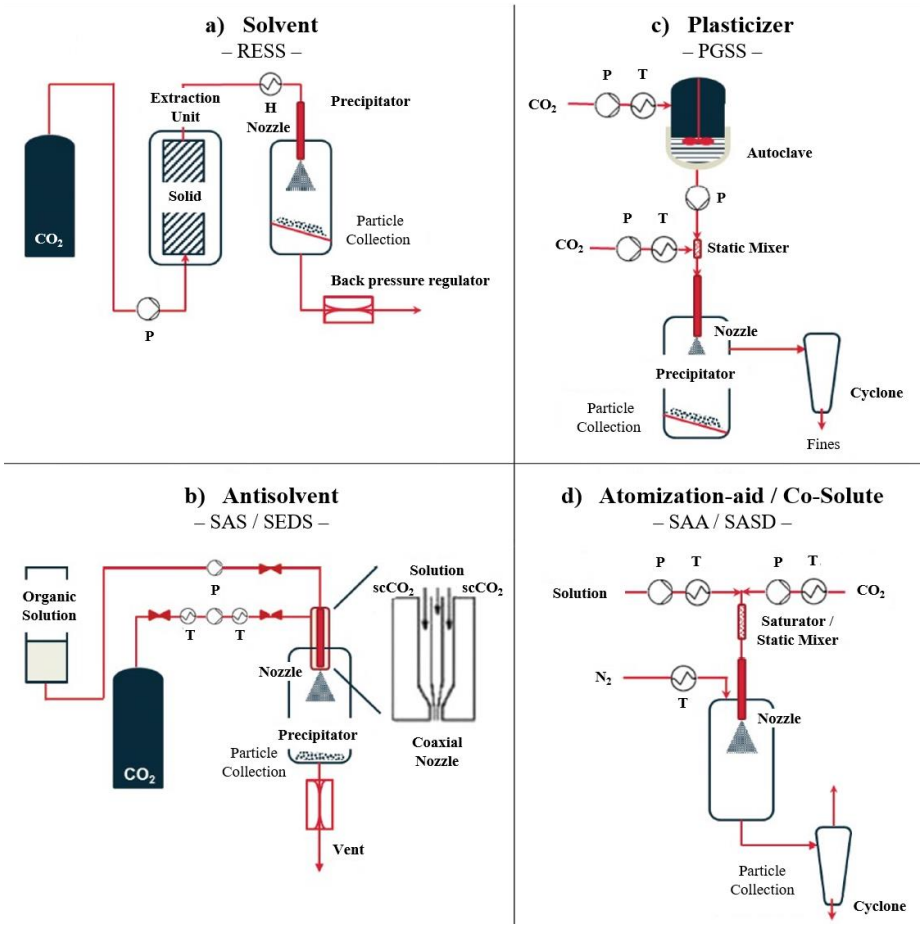

Figure 1.13 – Representation of the main SCF technologies according to the $scCO_2$ role. P: high-pressure pump; T: heat exchanger. Adapted from [117].

In short, the main pros and cons of supercritical processes are summarized in Table 1.3.

Table 1.3 – Synthesis of pros and cons of the main SCF processes [117,118,122,123].

Process	Advantages	Disadvantages
RESS	▪ Single-step process ▪ Environmental benignity: no solvents ▪ SCF reused in continuous process ▪ Moderated temperatures suitable for thermo-sensitive compounds ▪ Crystalline materials ▪ No additional drying steps	▪ Batch ▪ Safety: high pressures ▪ Poor solubility of most polymers and active ingredients in $scCO_2$ ▪ Poor predictive control of particle size and morphology ▪ Operational challenges: clogging and agglomerations
SAS SEDS	▪ Adaptable for continuous processing: large-scale production ▪ Suitable for poor $scCO_2$ solubility and hydrophobic compounds ▪ Control of particle size and morphology in the micro and nano range ▪ No additional drying steps	▪ Organic solvents required: traces in the final product (cytotoxicity) ▪ Safety: high pressures ▪ Complex mass transfer phenomena
PGSS PGSS-drying	▪ Continuous ▪ Versatile ▪ Scalable ▪ Moderate pressure ▪ Suitable for hydrophilic compounds	▪ Control of particle size ▪ Difficulty to obtain submicron-sized particles Melt processing: high temperatures (except for PGSS-drying) ▪ High CO_2 quantities required for PGSS-drying
SASD CAN-BD	▪ Continuous ▪ Scalable ▪ Moderate pressure and temperature ▪ Control of particle size and morphology ▪ Adaptable to the conventional SD apparatus	▪ Additional drying step ▪ High drying temperatures

1.4.5. Supercritical-CO_2 Assisted Spray Drying

Supercritical-CO_2 Assisted Spray Drying (SASD), or Supercritical Assisted Atomization (SAA) how was initially established by Reverchon in 2001 [124], is one of the most promising atomization techniques to produce DPFs at the micro-scale. In this process, the $scCO_2$ has two roles regarding the way it acts: as a co-solute, being miscible with the liquid solution at supercritical conditions and, thus, forming a possible ternary system CO_2/solvent/solute; as an atomization-aid during the atomization step. SASD enables the use of organic solvents or aqueous solutions to provide a better control in particle size, with the formation of homogeneous and smaller particles typically raging between 0.1 and 5 μm [123,125,126].

In the SASD, controlled amounts of $scCO_2$ are simultaneously pumped at the same time as a liquid solution is fed to the process, containing the active substance and the excipient. This two streams are mixed in the static mixer where the $scCO_2$ solubilization in the liquid solution promotes the formation of a homogeneous and near-equilibrium solution. Then, this mixture is sprayed out through a nozzle to a drying chamber at atmospheric pressure, in which a two-step

atomization occurs. Firstly, takes place the pneumatic atomization, where the first particles are formed by continuous heated drying gas flow (primary droplets, Figure 1.14a). Then, follows a decompressive atomization, in which the CO_2 expansion from within the first droplets to form particles of even smaller diameters (secondary droplets, Figure 1.14b). The heated air provides an efficient drying with the quick evaporation of the solvent from the droplets. The particles follow to a high-efficiency cyclone where they are separated from the gas stream and collected in a flask [111].

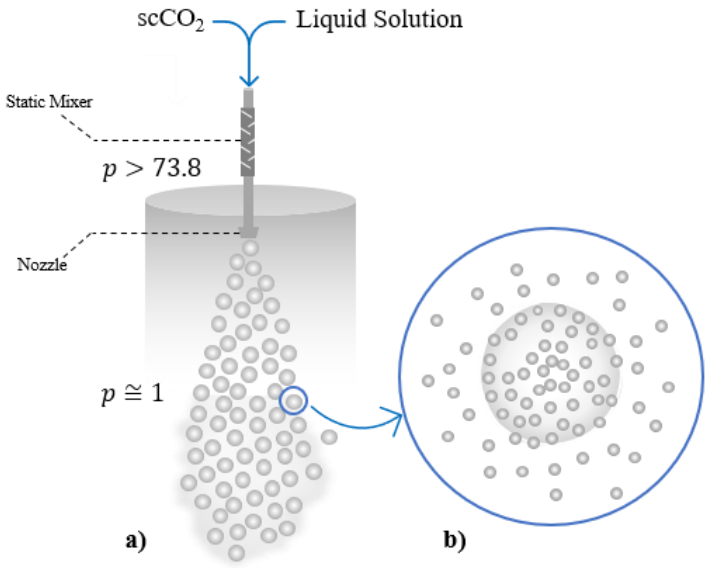

Figure 1.14 – Schematic representation of the two-step atomization: a) pneumatic and b) decompressive atomization. Adapted from [127].

A key-step in the atomization step efficiency is particularly related to the solubilization of the $scCO_2$ into the liquid solution that occurs in the static mixer [126]. The $scCO_2$ and the liquid solution feed ratio will determine the adequate residence time for the vapor-liquid equilibria (VLE) of the ternary system CO_2/solvent/solute [128]. It is generally advantageous to use an excess of CO_2 relative to the liquid solution to ensure the desired pressure conditions in the static mixer and lead to a good efficacy in the atomization [127][129]. Moreover, the pressure and temperature conditions, as well as the liquid system selected, will define the amount of $scCO_2$ solubilized. It is stated that the $scCO_2$ have shown a lower solubility in water when the process operates at lower temperature and pressure conditions, and falling into a two-phase gas-liquid region [126,127]. Hence, when aqueous solutions are used, it becomes more difficult to achieve the phase equilibrium and predict the phase behavior of such multicomponent systems involved in a real process.

The presence $scCO_2$ dissolved in aqueous solutions decreases the viscosity and the surface tension of the solution to be atomized. In contrast, if a low amount of $scCO_2$ is present in the

liquid phase, the viscosity of the solution tends to be higher. Such phase behavior is responsible for the poor CO_2 decompressive atomization and, therefore, leading to larger particles to be produced [126,128–131] Therefore, ethanol is usually used as a cosolvent to increase the $scCO_2$ miscibility in aqueous systems [132]. Ethanol is seen as a preferable cosolvent due to its price and toxicity when compared to others, since it is also FDA approved [133].

Indeed, there are some difficulties when it comes to processing thermosensitive compounds by SASD. The drying temperature during the atomization must be high enough to completely dry the solvents, but at the same time it cannot lead to the degradation or loss of activity of these substances. Moreover, polymers with a low glass transition temperature could difficult the atomization process [134].

1.4.6. Literature Studies

Supercritical-based techniques have been used to produce DPFs containing phenolic compounds from natural extracts. Aliakbarian et al. [135] used the SAA process to encapsulate natural polyphenols extracted from olive pomace, using maltodextrin (MD) as a carrier. Phenolic compounds were extracted by a high pressure-high temperature agitated reactor (HPTE) using ethanol:water 50:50 (%v/v) as a solvent. The different ratios of MD for the total solids of the extract (10 to 50 %wt/wt) as well as the drying temperature (75 to 95 °C) were the parameters studied. Particles with diameters below 1 µm and with antiradical capacity were obtained.

In another work, Di Capua et al. [136] also assessed the feasibility and efficiency of the use of SAA to encapsulate natural phenolic compounds present in a propolis ethanolic extract, using hydroxypropyl-*β*-cyclodextrin (HP-*β*-CD) and polyvinylpyrrolidone (PVP) as carriers. The solutions were prepared in a water:ethanol 30:70 (v/v) mixture with two different total concentrations (30 and 60 mg/mL) and at different dry extract/carrier ratios (wt/wt) (1:2, 1:3, 1:5 and 1:8). Microparticles were obtained with up to 100 % of the total polyphenol content present in extract and the phenolic compounds still maintaining their bioactivity after being processed by SAA.

At the best of our knowledge, no studies in the literature have used the SASD technology for the encapsulation of polyphenols extracted from VPR or other grape by-products, even pure phenolic compounds, such as resveratrol or gallic acid. Also, the HPC selection as excipient had never been done before to encapsulate natural phenolic compounds or extracts using SCF-based methods.

Table 1.4 – Recent supercritical fluid-based works reported in the literature to encapsulate grape phenolic extracts, raw resveratrol or raw gallic acid.

Method	Active Ingredient	Encapsulation Material	Solvent Used	Operational Conditions	Main Outcomes	Year	Ref.
SAS	Resveratrol (99.8% purity)	HP-β-CD	Ethanol	T = 40 ºC P = 120 bar $F_{solution}$ = 0.5 mL/min F_{CO2} = 30 g/min Molar ratio RV/HP-β-CD = 1:1 Solution concentration = 3% (w/v)	Enhancement in the solubility in an aqueous medium (up to 25.13 mg/mL)	2012	[137]
PGSS-drying	Resveratrol (98% purity)	β-glucans and soybean lecithin	Oil-in-water emulsion (with 20% w/v of tebu-conazole)	F_{CO2} = 167 g/min T_{CO2} = 125 ºC P_{CO2} = 9.5 bar CO_2:Liquid ratio = 30 w/w $T_{chamber}$ = 65–70 ºC	D_p = 100–150 µm (spherical) $\%_{EE}$ = 67–94 % Improvement of the antifungal action of RSV against Botrytis cinerea	2015	[138]
SAS	Grape pomace poly-phenolic extract	–	Ethanol	T = 40, 45 ºC (DoE) P = 100, 120 bar (DoE) x_{CO2} = 0.97, 0.99 (DoE)	D_p = 5–10 µm (irregular shapes)	2016	[139]
SAS	Grape pomace poly-phenolic extract	Poly(-lactic-co-glycolic acid (PLGA)	Ethyl acetate	P = 80, 110, 140 bar T = 35, 40, 45 ºC $[Extract]_{Feed}$ = 2, 4, 6 mg/mL $[PLGA]_{Feed}$ = 10 mg/mL $F_{solution}$ = 1.0, 2.0, 3.0 mL/min F_{CO2} = 1 kg/h	D_p = 4–11 µm (spherical) $\%_{EE}$ = 40 – 94 % Higher stability against degradation compared to the crude extract	2016	[140]
SEDS	Trans-resveratrol (99.0% purity)	'Poly(3-hydroxy-butyrate-co-3-hy-droxyvalerate (PHBV)	Acetone:Di-chloromethane 40:60 (v/v)	[Solute] = 4, 12, 20 mg/mL (DoE) P = 80, 115, 150 bar (DoE) T = 35 ºC $F_{solution}$ = 1 mL/min $F_{antisolvent}$ = 20 mL/min T,P_{CO2} = 5 ºC, 200 bar	D_p = 390–570 nm (spherical) $\%_{Encapsulat.}$ = 13.25–49.71 % $\%_{EE}$ = 58.6–99.5 % DPF particles free of organic solvent Higher AA of DPFs compared to raw RSV	2017	[141]
SAS	Trans-resveratrol (99.1% purity)	HPMC and HPMC + Surfactants	Dichloromethane: Methanol 1:1 (v/v)	T = 40 ºC P = 120 bar $F_{solution}$ = 1 g/min F_{CO2} = 40 g_{CO2}/min	D_p = < 300 nm (spherical) Nanoparticles Enhanced Oral and Skin Delivery Ƞ > 80 % $\%_{EE}$ > 97 %	2019	[60]

1.5. Quality-by-Design

1.5.1. Concept

Quality-by-Design (QbD) is a modern approach that was initially supported by the US FDA and the International Conference on Harmonization (ICH) for the improvement of the development phase of new pharmaceutical products [142]. According to what was established and documented by ICH, namely in the ICH Q8(R2) guideline 'Pharmaceutical Development', the QbD concept must be built through the application of design tests in the formulation and manufacturing process and not through product testing [143]. Besides that, this systematic approach allows not only to ensure speed and optimal robustness of the process, but also to ensure that the quality of the final product meets the required specifications.

The application of the QbD approach can follow the steps represented in Figure 1.15. It starts with the identification of the Target Product Profile (TPP) of the intended product, that is, the ideal product characteristics to ensure the desired quality and performance, as well as its safety and effectiveness. Therefore, the Critical Quality Attributes (CQAs) need to be well-identified. These attributes will establish the characteristics or properties (either chemical, physical, biological or microbiological) of the product that need to be observed so that it ensures the desired therapeutic effects. A risk assessment is performed for each step of the process to evaluate the impact of potential Critical Material Attributes (pCMAs) and Critical Process Parameters (pCPPs) on the CQAs. Then, experiments are performed according to the Design of Experiments (DoE) tool to assess the relationship between the pCMAs/pCPPs with the CQAs. The sum of acceptable variability in each of these parameters will define the design space and normal operating range (NOR). The QbD approach follows with performing a process risk assessment failure mode effects analysis (FMEA) which recognizes the parameters in terms of criticality and establishes suitable process control strategies [142,144].

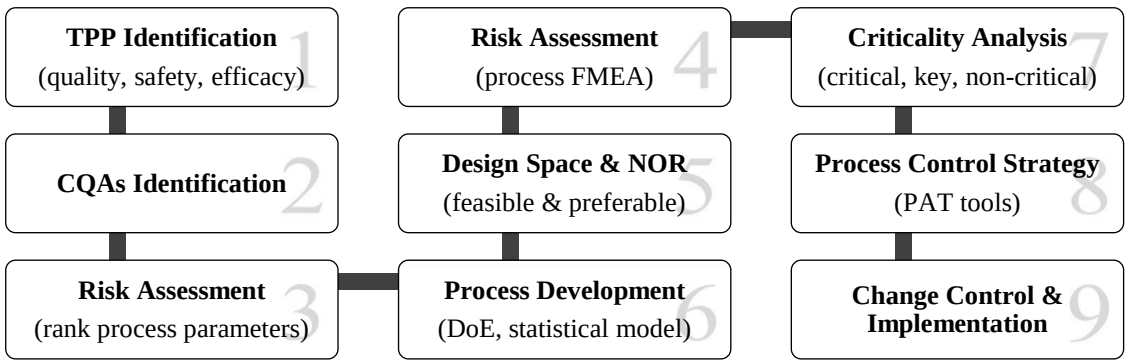

Figure 1.15 – Main steps of a Quality-by-Design approach. Adapted from [68].

1.5.2. Design of Experiments

The Design of Experiments (DoE) is a dynamic tool commonly used in the industry to decrease the manufacturing costs by minimizing process variation and the time consumption for rework and inspections. A set of experiments based on a quality criticality analysis are carried out and further used in a modeling approach to quantify the impact of the parameters in the dry power properties and performance.

The two most used models to predict this effect are the mechanistic and statistical approaches. While the mechanistic models extrapolate a design space based on process descriptions and first principles, statistical models use the range of the parameters observed to make systematic approaches in DoE and statistically correlate the CPPs and the CQAs. The statistical approach is capable to detect the degree of correlation between variables without any knowledge of the process. However, a high number of tests are needed, compared to the mechanistic, to achieve a high level of confidence and extrapolating relationships to other scales which can become a higher constrain [68].

A statistical modeling approach for the development of a new formulation should involve three stages: screening, optimization and robustness (Figure 1.16). In the first phase, the factors that most influence the final powder properties are identified and the process parameter ranges are determined. A low number of experiments relative per number of factors are performed at this stage since it is unnecessary to be strict in quantifying the effects. In the optimization phase, the objective is to investigate the range of the parameters that showed statistical significance and within this range, found the combination of factors that led to an optimized process or product. Hence, a higher number of experiments are required to evaluate all possible interactions between parameters. Finally, the main goal of the robustness phase is to access the CQAs sensibility towards small variations in the process parameters of the studied factors and to be able to potentiate fluctuations in the process/product [145,146].

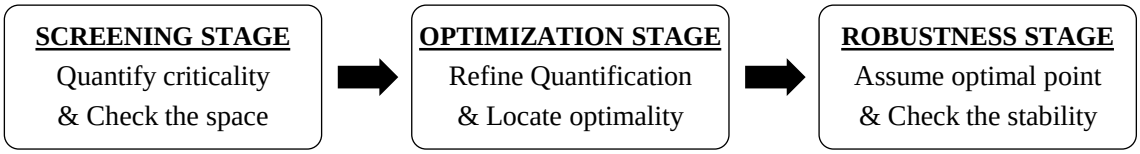

Figure 1.16 – Sequence of the Design of Experiments stages. Adapted from [146].

Although the DoE helps to achieve the ideal conditions of the process, we must keep in mind that the conclusions and observations we reach by the application of this tool are conditioned by the factors and ranges that have been selected [144].

The use of the DoE tool and the consequent statistical analysis can be applied for the optimization of drying processes to correlate the effect of CPPs with the properties of the DPFs. Usually, the common parameters studied either for conventional or supercritical-assisted spray drying techniques are based in the temperature and pressure conditions, nozzle diameter, feed flow rates and the solids content in the liquid solution. When it is intended to use different types of excipients, this can also be a variable under study, as well as the drug/excipient ratio. [111,128].

Recently, some authors have applied DoE methodology to optimize the SASD process. Cabral et al. [147] studied the effect of the CO_2 to liquid flow ratio, the precipitator temperature and the use of a model active ingredient on the final aerodynamic properties of the composite dry powders. Aliakbarian et al. [135] studied different ratios of MD to total solids of the extract and drying temperatures, to encapsulate phenolic compounds using SASD. The yield as well as the physical characteristics, phenolic content and antioxidant power were assessed. Tavares et al. [148] optimized the formulation of dry powder microparticles for potential vaccine delivery to the lungs, varying the absence or presence of both BSA and L-leucine and two CO_2 to liquid flow ratios. The effects of these parameters were evaluated both on aerodynamic performance and on the microparticles size distribution. Moura et al. [149] also implemented DoE tool for the optimization of SASD for the production of inhalable composite particles and improvement of the aerodynamic performance, along with process yield and powder properties when compared to particles obtained by conventional SD.

A summary table with the main parameter values applied in these studies is presented next.

Table 1.5 – Recent SASD reported works in the literature using QbD approach based on DoE tool.

Compound/ excipient	Solvent	DoE	Optimization parameters	Operating conditions	Year	Ref.
Ibuprofen (IBP) / Chitosan	1% acetic acid aqueous solution w/ 18.6% (v/v) of ethanol	2^{3-1} factional factorial + c.p.	IBP (%w/w) = 0, 6.7, 13.4 $R_{CO2/liquid\ ratio}$ (w/w) = 5.3, 7.1, 8.9 T_{in} (ºC) = 60, 70, 80	P = 100 bar	2016	[147]
Polyphenolic extract / Maltodextrin (MD)	Ethanol/ water 50:50 %(v/v)	3^2 full factorial	MD (%w/w_{solids}) = 10, 30, 50 $T_{chamber}$ (ºC) = 75, 85, 95	T_{in} = 95 ºC T_{SM} = 75 ºC T_{in} = 100 ºC F_{CO2} = 10 g/min $F_{solution}$ = 4 g/min	2016	[135]
Bovine serum albumin (BSA) / PLGA / L-leucine	Acetonitrile/ water 83:16 %(v/v)	2^3 full factorial + c.p.	BSA (%w/v) = 0, 0.09 IBP (%w/v) = 0, 0.02 $R_{CO2/liquid\ ratio}$ (w/w) = 8.3, 5.0	T_{SM} = 40 ºC P = 90 bar T_{in} = 100 ºC	2017	[148]
Trehalose / L-leucine	Ethanol/ water 20:80 %(w/w)	3^3 full factorial	F_{feed} (kg/h) = 3.5, 5.5, 7.5 T_{in} (ºC) = 85, 115, 150 P_{SM} (bar) = 90, 103, 117	C_{solids} = 2 %w/w $R_{t/leu}$ = 80/20 %wt F_{CO2} = 25 mL/min T_{SM} = 80 ºC	2019	[149]

2. Experimental Section

2.1. Microparticles Production

2.1.1. Materials

Hydroxypropyl cellulose (HPC, Mw ~18,000), gallic acid monohydrate (GA, ≥ 98.0 % purity, Mw = 188.13 g/mol) and 2,2-Diphenyl-1-picrylhydrazyl (DPPH•, Mw = 394.92 g/mol) were purchased from Sigma-Aldrich. Resveratrol (RSV, >99.0 % purity) was purchased from Tokyo Chemical Industry (TCI, Japan). Deionized water was prepared by reverse osmosis (Milli-Q, Millipore). Ethanol absolute anhydrous (EtOH, 99.8 % purity) was purchased from PanReac ITW Reagents (Barcelona, Spain). All compounds were used without further purification. Industrial carbon dioxide (purity ≥ 99.93 %) from Air Liquid was used. Phosphate Buffer Solution (PBS) pH 5.5 was prepared according to European Pharmacopeia's procedure [150].

2.1.2. Formulation and SASD Apparatus

In the pre-processing phase, water/ethanol solutions were prepared in order to create a model system with each of the two phenolic compounds, namely gallic acid (GA) and resveratrol (RSV). Two different solution volumes, 25 mL and 50 mL for GA and RSV solutions, respectively, were prepared. Hydroxypropyl cellulose (HPC) was used as excipient in both system solutions. The percentage of the phenolic compound was 1% w/w for the total percentage of solids in all formulations. While HPC solution was prepared in part of the deionized water and left under continuous stirring one day before processing, both GA and RSV were prepared in ethanol, a few minutes before being processed. After the complete dissolution, the GA or RSV ethanolic solution was added to the HPC aqueous solution. The resultant solution was then filtered to an amber flask to protect it from light exposure while it is fed to the process.

In this process (Figure 2.1), two independent streams are fed to the process: a homogeneous liquid feed solution containing both bioactive compound and excipient was pumped through a high-pressure liquid pump (Smartline Pump 1000, Knauer); liquefied CO_2 from a cylinder (TP) was first cooled in a cryogenic bath and then pumped with a high-pressure liquid pump (HPLC pump K-501, Knauer), since this pump is only suitable for liquid solutions. Liquefied CO_2 was heated in an oil bath and then sent to the static mixer (SM) that promotes its solubilization and homogenization with the liquid solution, creating near-equilibrium conditions before the atomization. Pre-atomization pressure at the SM was controlled by a Setra pressure transducer (0.1 psig stability). The temperature of SM is assured by a set of heating tapes and is connected to a Shinko

temperature controller. The mixture was then sprayed and depressurized through a nozzle into an aluminium precipitator vessel (with a glass window frame) at near-atmospheric pressure. Simultaneously, an inlet heated compressed air/N_2 flow at 30 kg/h allowed the evaporation of the liquid solvent from the droplets to form particles. The particles exit from the bottom of the precipitator to a high-efficiency cyclone, where they were separated from the gas stream and collected in a glass flask. The powder was stored in amber flasks inside a desiccator.

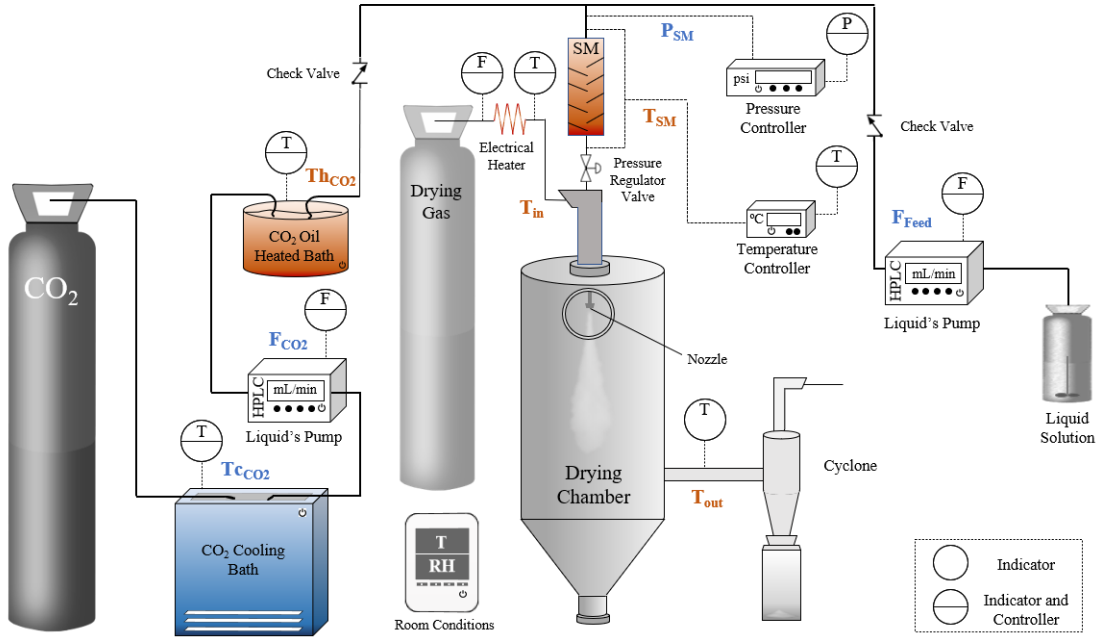

Figure 2.1 – Schematic representation of the Supercritical CO_2-Assisted Spray Drying (SASD) apparatus.

The following SASD parameters were kept constant: CO_2 flow rate (F_{CO2}), liquid feed solution flow rate (F_{Feed}), inlet drying gas temperature (T_{in}), saturator temperature (T_{SM}), CO_2 oil bath temperature (Th_{CO2}), CO_2 cooling bath temperature (Tc_{CO2}) and saturator pressure (P_{sat}). The SASD parameter values are summarized in Table 2.1. The pressure and temperature conditions have been selected according to the vapor-liquid equilibria (VLE) data of CO_2/ethanol/water system to work above CO_2 critical point and form a homogenous supercritical state [151]. Also, the selected conditions were optimized according to previous work using this apparatus [149].

Table 2.1 – Constant parameters in SASD process.

F_{CO2} (mL/min)	F_{Feed} (mL/min)	T_{in} (ºC)	T_{SM} (ºC)	Th_{CO2} (ºC)	Tc_{CO2} (ºC)	P_{SM} (MPa)	d_{nozzle} (µm)
25	3.5	100	80	80	–20	10	150

The experiments were performed in a hand-made laboratory-scale SASD apparatus available at LAQV/REQUIMTE's laboratory (FCT/NOVA), as shown in Figure 2.2.

In a typical experimental assay, the following steps were taken:

1. Injection of the CO_2 with a solvent washing solution;
2. Stabilization of the required conditions of temperature and pressure;
3. Switch to the liquid feed solution until it is completely processed;
4. Switch to the solvent washing solution to drag residual feed solution;
5. Injection of CO_2 for removing the residual liquid solvent;
6. Let the installation cooling to recover the powder.

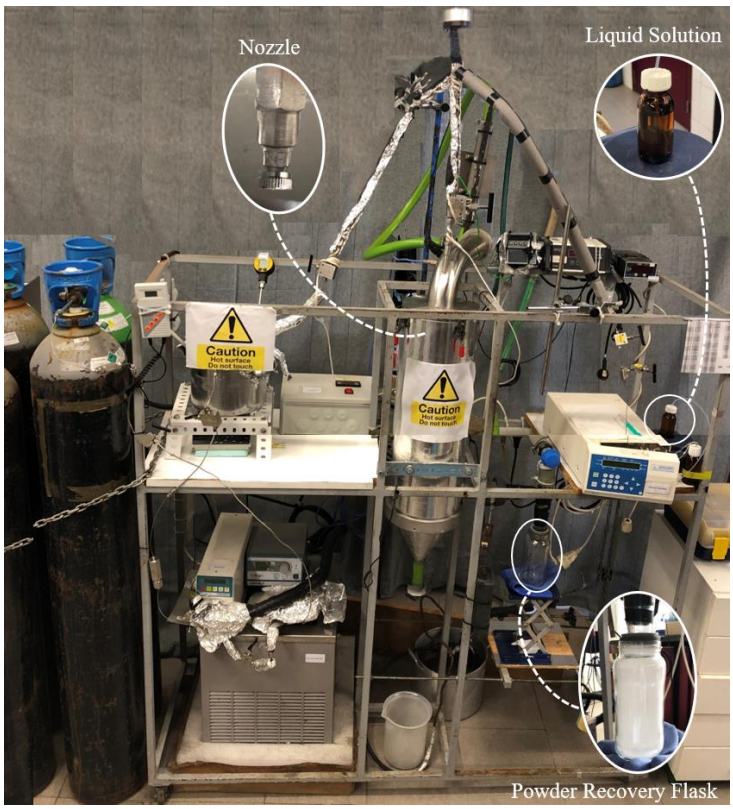

Figure 2.2 – SASD laboratory scale apparatus used to produce DPFs.

2.1.3. Design of Experiments

A 3^2 full factorial design DoE approach was applied to study two formulation variables in the optimization of SASD process for the production of DPFs with GA or RSV: 8 points plus 1 central point (Figure 2.3). The effect of the content of solids (C_solids, %w/v – Factor A) and ethanol volume (V_ethanol, %v/v – Factor B) in the liquid solution were studied with the respect to process yield, particle size, span and encapsulation efficiency of the bioactive compound in the polymeric matrix. The content of solids was ranged between 2.5–7.5 %w/v whereas the ethanol volume was ranged between 20–75 %v/v. The range of values for the solids content was based on recent studies by Rahman et al. [152,153], where HPC was co-atomized with a poorly soluble

drug. To assess the reproducibility of the process, the experiments were replicated for each combination of factors, for a total of 18 experiments for each of the phenolic compounds.

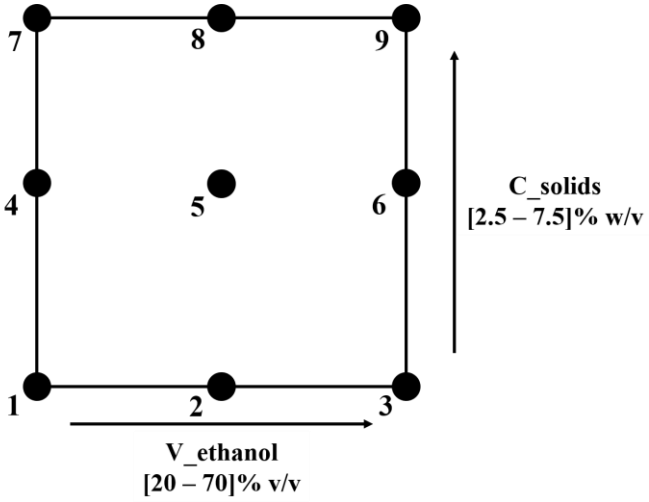

Figure 2.3 – Schematic representation of the 3^2 full factorial design DoE.

These are selected as potential critical process parameters (pCPP) and were studied using three levels – low (–1), medium (0) and high (+1) – as shown in Table 2.2. The standard order of the experiments obtained by the DoE is presented in Table 2.3.

Table 2.2 – Parameter level values used in 3^2 full factorial design.

		Level of factors used in the formulation		
Factor		**–1**	**0**	**+1**
A	C_solids (%w/v)	2.5	5.0	7.5
B	V_ethanol (%v/v)	20	45	70

Table 2.3 – Standard order matrix of the experiments.

Exp. No.	**A**	**B**
1	–1	–1
2	–1	0
3	–1	+1
4	0	–1
5	0	0
6	0	+1
7	+1	–1
8	+1	0
9	+1	+1

The possible correlations of the dependent and independent variables as well as their level of significance under the results obtained from different experiments were studied by statistical analysis through the *Statistica V12* (StatSoft, Inc.) *software*.

2.1.4. Process Yield and Encapsulation Efficiency

The process yield was determined by the ratio between the mass of powder collected in the flask, placed at the bottom of the high-efficiency cyclone at the end of the process, m_p, and the solid content uploaded in the initial feed solution, m_s.

$$\eta\ (\%) = \frac{m_p}{m_s} \times 100 \tag{2.1}$$

The quantification of the encapsulated phenolic compound in each RSV-DPF and GA-DPF was performed by High-Performance Liquid Chromatography (HPLC), based on the method described by Ahmad et al. [154] with some modifications. The analysis was performed with a Thermo Kromasil Keystone C18, 5 µm, 4,6 mm × 250 mm column and a UV-Vis detector. The mobile phase (eluent) consisted of a mixture of 0.5 %v/v acetic acid in methanol:water (50:50 v/v), pumped at a flow rate of 1 mL/min and at 30 ºC. Previously, a calibration curve for each phenolic compound was prepared from eight calibration standards solutions with the same eluent, with concentrations from 0.5 to 52 mg/L (see Appendix H).

The preparation of the solution to be analyzed was made dissolving 1 mg of DPF in 1 mL of eluent. The volume injected in the HPLC column was 20 µL. RSV and GA were identified by comparison of the retention time and the detected peaks by UV-Vis spectra with those obtained for standards. The retention time of approximately 6 and 2.7 min was observed for RSV and GA, respectively. The RSV-DPF solutions to be analyzed were read at a wavelength of 304 whereas the GA-DPF solutions were read at 280 nm.

Then, to quantify the RSV or GA in the DPFs, the peak area given in the HPLC chromatogram was replaced in the linear regression obtained by the standard point of phenolic concentration *versus* peak area. The encapsulation efficiency (EE) was determined by the ratio of the encapsulated mass detected by HPLC and the phenolic mass input (equation 2.2). All data were treated using the Excel *software*.

$$\%\ \mathrm{EE} = \frac{\text{Mass of Compound Encapsulated}}{\text{Input Mass of Compound}} \times 100 \tag{2.2}$$

2.2. Microparticles Characterization

2.2.1. Particle Size and Particle Size Distribution

The particle size (PS) and the particle size distribution (PSD) were measured by Morphologi G3 equipment (Malvern Instruments, UK). This equipment has an automatic sample dispersion unit coupled to a microscope in which different objectives are controlled by a proper software. For a good feasibility analysis of the results, at least 30,000 particles are photographed and statistically analyzed according to different geometrical factors, that is, the particle diameter in volume (D_v) and number (D_n) corresponding to 10, 50 and 90% of the total population. Also, a measure of the width of the particle size distribution (span) considering the $D_{v,10}$, $D_{v,50}$ and $D_{v,90}$ was determined as represented in equation 2.3.

$$\text{Span} = \frac{D_{v,90} - D_{v,10}}{D_{v,50}} \tag{2.3}$$

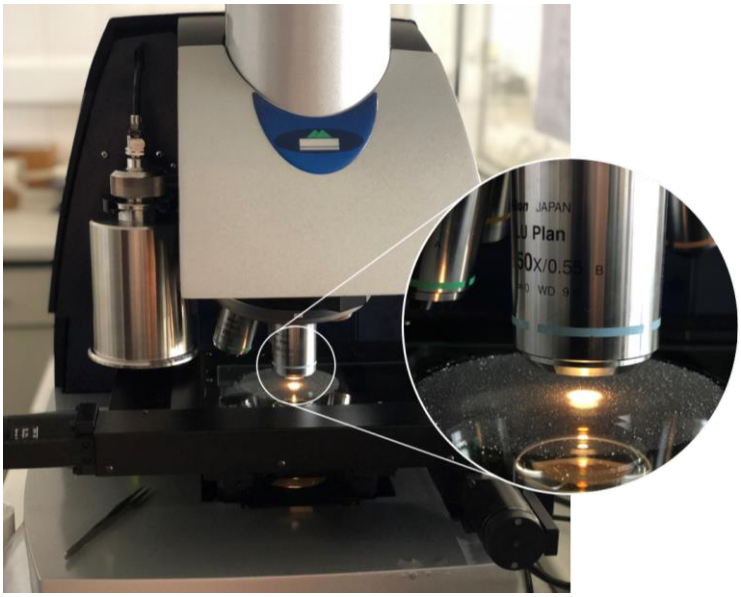

Figure 2.4 – PS and PSD analysis using Morphologi G3 equipment.

2.2.2. Particles Morphology

The shape and surface morphology of the atomized DPFs in the SASD were observed by Scanning Electron Microscopy (SEM). The samples were coupled to adhesive carbon tapes and the excessive powder was removed by a jet of compressed air. Then, the samples were analyzed by a Hitachi S2400 with an accelerating voltage set to 15 kV and at magnifications of 500, 1,000 and 3,000×.

2.2.3. X-Ray Powder Diffraction

The amorphicity and crystallinity of the native compounds, physical mixtures (PMs) and DPFs were assessed by X-Ray Powder Diffraction (XRPD). The PMs were prepared in the same HPC/compound ratio as the SASD processed formulation by gently mixing with a ceramic mortar and pestle. The measurements were performed in a RIGAKU X-ray diffractometer (model Mini-flex II) with automatic data acquisition (Peak search for Windows v. 6.0 Rigaku) using CuKα radiation (λ = 0.15406 nm or 1.54 Å) and working at 30 kV/15 mA. Diffraction patterns were collected in the range 2θ = 5–90 ° with a 0.02 ° step size and an acquisition time of 1 º/min.

2.2.4. BET Specific Surface Area

The specific surface area (expressed in m^2/g) of the native compounds and DPFs were measured by porosimetry of adsorption with N_2 at 77 K, based on the method applied by Badawy et al. [155]. Before the measurements, the powder was loaded into a sample cell and degassed by N_2 flow for at least 2 hours under vacuum at 60 ºC. The data was obtained by a Surface Area Analyzer ASAP Model 2010 (Micromeritics Instrument Corporation) based on the Brunauer, Emmett, and Teller (BET) equation.

2.2.5. Attenuated Total Reflection Fourier Transform Infra-Red (ATR-FTIR)

ATR-FTIR was performed to study the interactions between the excipient and the bioactive compound. Samples of raw phenolic compounds, two DPFs, with each compound, and also their physical mixtures (PM) were analyzed. The physical mixtures were prepared by the same method as described above. The analysis was carried out on a Spectrum Two FTIR spectrometer (Perki-nElmer, Inc.). A proper amount of each sample was placed in a crystal diamond plate, completely covering the prism surface. Each spectrum was recorded with 16 scans from 400 to 4000 cm^{-1}.

2.2.6. Differential Scanning Calorimetry

The thermal behavior of the DPFs and PMs was assessed using a differential scanning calorimetry equipment (DSC Q2000, TA Instruments) with a refrigerated cooling system. The physical mixtures were prepared by the same method as above. Approximately 5 mg of sample were accurately weighed into a pinhole aluminium pan hermetically crimped (Tzero Hermetic Lid, TA) and heated under a continuous dry nitrogen purge (50 mL/min).

The main procedural steps of the DSC test are summarized in Figure 2.5. The first heating ramp (Run 1) starts at –90 ºC and goes up to 250 ºC, at a heating rate of 10 ºC/min, to eliminate the water content in the sample. Then, a cooling ramp brings the temperature down to -90 ºC, at a cooling rate of 10 ºC/min, in order to start the second heating ramp (Run 2) up to 250 ºC again,

at the same previous heating rate. Here, either the glass transition and the melting point can be identified by a sigmoidal difference in the thermal baseline or by an endothermic peak, respectively. DSC data and thermograms were extracted by TA Instruments *software* (Universal Analysis 2000).

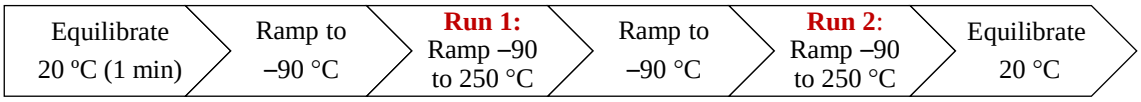

Figure 2.5 – Sequential procedure segments in DSC.

2.2.7. Moisture Content

The residual moisture content present in the atomized DPFs was determined using the Karl Fisher (KF) titration method (756/831 KF Coulometer, Metrohm Ion Analysis, Ltd.). Since the equipment was generally used for liquid samples, the DPFs were dissolved in a suitable dry solvent. About 30 mg of DPF sample were accurately weighted and dissolved in 600 µL of dried ethanol. The sample was placed under continuous stirring until the total dissolution of the powder. Absolute ethanol 99.8 %v/v was dried in a close flask with activated molecular sieves for at least 3 days before preparing the solution, to reduce as much as possible its moisture content. A blank value correction was made for the solvent. For each DPF, three replicas were made. Using a syringe (B|Braun, Injekt®-F 0.01 mL–1 mL), an aliquot of 0.3 mL was removed from the solution and weighed before and after being titrated. The Karl Fisher reagent, which reacts selectively and quantitatively with the water of the injected solution. The percentage of H_2O normalized per gram of sample is further calculated using Excel *software*. A schematic representation of the described method is present in Figure 2.6.

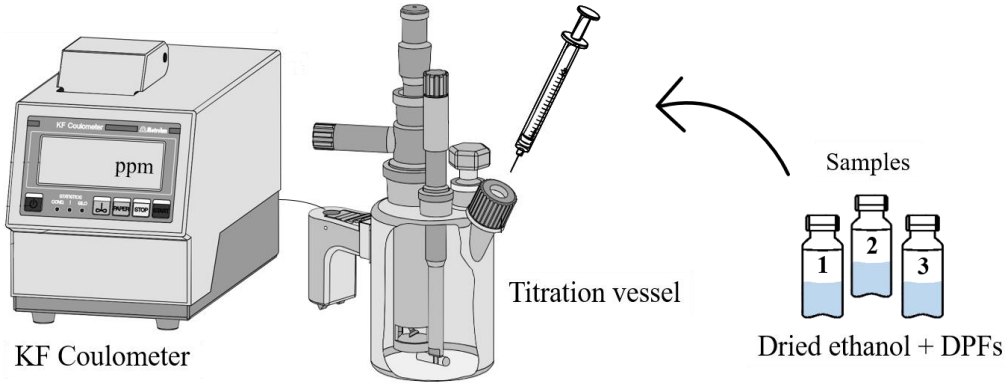

Figure 2.6 – Schematic representation of the Karl Fisher titration method. Adapted from [156].

2.3. Antioxidant Activity

The antioxidant activity of the DPFs was assessed by the scavenging capacity of the DPPH radical, following the method applied by Medina-Torres et al. [157], with some modifications. The tests were also performed for each of the pure phenolic compounds (RSV and GA) as a term of comparison to the antioxidant activity of the DPFs. The procedure of the tests followed the next steps: 1) a stock solution of DPPH• at a concentration of 26 mg/100 mL (6.6×10^{-4} M) was prepared in ethanol; 2) an aliquot of the previous DPPH stock solution was mixed with ethanol at a volume ratio of 1:4.5 to form a solution with a DPPH concentration of 1.2×10^{-4} M; 3) a stock solution with the bioactive samples was prepared separately in ethanol to subsequently allow seven dilutions from 100 to 2100 µM for RSV samples and from 50 to 470 µM for GA samples. Then, an aliquot of 0.2 mL was removed from each of the seven dilution to mix with 1.8 mL of the DPPH• solution prepared in 2) and hand-stirred. The samples were prepared in triplicate for each concentration and kept in the dark (in an amber vial) for 30 min at room temperature. The absorbance was measured at 517 nm in a Evolution™ 201 UV-Vis spectrophotometer with Thermo Insight *software* (Thermo Fisher Scientific) by adding an aliquot of sample to a 1 mL cuvette. Previously, the reference blank ($A_{DPPH\bullet}$) was measured, corresponding to the diluted ethanolic solution of DPPH• prepared in 2). The percentage of DPPH free radical scavenging activity was determined by the Equation 2.4 and plotted against concentration.

The EC_{50} value, which is defined as the minimum effective concentration of antioxidant necessary to scavenge 50% of the initial DPPH free radical, is determined by the analytical method described by Alexander et al. [158].

$$\%\ \text{DPPH radical scaveging activity} = \frac{A_{DPPH\bullet} - A_{sample}}{A_{DPPH\bullet}} \times 100 \quad (2.4)$$

2.4. *In vitro* Aerodynamic Performance

The aerodynamic performance of the DPFs was evaluated gravimetrically using an 8-stage aluminum Andersen Cascade Impactor (ACI) apparatus (Copley), following the European Pharmacopeia procedure [159]. The analyzed DPFs were previously stored for two weeks in atmospheres with different relative humidity conditions (20 and 45 %RH) to evaluate their aerodynamic performance.

Before starting the tests, the airflow of the ACI was regulated on a critical flow controller model TPK (Copley), with an empty capsule, to adjust the pressure drop for 4 kPa (admitted pressure drop in nasal administration up to the lungs). The airflow rate was measured using a flowmeter model DFM3 (Copley) and adjusted to the previous pressure drop, which is generally 61.0 ± 1.0 L/min. The test duration for each run was then determined using the Equation 2.5,

where Q_{air} (L/min) is the airflow measured with the flowmeter. A critical flow must be guaranteed by maintaining P3/P2 ≤ 0.5.

$$t\,(s) = \frac{4 \times L}{Q_{air}} \times 60 \tag{2.5}$$

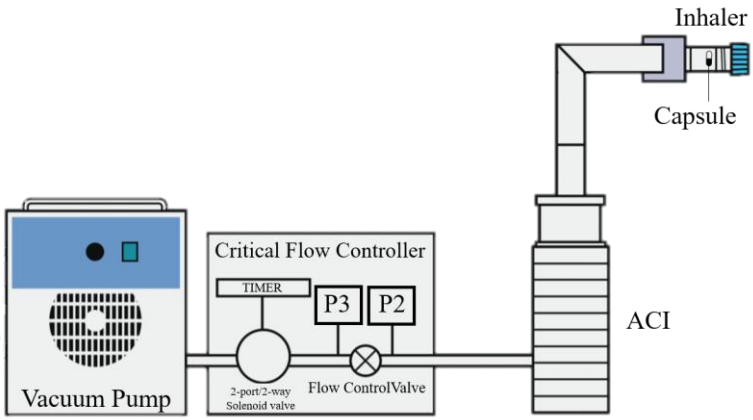

Figure 2.7 – Andersen cascade impactor (ACI) apparatus. Adapted from [160].

For each assay, approximately 30 mg of powder was hand-filled in hypromellose (HPMC) nº 3 capsules (Aerovaus). The capsule is placed in a handheld breath-activated inhaler device (Aerolizer Plastique 60 LPM–Model 7 dry powder inhaler (DPI)), attached to the inlet of the ACI that was fixed on the testing stand horizontally. The flow rate was maintained by a high capacity pump model HCP5 (Copley) through the sampling apparatus to simulate inhalation. The tests were performed in triplicate for each sample. Before starting the test, the inhaler and all the glass microfiber filters (MFV1 80 mm, Filter Lab) were weighed on an analytical balance. The filters were placed in all plate stages before the assay. After the three capsules release, the total mass of powder deposited in each stage filter is determined. The capsule and the inhaler device are weighed to determine the amount of residual powder present in each. The fine particle fraction (FPF) was determined by the interpolation of the percentage of the particles collected in each ACI experiment containing an aerodynamic diameter less than 5 μm. The mass median aerodynamic diameter (MMAD) was determined as the particle diameter corresponding to 50 % of the cumulative distribution. The geometric standard deviation (GSD) was determined by the following equation:

$$GSD = \sqrt{\frac{d_{84}}{d_{16}}} \tag{2.6}$$

where d_{84} and d_{16} is the diameter corresponding to 84 and 16 % of the cumulative distribution, respectively.

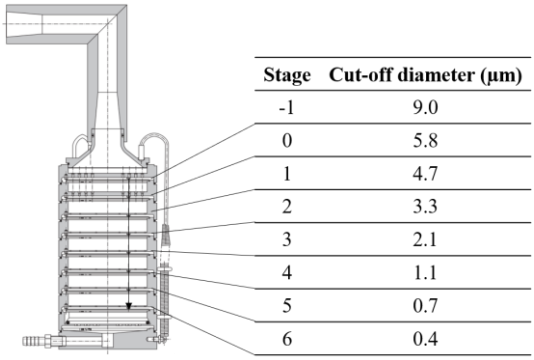

Stage	Cut-off diameter (µm)
-1	9.0
0	5.8
1	4.7
2	3.3
3	2.1
4	1.1
5	0.7
6	0.4

Figure 2.8 – Andersen cascade impactor (ACI) device and the effective aerodynamic cut-off diameter (µm) of each stage.

2.5. *In vitro* Phenolic Release

The release profiles of both RSV and GA bioactive compounds were evaluated to later compare its release behavior. For each compound, the assays were performed both with native (compound non-encapsulated) and DPF (compound encapsulated) samples with 1 mg of RSV/GA. The sample was weighted into a SnakeSkin® (Dialysis Tubing, Thermo Scientific, USA) and closed in a candy shape, as shown in Figure 2.9. The sample was then putted into amber flasks containing 25 mL pH 5.5 phosphate-buffered saline (PBS) as a dissolution medium. The experiments were made in triplicate for each sample. The release was performed inside an incubator agitator (IKA KS 4000 I control) at 100 rpm and a controlled temperature of 32 ºC. Aliquots of 1 mL were withdrawn each time at specific time intervals from 0.03 to 72 hours. The amount of compound released through the SnakeSkin® was quantified by HPLC, as previously described for the encapsulation efficiency tests, but in this case, a blank sample was made for the pH 5.5 PBS solution, since the samples were prepared and injected in this solvent.

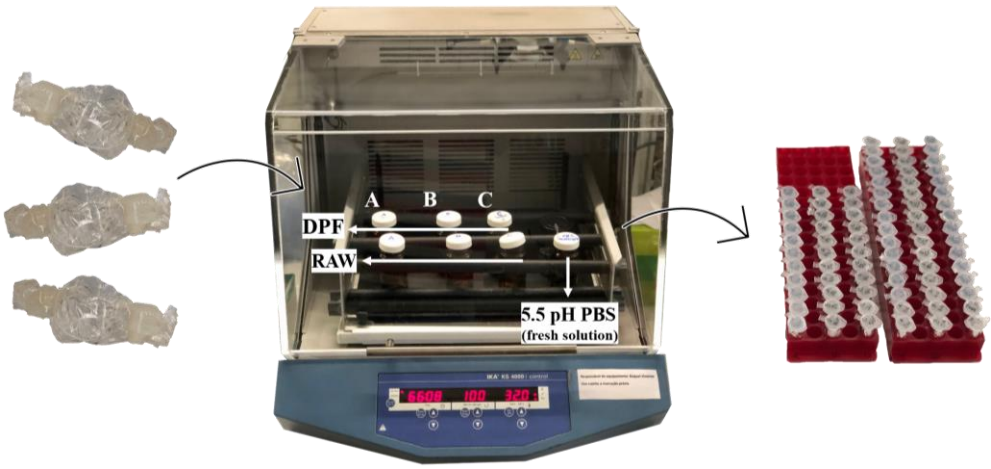

Figure 2.9 – Powder samples within SnakeSkin® and the incubator agitator at desired conditions.

The total mass of released phenolic in each moment of the experiment was determined considering the aliquots taken and the dilution generated by the addition of fresh buffer.

After the *in vitro* release assays, quantification tests were performed on both RSV-DPF and GA-DPF samples used in the tests. A known quantity of each DPF was directly dissolved in ethanol in the same volume used in the tests (25 mL). The same procedure was repeated, but for new PBS solutions for each DPF. These quantification tests were performed in triplicate for each sample and each solvent.

The mechanism of transport associated to the phenolic release from the DPF was assessed by the application of two mathematical models, Higuchi and Korsmeyer-Peppas, according to Equation 2.7 and 2.8, respectively [161,162]. The models were fitted for the first 60 % of release, regardless the particle geometry.

$$\frac{M_t}{M_\infty} = kt^{\frac{1}{2}} \tag{2.7}$$

$$\frac{M_t}{M_\infty} = kt^n \tag{2.8}$$

The M_t/M_∞ is defined as the fraction of phenolic compound released at time t, where M_t is the phenolic mass released at the t and M_∞ is the initial loading of phenolic in the DPF.

The release rate constant (k) is obtained from the slope of the representation of M_t/M_∞ *versus* $t^{1/2}$ according to Higuchi model. In accordance with Korsmeyer-Peppas model, the constant k derives from the interception of the representation of natural log (M_t/M_∞) *versus* natural log (t).

In Korsmeyer-Peppas equation, the parameter n corresponds to the diffusional release exponent. It is obtained by the slope of the representation of the natural log (M_t/M_∞) *versus* natural log (t) and it will define the type of mechanism associated to the release of RSV/GA. For spherical geometries, the release mechanism can be a contribution of a Fickian diffusion for $n \leq 0.43$, an anomalous non-Fickian diffusion for $0.43 < n < 0.85$ or as a Case-II transport for $n \geq 0.85$ [162]. This model was developed exclusively for the release of an active molecule from a polymeric matrix.

All graphics were represented and treated using OriginPro 2018 *software*.

3. Results and Discussion

The main goal of this work is to effectively to encapsulate the bioactive compounds with antioxidant potential, which is normally characteristic in the chemical composition of residues produced during viticulture activities. Supercritical CO_2-Assisted Spray Drying (SASD) was the method used for the production of dry powder formulations (DPFs) with bioactive properties. A model formulation was created with two natural phenolic compounds: gallic acid (GA), for being present at higher concentrations in the composition of the vine-cane extracts, and resveratrol (RSV), because it is known as one of the polyphenols with the greatest antioxidant potential. Since these compounds have a hydrophobic nature, when administrated in their free form, they presented a low bioactivity and bioavailability. For this reason, the use of excipient it is important to preserve and increase its bioactivity and bioavailability when administered, either as cosmetic or food additive. Therefore, hydroxypropyl cellulose (HPC) was selected as a model excipient.

Another purpose of this work is to study a simple DoE approach by applying a 3^2 full factorial design to access the impact of some formulation parameters in the produced powders through the SASD process and their characteristics. Effectively, it is of the most interest to know if the compounds encapsulated are able to maintain their bioactivity. Finally, will be studied the release behavior of two powders, with different phenolic composition, with the application of two kinetic release models in in conditions that mimic the surface of the normal adult skin.

3.1. SASD Conditions

Good efficiency and performance in the atomization and particle formation depend on the selection of the ideal process conditions. Such conditions are important for the formation of a homogeneous mixture in the static mixer, which is directly related to the phase equilibria of the $scCO_2$ and the liquid solution [129]. The $scCO_2$ to liquid solution flow ratio of approximately 7.1 was considered in order to have an excess $scCO_2$ to ensure a pressure of 10 MPa in the static mixer [129]. Also, the higher the ratio $scCO_2$/liquid solution ratio, the higher amount of CO_2 solubilized in the liquid solution [163]. The solubilization of the $scCO_2$ in the liquid solution is promoted by a water/ethanol system since ethanol increases the water affinity in $scCO_2$. A drying gas temperature near to 100 ºC is important to assist the evaporation of the solvents from the droplets during the atomization. Ethanol was also used in the formulations to increase the phenolics solubility in aqueous solutions.

The parameters recorded during all the SASD experiments can be found in Appendix A.

3.2. HPC Preliminary Studies

Before the co-atomization of the excipient and bioactive compounds, some tests were performed to study the feasibility of processing HPC in the SASD apparatus. In recent literature, the conventional spray-drying method was applied to produce amorphous solid dispersions (ASDs) using HPC along with a surfactant to encapsulate a poorly water-soluble model drug. Here, an acetone/water system was used with HPC concentrations of 2.5, 7.5, and 12.5 %w/v to 2.5 %w/v of drug [153]. So, based on this recent work, the decision was to prepare solutions with 5.0, 7.5, and 10.0 %w/v of HPC on our first testing formulations. An ethanol volume of 18.6 %v/v in the feed solution, as well as the process operating conditions, were established according to previous studies carried out on the same SASD apparatus, selected as the optimized conditions [147,149].

It was observed that the higher the concentration of HPC in the solution, the more viscous it became. It was also observed that the liquid solution had a relatively high degree of viscosity, especially with a concentration of HPC of 10 %w/v. Therefore, since this could affect the operationality of the SASD (e.g. system's clogging), this hypothesis was excluded. Instead, solutions with 2.5, 5.0, and 7.5 %w/v of HPC proved to be reasonably processable under the pre-established operation conditions. With these conditions it is possible to observe the formation of a fine and well-defined conical spray at the outlet of the nozzle (Figure 3.1).

Figure 3.1 – Nozzle's spray in the atomization step in the SASD.

The recovered particles were collected as free-flowing dry powders and presented a white color. However, it tends to easily form agglomerates, probably due to the hygroscopicity of the HPC after the drying. The potential moisture uptake of HPC from the surrounding environment is a key parameter in the long-term physical and chemical stability [67]. That is why relative humidity (RH) of the room air was also one of the parameters recorded during the SASD assays.

3.2.1. Process Yield and Solid-State Characterization

SASD allowed to recover up to 66 % of initial solids content from the feed solution. It was noticed that some losses occur at the internal walls of the precipitator chamber, possible due to the static electricity of the powder after the atomization, that typically occur in spray drying processes. This can also be one of the factors that affects the yield of the process.

Table 3.1 – Process yield and physicochemical characteristics of the HPC powders produced by SASD.

HPC (%w/v)	**Yield, ɳ (%)**	**$D_{v,50}$ (µm)**	**span**	**Moisture Content (%H_2O/g_{powder})**	**a_{BET} (m^2/g)**	**SEM (shape/ surface)**	**XRPD (solid-state)**
2.5	34	20.24	1.39	n.a.*	1.95	n.a.	Amorphous
5.0	66	19.95	1.44	4.3 ± 0.6	2.62	n.a.	Amorphous
7.5	49	18.26	1.52	4.6 ± 0.4	2.08	Irregular/ smooth	Amorphous
Raw	n.a.	n.a.	n.a.	2.5 ± 0.4	0.80	n.a.	Amorphous

* Test not performed due to the insufficient powder amount required for the characterization; n.a. = not available.

As it is shown in Table 3.1, microparticles with geometric particle size in the range of 18 to 20 µm were produced. The higher the HPC concentration in the liquid feed solution, the lower the particle size is obtained, which shows that the concentration influences the particle size and particle size distribution. This tendency is not normally observed, since more concentrated solutions have higher viscosity and induce the formation of larger droplets in the atomization step. According to the results, formulations prepared with lower content of solids lead to a more homogeneous particle size distribution (lower span values).

According to the images obtained by the analysis of Morphologi G3 (Figure 3.2), there was a good dispersion of the particles. At the higher magnification, some larger particles appear to be the conjugation of two or three particles, with the formation of some aggregates.

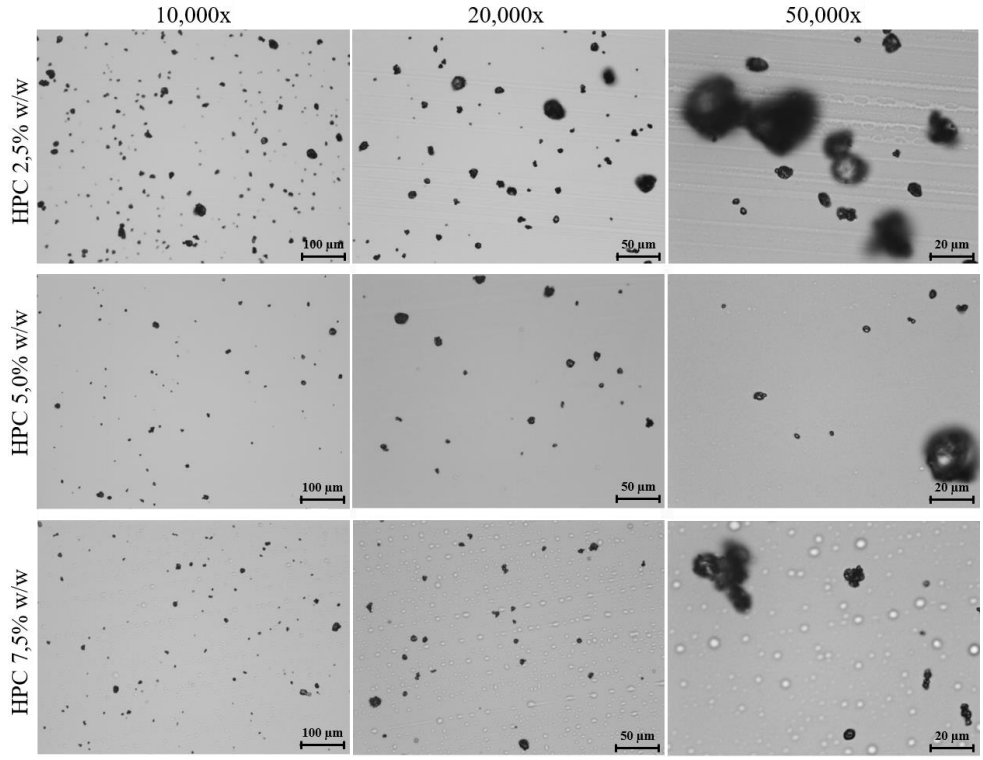

Figure 3.2 – Morphologi G3 images of the DPFs microparticles with 2.5, 5.0 and 7.5 %w/v of HPC at different image magnifications: 10,000×, 20,000× and 50,000×.

The SEM micrographs of the DPF with the higher solid concentration present in Figure 3.3 show that the morphology of the microparticles appears to have an irregular but slightly smooth surface, with the larger particles approaching a more rounded surface. These images clearly show the number of aggregates formed, with the smallest particles surrounding the larger ones.

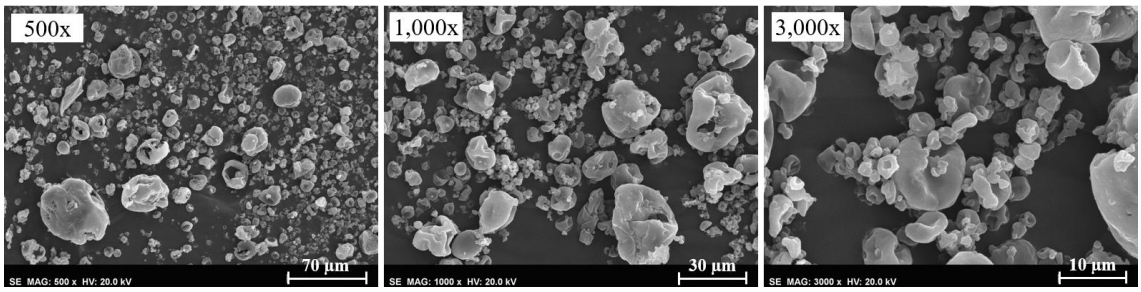

Figure 3.3 – SEM images of HPC microparticles with 7.5 %w/v of HPC at 500×, 1,000× and 3,000× magnifications.

The moisture content percentage (Table 3.1) of the SASD processed HPC was not even 5 % H_2O per gram of powder. A slightly higher percentage was detected for the unprocessed HPC. These percentage values are in line with what was expected by the literature of the HPC [67]. One

reason for the increased moisture content in the processed HPC powder, compared to the raw HPC may be due to the incomplete drying.

The solid-state characterization for both unprocessed and SASD processed HPC was realized to assess if SASD has some direct effects in the structure of the polymer. According to the XRPD analysis diffractograms (Figure 3.4), both non-processed HPC and processed HPC exhibited two peaks at about 8 º and 20 º, indicating that this polymer has an amorphous domain. Diffractograms obtained by Rahman et al. [153] also confirm the same peaks for the non-processed HPC. The HPC powder processed with different concentrations depicts the same peaks, however, it can be noticed that the intensity of the peaks is slightly lower for the SASD processed HPC. In similar results reported in the literature, in addition to these two broad peaks, a few small crystalline peaks were observed between 29–47 º [164].

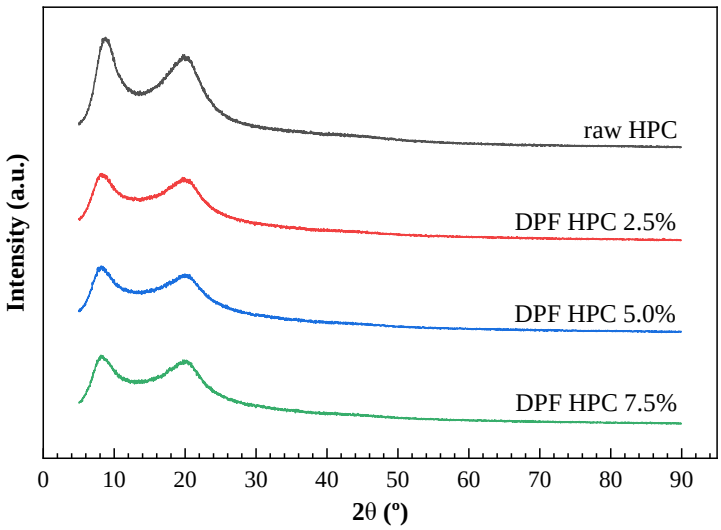

Figure 3.4 – XRPD diffraction spectra of raw HPC powder and DPFs with 2.5, 5.0 and 7.5 %w/v HPC.

According to the DSC thermogram of raw HPC present in Figure 3.5, the Run 1 shows a broad endothermic peak between 25 and 100 ºC associated to the water evaporation from the sample. In the Run 2, it was detected a small endothermic peak around 190–200 ºC, also reported by Rahman et al. [153]. This peak is probably the fusion of the small crystalline fraction of largely amorphous HPC or a liquid crystal isotropic transition [76,165]. This low crystallinity was not detected before by XRPD.

A low glass transition temperature in the range of -20 to 0 ºC was expected for this polymer according to Sarode et al. [76], but from the thermogram reported below this was not detected. Cellulose ethers usually show a glass transition of low intensity and the associated change in heat

capacity is too small to be detected using conventional DSC [72]. Different transitions values were reported in the literature for HPC at 19, 25, 30 and 124 ºC [76,165].

It is likely that the reticulated morphology of the structure of this cellulose ether makes it difficult to determine the T_g value. The different degrees of substitution that the HPC may have also could explain that there is no common behavior for the transition of this polymer.

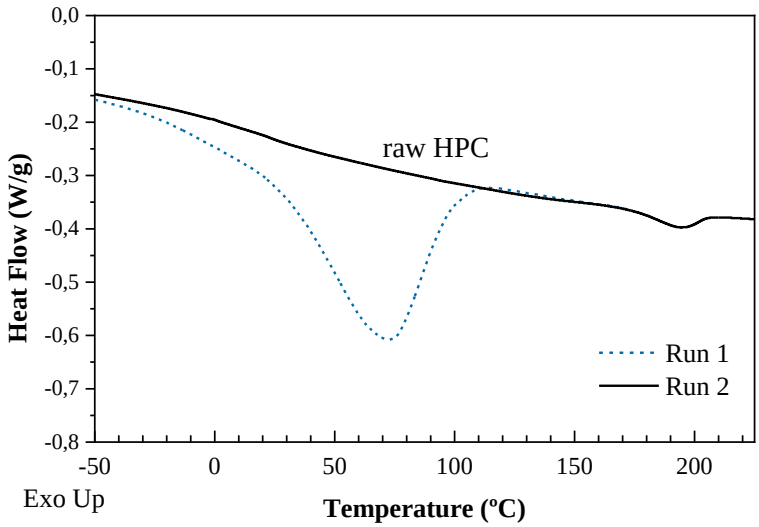

Figure 3.5 – DSC thermogram of unprocessed HPC (raw).

ATR-FTIR analysis was used to evaluate the composition of the powder and compare the processed HPC powder spectra with the native HPC powder spectrum. Figure 3.6 shows that the spectra of the processed HPC and the spectrum of the unprocessed HPC are coincident. This means that all DPFs after being processed by SASD maintained the same composition and chemical structure as the unprocessed HPC.

The FTIR spectrum depicts four main absorption bands for HPC: at 3400 cm^{-1}, corresponding to O–H stretching vibration of the hydroxyl groups in the pyranose unit; at 2900 cm^{-1}, assigned to the C–H stretching vibration band; at 1330–1450 cm^{-1}, corresponding to the O–H, C–H bending and $–CH_2$ deformation bands; and at 1100 cm^{-1}, C–O stretching vibration of the ether bond [166–168].

According to Varshosaz and Ghassami [169], the most important characteristic peak of the HPC is the ether bond of C–O at about 1000 cm^{-1}. On the one hand, the OH groups can act as hydrogen bond donors, on the other hand, the ether groups of HPC might act as hydrogen bond acceptors [170].

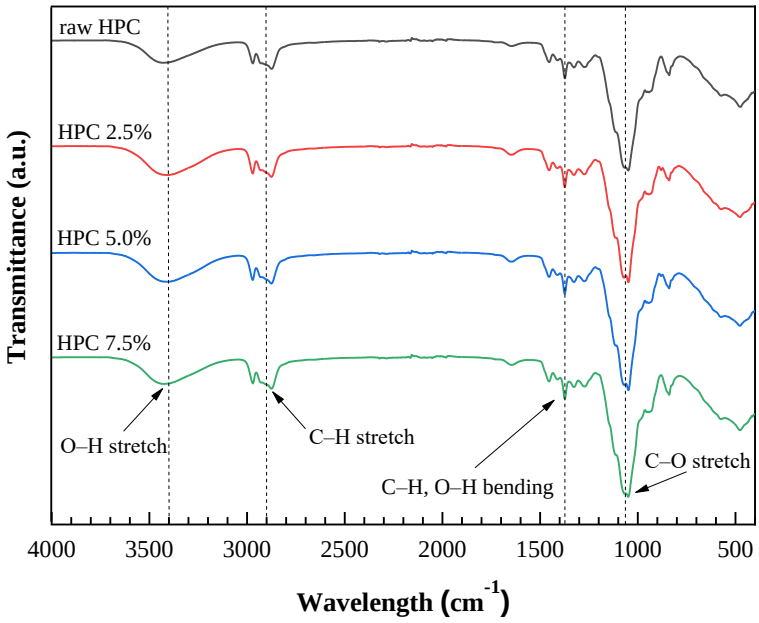

Figure 3.6 – FTIR spectra of unprocessed HPC (raw) and SASD processed HPC formulated with 2.5, 5.0, and 7.5 %w/v of solids content.

Aerodynamic performance tests were performed for the 5.0 and 7.5 %w/v DPFs to understand how their deposition distribution would be over the eight stages of the Andersen Cascade Impactor (ACI). These tests also aimed to assess whether the administration by inhalation of these powders, in a first phase containing only the polymer, was viable. The mass distribution of the powder trapped in each stage (see Appendix D) since it was released by the capsule, reveals that it was mostly retained in the induction port (i.p.). The sticky properties of the HPC may be a strong reason to explain the adhesion of the particles in the upper airways that simulates the respiratory tract.

It is possible to verify according to the results obtained (Table 3.2) that low values for fine particle fraction (FPF) were obtained, which means that only a small percentage of the DPF would reach the deep lung. The mass median aerodynamic diameter (MMAD) of the microparticles is similar for both analyzed DFPs.

Table 3.2 – Aerodynamic properties of SASD process powders determined by ACI.

Sample	MMAD (µm)	FPF (%)	GSD
HPC 2.5 %w/v	n.a.	n.a.	n.a.
HPC 5.0 %w/v	4.3	18.4	2.1
HPC 7.5 %w/v	5.0	15.1	1.8

3.3. Co-atomization with bioactive compounds

After preliminary tests, the phenolic compound was now processed along with HPC in a bioactive/excipient ratio of 1:99 w/w. In order to complement this study a Design of Experiments (DoE) approach was applied in two formulation parameters. The DPFs obtained were also subjected to a solid-state characterization, as well as bioactivity and release tests in an aqueous media.

3.3.1. Statistical Analysis

A 3^2 full factorial DoE was performed in which all combinations of factor levels were tested, two by two. The solids content and ethanol volume in the initial formulation were the variables selected, while the process yield, particle size, span and encapsulation efficiency were adopted as response variables.

Through the Analysis of Variance (ANOVA) table, it is possible to identify, for a significance level less than 5 % ($p < 0.05$), which are the significant effects of the factors for each of the studied response variables. In this case, as the factors are studied at three levels, these should be studied in the linear and quadratic components: if there is a significant effect on the linear component, it is expected that the best response to the factor is at the high (+1) or low (-1) level; a significant effect in the quadratic component means that the best response is at the intermediate level (0).

Before studying the factors, it is also important to clarify that for the process yield and encapsulation efficiency it is intended to maximize the response whereas for the particle size and the span it is intended to minimize the response. Regarding RSV-DPFs, Table 3.3 shows the results obtained for the different responses according to the factors studied.

Table 3.3 – SASD processed RSV-DPFs results following the 3^2 full factorial design.

Exp. No.	C_solids (%w/v)	V_ethanol (%v/v)	Yield (%)	EE (%)	$D_{v,50}$ (µm)	span
1	2.5	20	49 ± 22	76 ± 1	24 ± 4	1.39 ± 0.06
2	2.5	45	44 ± 6	82 ± 12	22 ± 4	2.2 ± 0.3
3	2.5	70	53 ± 9	91 ± 2	28 ± 4	1.59 ± 0.05
4	5.0	20	53 ± 11	74 ± 8	19.64 ± 0.04	1.34 ± 0.03
5	5.0	45	55 ± 12	100 ± 2	18 ± 3	2.2 ± 0.4
6	5.0	70	36 ± 21	100*	19.6 ± 0.6	1.8 ± 0.4
7	7.5	20	56 ± 2	88 ± 6	20 ± 1	1.33 ± 0.04
8	7.5	45	51.5 ± 0.5	100*	15.6 ± 0.3	1.99 ± 0.02
9	7.5	70	72 ± 2	100*	15 ± 1	2.8 ± 0.2

* value considered when the average value of EE > 100%.

Figure 3.7 shows the representation of the response surfaces obtained from ANOVA tables corresponding to the RSV-DPFs (Appendix E). The effects of both factors in the study of each response are described below.

- **Yield**: both C_solids and V_ethanol variables show no statistical significance ($p > 0.05$) regarding the final process yield for the RSV-DPFs;
- **Encapsulation Efficiency (EE)**: both parameters indicate a significant effect on the linear component. EE increases with the increase of both variables, C_solids and V_ethanol;
- **Particle Size ($D_{v,50}$)**: C_solids variable exhibits significant effect in the volumetric diameter of the microparticles, in the linear component. Higher solid concentrations in the solution to be atomized yield smaller particles, regardless of the ethanol volume, contrary to what was expected.
- **Span**: the width of particle size distribution is affected with significance by the V_ethanol variable, while the C_solids variable shows only a slight decrease in the span values, although with no level of significance. Thus, the V_ethanol variable shows a significant effect in both linear and quadratic components. Lower span values are obtained when low and high levels are applied to the solution to be atomized., regardless of the solids content. There is also a certain level of significance in the interaction of the linear components of both C_solids and V_ethanol variables, easily observed in the response surface below.

a)

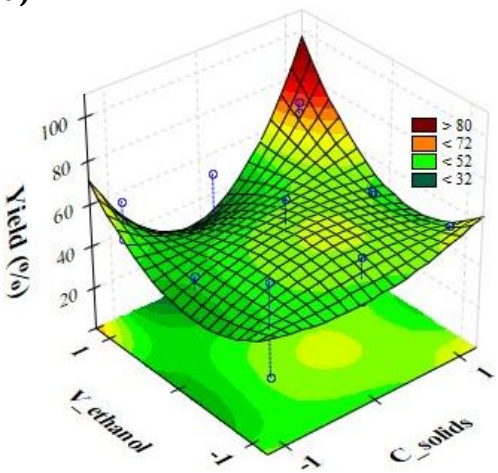

b)

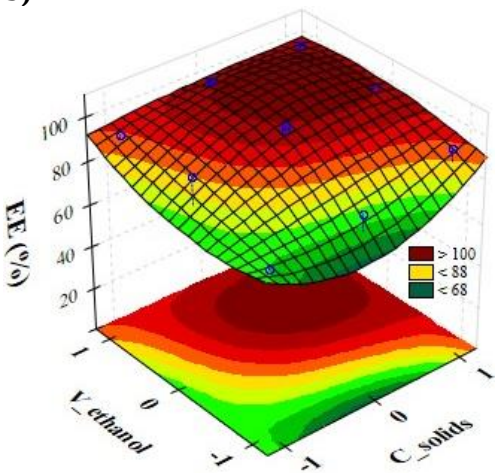

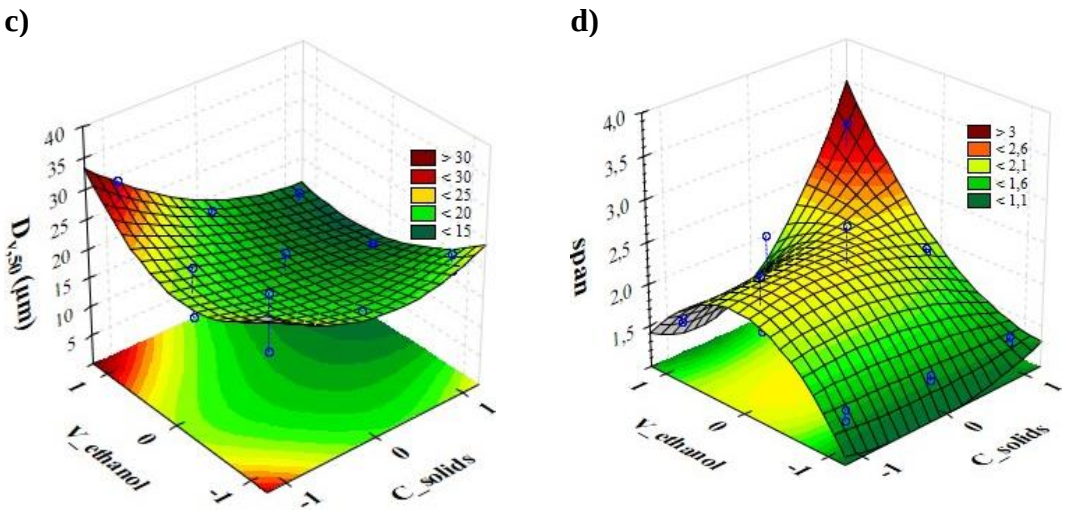

Figure 3.7 – Fitted surface plots from ANOVA for each response (RSV-DPFs): a) process yield, b) encapsulation efficiency, c) particle size ($D_{v,50}$) and d) span.

For the GA-DPFs, the results of the studied variables are shown in Table 3.4.

Table 3.4 – SASD processed GA-DPFs results following the 3^2 full factorial design.

Exp. No.	C_solids (%w/v)	V_ethanol (%v/v)	Yield (%)	EE (%)	$D_{v,50}$ (µm)	span
1	2.5	20	42.5 ± 0.5	48 ± 4	22 ± 2	1.37 ± 0.08
2	2.5	45	21 ± 5	100*	26 ± 8	2.0 ± 0.8
3	2.5	70	59 ± 4	88 ± 11	30 ± 1	1.8 ± 0.1
4	5.0	20	55 ± 3	65 ± 7	22 ± 4	1.5 ± 0.2
5	5.0	45	41 ± 15	94 ± 6	18 ± 4	2.2 ± 0.8
6	5.0	70	58 ± 2	100*	23 ± 2	2.0 ± 0.2
7	7.5	20	51 ± 3	78 ± 7	21 ± 1	1.34 ± 0.02
8	7.5	45	58 ± 5	100*	14 ± 2	2.3 ± 0.2
9	7.5	70	61 ± 2	96 ± 3	16 ± 2	1.9 ±0.2

* value considered when the average value of EE > 100%.

Response surfaces from ANOVA tables corresponding to the GA-DPFs (Appendix E), are represented in Figure 3.8. The effects of both factors in the study of each response are described below.

- **Yield**: a high significance level affecting the process yield is noticeable in the quadratic component for the V_ethanol variable. Lower yields are obtained when the ethanol volume is at the intermediate level. The C_solids variable shows a significant effect on the yield in the linear component. There is also a significant effect on the interaction of the linear component of C_solids with the quadratic component of V_ethanol.

- **Encapsulation Efficiency (EE)**: both variables indicate a statistical significance in the EE. Increasing the C_solids shows a linear increase of the EE while a variation in the V_ethanol from 20 %v/v to higher volumes is shown to have a greater effect on the linear component, although the quadratic component also affects EE;
- **Particle Size ($D_{v,50}$)**: as for the RSV-DPFs, the C_solids variable indicates a high significance level for the volumetric diameter of the microparticles of GA-DPFs, in the linear component. Higher concentrations in the solution to be atomized lead to smaller particles;
- **Span**: The ethanol volume proves to be a significant factor in the quadratic component, as can be clearly seen in the corresponding response surface.

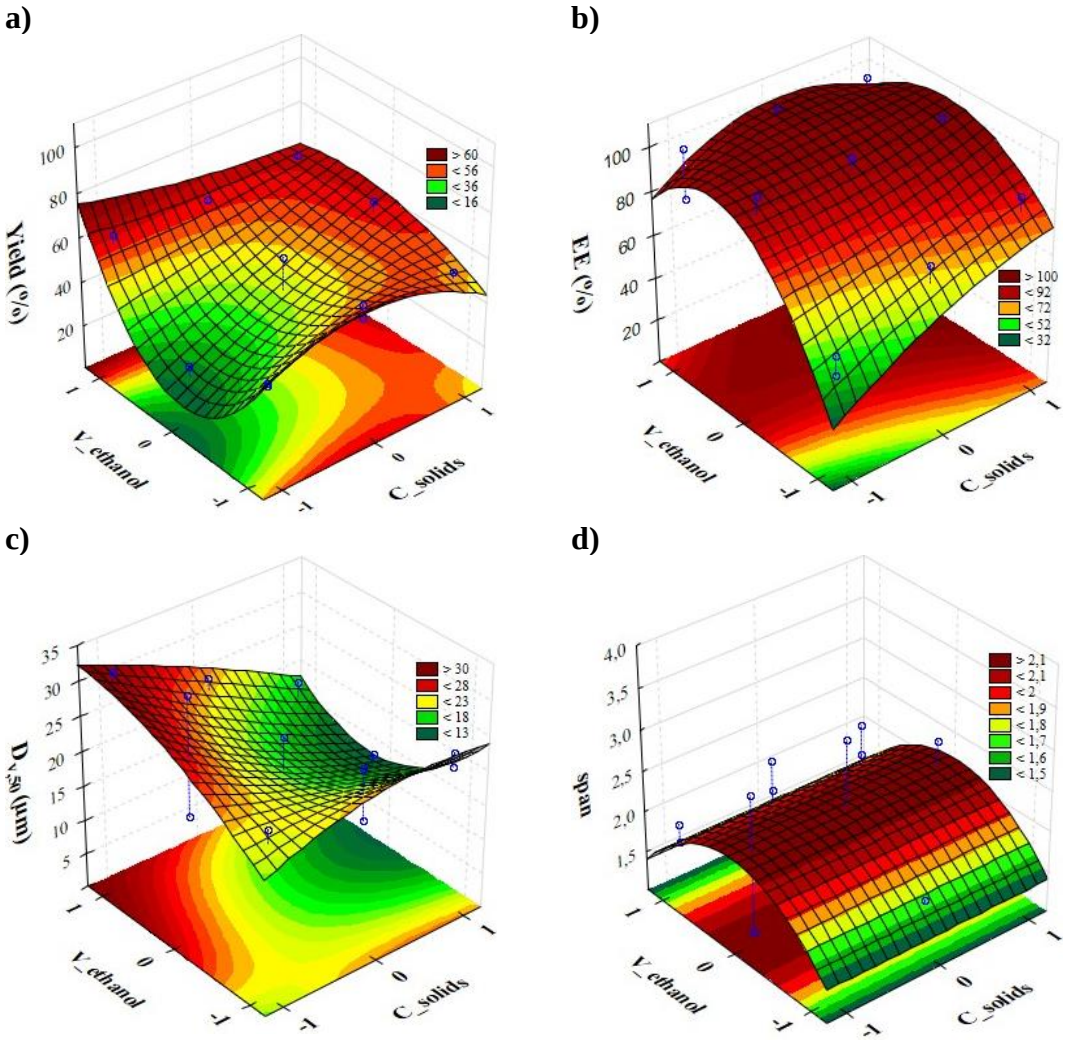

Figure 3.8 – Fitted surface plots from ANOVA for each response (GA-DPFs): a) process yield, b) encapsulation efficiency, c) particle size ($D_{v,50}$) and d) span.

The analysis of variance is completed with the validation of the assumptions, namely, the normality of the residues, homogeneity of the variance, and the independence of the residues (Appendix E).

3.3.2. Process Yield and Encapsulation Efficiency

The yields obtained from the process lead us to believe that the process has some discrepancies in the reproducibility of the process as observed in Figure 3.9. This appears to be more evident for RSV-DPFs, while GA-DPFs had a more consistent reproducibility. Overall, process yields ranged from 40 to 70 %. Some values below this range were obtained, due to several factors that unexpectedly influenced the performance of the SASD. Among these are blockage of the nozzle or even rupture of the nozzle's O-ring which has often led to the stoppage and retake of the process. The amount of powder that was sometimes retained on the inner wall of the precipitator chamber and cyclone (still recoverable from the latter) may also have influenced yield losses.

Similar process yield were reported by Aliakbarian et al. [133] in processing a phenolic ethanol:water extract using SAA, with powder recoveries of up to 65 %. The solids content was also studied, with no trend found in the final yield of the process. Moura et al. [149] also achieved yields in the range of 54–70% using the same SASD apparatus, showing that the yields obtained in this work are typical expected results.

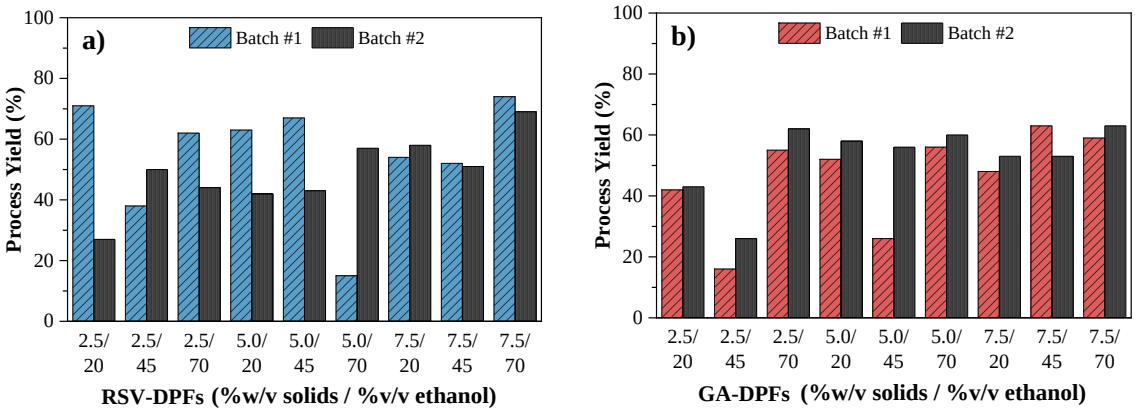

Figure 3.9 – Process yields of Batch #1 and #2 (replicates) for a) RSV-DPFs and b) GA-DPFs.

One of the greatest indication that a process performed an efficient co-atomization is the percentage of the bioactive compound that has been encapsulated. Encapsulation efficiencies (EE) up to 100 % were achieved from both RSV-DPF and GA-DPFs. The results in Table 3.3 and Table 3.4 suggest that the phenolic loading is higher for a content of solids in the solution to be atomized above 2.5 %w/v and ethanol volumes above 45 %v/v.

As expected, the increase of the concentration of solids, composed mostly by HPC, creates more viscous solutions due to the nature of this polymer. When dissolved in a water:ethanol liquid system, the sticky texture of the solution might enhance the entrapment efficiency of the compound [169]. As reported in the literature, similar encapsulation efficiencies values (around 95%) were achieved using HPC as carrier to encapsulate poorly water soluble drugs by conventional spray drying [169].

Generally, when atomization and drying of droplets occurs, the components tend to separate from each other due to diffusion factors. The rapid evaporation of the solvent can be a primary factor in the encapsulation of the phenolic compounds. Due to its hydrophobic nature, it is likely that they tend to go more towards the center of the droplet. HPC, being a hydrophilic molecule, tends to be more on the surface in contact with the aqueous medium and to start the coating of the phenolic. In addition, as it is on the particles surface that the solvent evaporates first, the molecules become more concentrated in the outermost layer of the particle. Therefore, as the molecules tend to balance their concentration across the particle, there is a concentration gradient that makes the small molecules tend to diffuse inwards. As HPC has a high molecular weight, its molecules have a lower diffusion velocity and preferably stay more in the outer layer of the particle, making the coating. In contrast, RSV and GA molecules, with a lower molecular weight, have higher diffusion coefficients and therefore are more easily located inside the particle.

In some cases, it is noticed that the EE exceeds 100 %. The reasons for this to happen may be due merely to error in the quantification assays. In this way, the sample sent for analysis could have a higher concentration of compound than what was expected (0.01 g phenolic per g sample).

3.3.3. Particle Size and Particle Size Distribution

For RSV-DPFs, the mean particle volumetric diameter for 50 % of the population ($D_{v,50}$) ranged from 15 µm to 28 µm, for the solutions with the highest and lowest concentration, respectively. In the GA-DPFs, the same trend was followed, with particles with a mean volumetric diameter of approximately 13 and 30 µm.

Regarding the span, the closer the value is to 1, the narrower the range of particle size distribution and therefore the more homogeneous is the population. Span values closer between 1.33–1.53 were obtained for both RSV-DPF and GA-DPFs. It is observed that span values closer to 1 were obtained when the ethanol volume in solution is the lowest and higher when ethanol volume of 45 %v/v are used. Overall, a narrow size distribution is obtained for all DPFs.

3.3.4. Particles Morphology

Scanning electron microscopy (SEM) analysis was used to evaluate the morphology and particle size of the bioactive compounds in their native form and after being processed along with HPC to form the dry powder formulations. In Figure 3.10, it is possible to see the crystalline form of both raw GA and raw RSV. The morphology of raw GA exhibits uniform rods crystals with a broad particle size distribution whereas raw RSV exhibits a geometric crystallized shape with a particle diameter of 0.1–30 µm.

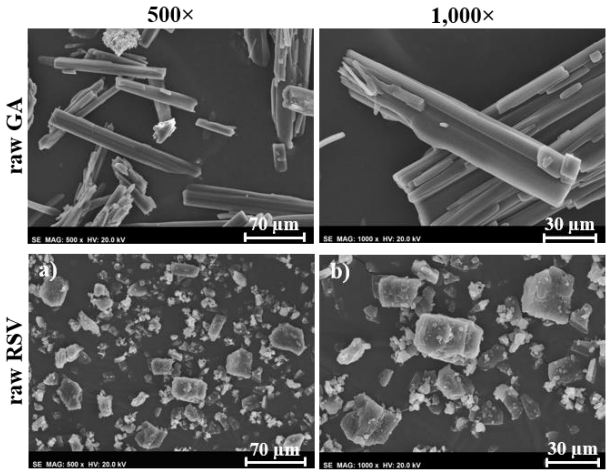

Figure 3.10 – SEM images of raw GA and raw RSV at 500× and 1,000× magnifications.

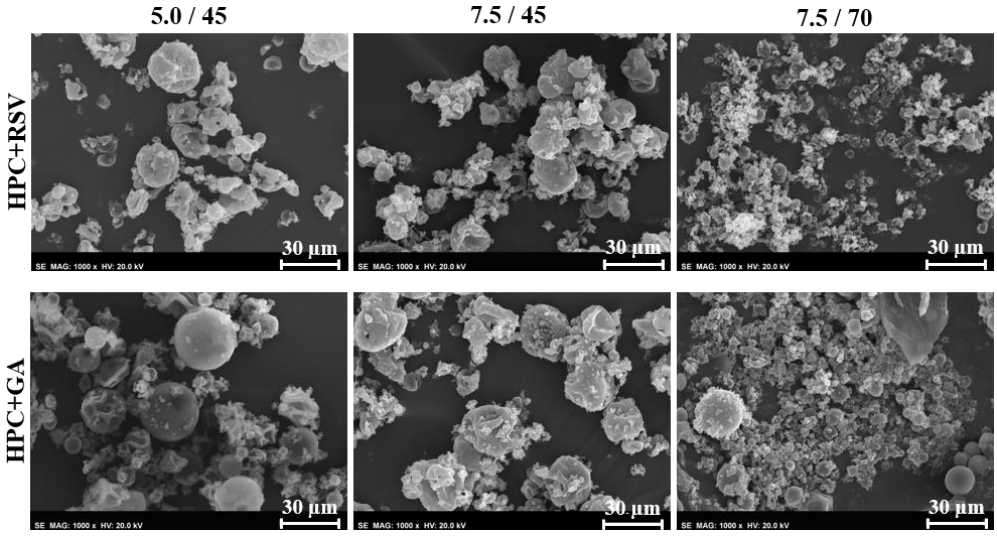

Figure 3.11 – SEM images of both HPC/RSV and HPC/GA dry powder formulations with 5.0 and 7.5 %w/v of solids and 45 and 70 %v/v of ethanol at 1,000× magnification.

Regarding the morphology of the SASD processed microparticles of RSV-DPF and GA-DPF (Figure 3.11), a broad particle size distribution and particles agglomerates for all the three powders analyzed were observed. These have an analogous morphology as the HPC processed microparticles obtained in the preliminary studies, with a wrinkled surface. This can be the result of a rapid evaporation of the solvents during the decompressive atomization. The formation of agglomerates may be on account of the electrostatic and Van der Waals forces that the molecules of HPC present, due to the high carbohydrate content. Furthermore, microparticles with smaller dimensions have a rounded irregular shape while microparticles with larger dimensions have a spherical shape with a smoother surface.

For both 7.5 %w/v HPC/RSV and HPC/GA microparticles, it can be seen that the increase in the volume of ethanol in the formulation from 45 to 70 %v/v leads to a smaller particle size distribution. There are no significant differences in the size distribution, varying only the concentration of solids. This can be confirmed not only by the results obtained for the size and distribution of the particles, but also by the conclusions of the analysis of variance. These results confirm the encapsulation of both antioxidants by the HPC.

3.3.5. BET Specific Surface Area

The bioavailability of a model substance or drug of a DPF is relied on the particle's morphology and surface. Knowing the specific surface area of the co-atomized powders can be useful to predict the dissolution rate, since the higher the specific surface area, the higher will be the dissolution rate [171].

According to the BET isotherms (see Appendix C), both DPFs represent a material with residual adsorption and similar to type II isotherm. Hence, this isotherm is representative of a low or non-porous material and, if there are pores, these will be macropores. The vertical slope at the end of the isotherm may indicate macroporosity, but this must be confirmed by MIP (mercury intrusion porosimetry). However, considering the residual volume of nitrogen adsorption and the absence a of defined hysteresis, this effect can also be some adsorption in the inter-particular space and not in the pores. The gradual curvature (or "knee") represented by point B indicates the monolayer coverage and the onset of multilayer adsorption. The ordinate of point B indicates an estimate of the amount of adsorbate needed to form a monolayer and from which the multilayers begin to form at higher relative pressures [172].

As shown in Table 3.5, RSV-DPF and GA-DPF have specific surface areas of 4.2 and 2.0 m^2/g, respectively. The material has a very low area regarding the technique resolution (< 5.0 m^2/g) and therefore, these values are merely estimates and unreliable. These values are in line

with the specific surface area values of the HPC microparticles produced by SASD with different solid contents (1.95–2.6 m^2/g).

Table 3.5 – Specific surface area (m^2/g) of both raw phenolics and respective RSV-DPF and GA-DPFs.

Sample	BET Specific Surface area (m^2/g)
raw RSV	2.19
raw GA	1.25
RSV-DPF	4.20
GA-DPF	2.04

3.3.6. Moisture Content

The results obtained with the Karl Fisher (Table 3.6) showed that the residual moisture content of the dry powders produced after the co-atomization of HPC/RSV and HPC/GA was in the range of 2.5–3.0 $\%H_2O/g_{powder}$, thus indicating good drying efficiency of the SASD process. Different water/ethanol ratios used in the formulations seemed not have any effect on the final moisture content. These values were expected, but slightly lower, according to the results obtained previously with HPC in the preliminary studies. Small differences in moisture content can be influenced by small variations in the flow rate of the compressed drying air. Water uptake from the produced DPFs tends to increase when the RH conditions of the surrounding air are higher [67,74]. The recorded humidity values can be found in Appendix A.

In a study reported in the literature, the particles obtained for the encapsulation of phenolic compounds within maltodextrin presented a moisture content of 3.1–5.6 %w/w, using the SASD (SAA) process [135].

Table 3.6 – Moisture content of DPFs obtained by SASD with different water/ethanol ratios in the initial solutions. Results were expressed in percentage of water per gram of powder ($\%H_2O/g_{powder}$).

DPF sample	Ratio water/ethanol (v/v)	Moisture Content ($\%H_2O/g_{powder}$)
RSV-DPF (7.5% w/v)	80:20	2.9 ± 0.1
	55:45	3.04 ± 0.07
	30:70	2.9 ± 0.8
GA-DPF (7.5% w/v)	80:20	2.8 ± 0.1
	55:45	2.9 ± 0.1
	30:70	2.5 ± 0.1

3.3.7. X-Ray Powder Diffraction

The XRPD was employed to determine the physical state of raw phenolic compounds, as well as the physical state of PMs and DPFs of HPC/RSV and HPC/GA. The diffractograms for both studied systems are shown in Figure 3.12. Unprocessed RSV depicts many diffraction sharp peaks at approximately 2θ = 6º, 16º, 19º, 22º, 23.5º and 28º, whereas unprocessed GA depicts the main sharp peaks at approximately 2θ = 8º, 12º, 16º and 19º. Their diffraction patterns confirm the crystalline state of both raw compounds. The RSV and GA patterns are in concordance with the literature [141,173].

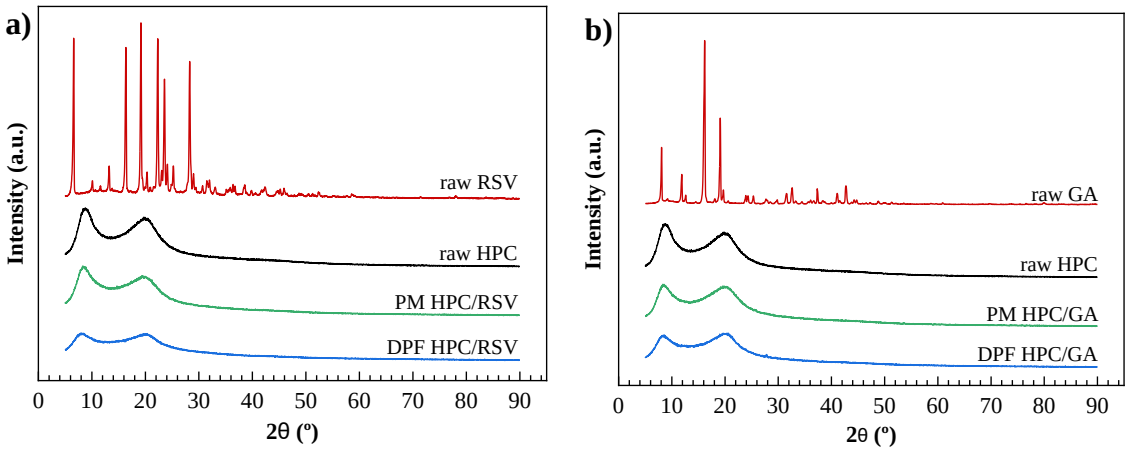

Figure 3.12 – PXRD diffractograms of a) HPC/RSV and b) HPC/GA systems.

Given the high polymer/compound ratio (99:1 w/w), the PM resulting from both phenolics with HPC does not present any characteristic peaks of crystalline RSV or GA. Co-atomized powders are amorphous, possibly indicating that both RSV and GA are molecularly dispersed in the polymeric matrix. Thus, it was possible to obtain solid amorphous dispersions with approximately 1 % of bioactive substance using SASD technology.

3.3.8. DSC

DSC was performed to evaluate potential thermal behavior changes in the SASD powders and also in the respective physical mixtures. DSC thermograms of both systems studied are reported in Figure 3.13. Run 1 was not represented graphically because it meets the profile already represented in the preliminary studies and explained by the removal of the residual water.

The thermal profiles of the DPFs and PMs for both HPC/RSV and HPC/GA systems are identical to those of the raw HPC. All thermograms show a reproducible endothermic peak around 190–200 ºC related to the melting point of the small crystalline domain of HPC, as previously

discussed in the preliminary studies. This means that the melting temperature of the HPC processed by SASD was not affected in the presence of the phenolic compound.

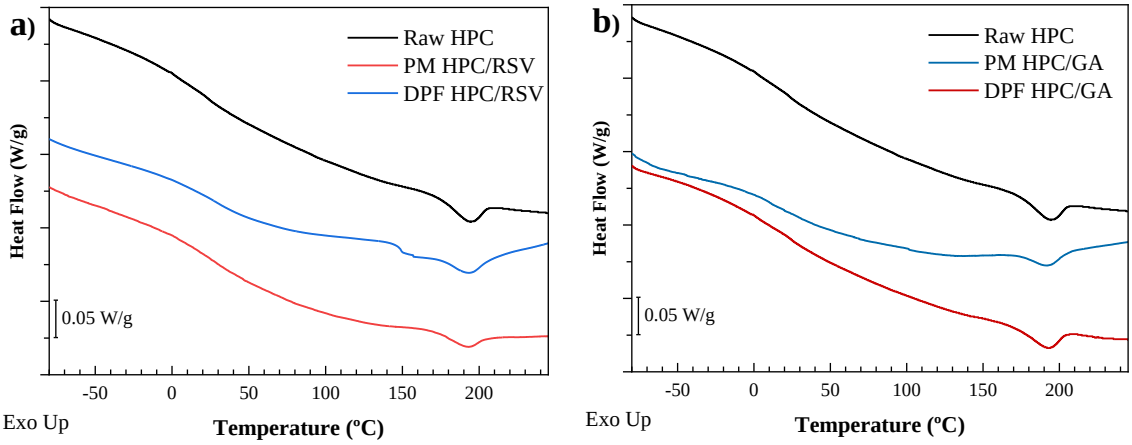

Figure 3.13 – DSC thermograms (Run 2) for a) HPC/RSV and b) HPC/GA systems.

The sharp peaks of melting respective to crystalline phenolic compounds (RSV and GA) reported in the literature usually appear in the range of 250–270 ºC [60,174]. As the DSC equipment was not calibrated to testing the samples at temperatures above 250 ºC, it was not possible to observe any attainable change in the thermal profile of the PMs or DPFs. Only thermograms performed up to about 280 ºC exclusively for each of the pure phenolic compounds are present in the Appendix F. If an endothermic melting event occurred in the thermal profile close to the melting temperature of each phenolic compound, it would indicate that it was encapsulated in its crystalline state. On the other hand, if such behavior was not observed, it is likely that the phenolic was encapsulated in its amorphous state or molecularly dispersed in the structure of the HPC [60], owing to the high content (~99.9 %w/w) of amorphous HPC in the PMs and DPFs.

3.3.9. ATR-FTIR

Figure 3.14 shows an overlapping of the ATR-FTIR spectra of the raw compounds, physical mixtures (PM) and DPFs, for both HPC/RSV and HPC/GA systems, respectively. Regarding the wavelength signals of both antioxidant compounds, it was shown a broad peak present around 3200 cm^{-1} associated with the phenolic hydroxyl bonds (O–H stretch). The RSV spectrum shows its characteristic absorption bands: at 1600, corresponding to the stretching of C=C bond of the aromatic ring; at 1580 cm^{-1} assigned to the stretching of the C=C olefinic bond; at 1380 cm^{-1} relative to the O–H bending; at 1143 cm^{-1}, confirming the C–O stretching for phenolic compounds; at 965 cm^{-1}, confirming the alkene (=C–H bending) of the *trans*- form of the RSV; at 828

cm^{-1}, with respect to the =C–H vibration bands of arene conjugated to the olefinic group; and the deformation bands at 671–500 cm^{-1}, corresponding to the =C–H of the olefinic group.

The GA spectrum shows its characteristic absorption bands: at 1690 cm^{-1}, corresponding to the stretching of C=O bonds of the carboxylic acid; at 1610, 1533, and 1440 cm^{-1}, typical of the stretching vibrations of C=C bonds of the aromatic ring; at 1300–1200 cm^{-1} range assigned to the CO–OH stretching and bending, indicating the combination of O−C–C asymmetric stretching and the OH bending; and at 1020 cm^{-1}, related to the C–O stretching. These results were in agreement with the literature for both phenolic compounds [157,175,176].

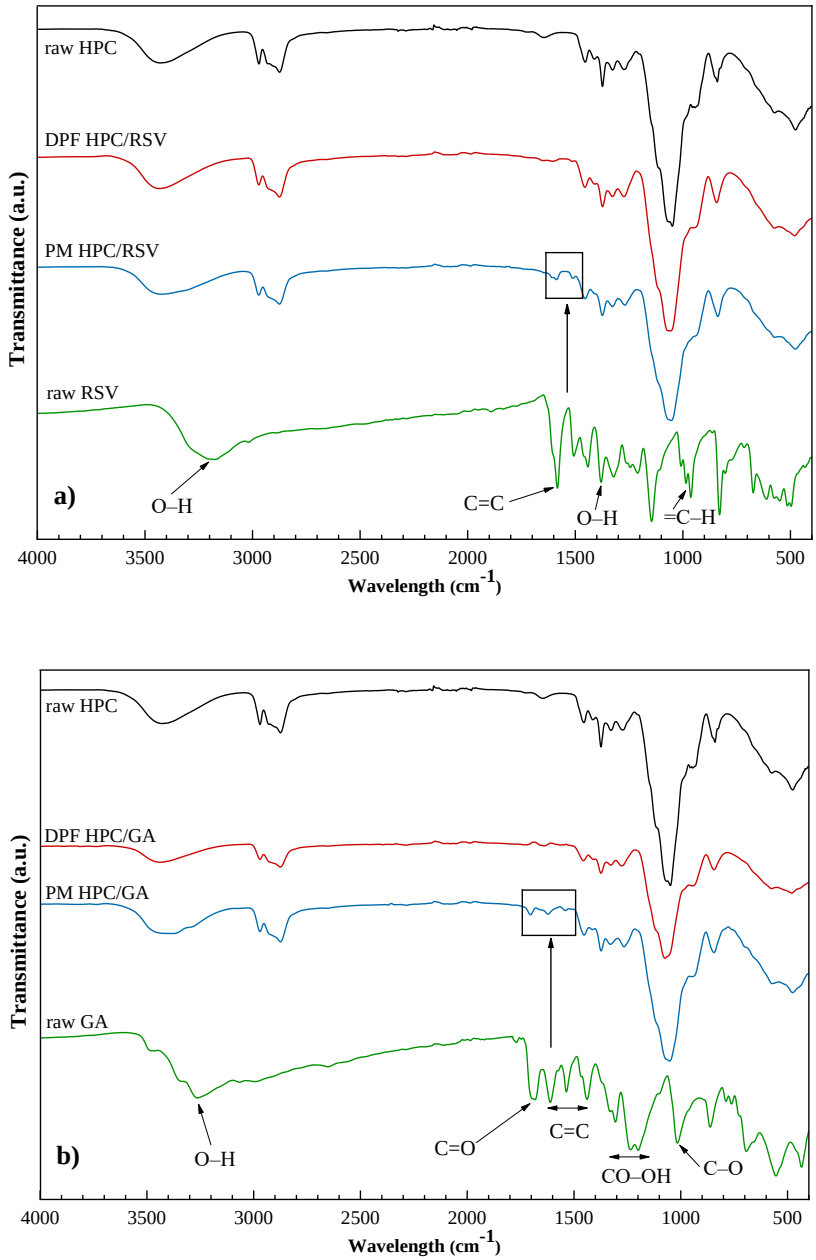

Figure 3.14 – ATR-FTIR spectra for the a) HPC/RSV and b) HPC/GA systems.

Taking special attention to the low-intensity bands observed at 1589 and 1500 cm^{-1} for RSV-PM and at 1703, 1618 and 1540 cm^{-1} for GA-PM, it appears that these are not so evident in the raw HPC spectrum. The correspondent peaks of these bands are more characteristic of the raw RSV and GA and therefore, may show a discreet presence of their functional groups in these bands. The DPF samples presented a similar spectra to unprocessed and processed HPC (in the preliminary studies), suggesting that the compounds are probably not detected on the surface of the particles.

3.4. Antioxidant Activity

Antioxidant activity tests were performed in order to assess whether the RSV or GA co-atomized with HPC by SASD maintained their ability to eliminate DPPH free radicals, using both bioactive compounds in their pure form as reference. Three SASD powders, considered the best in encapsulation efficiency, were selected for this study. After 30 minutes since the DPPH• solution was added to the compound solution it was expected a degree of discoloration from a deep violet hue to a more yellowish hue, which indicates the scavenging potential of the antioxidant compounds. In other words, the free radical DPPH• in the reaction solution is reduced to its non-radical form (DPPH•-H).

For tests performed with RSV, it was possible to verify, according to Figure 3.15, that the color changes as the RSV concentration in each solution increases. The intensity of the violet color gradually reaches a yellow-golden hue from the last two concentrations.

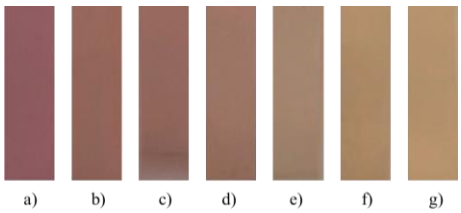

Figure 3.15 – Color of the reaction solution after 30 minutes, at different RSV concentrations: a) 100, b) 400, c) 800, d) 1200, e) 1500, f) 1800 and g) 2100 µM.

Figure 3.16 shows the percentage of DPPH radical scavenging plotted as a function of RSV concentration. From this, it can be noticed that all the processed DPFs have a slightly lower antioxidant activity compared to the raw RSV. Among these, the two RSV-DPFs with higher solid content, namely RSV/7.5/20 and RSV/7.5/70, exhibit greater antioxidant activity compared to DPFs with lower solids content. This certainly indicates that a higher RSV concentration in the initial SASD feed formulation increases the antioxidant capacity of the final DPF. At

concentrations reaching 2000 µM, the curve tends to have a stabilizing behavior for all samples, meaning that the antioxidant power of RSV is running out, as it presents itself as a limiting reagent.

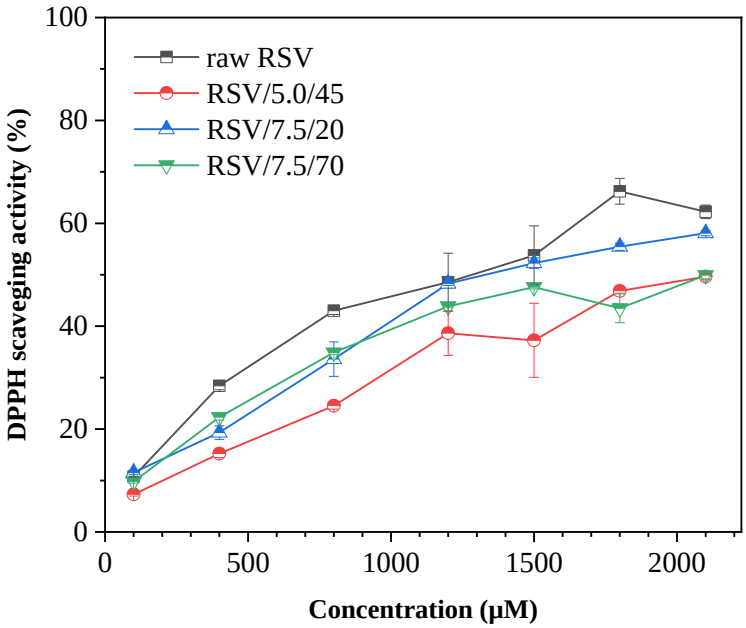

Figure 3.16 – Antioxidant activity of unprocessed RSV and SASD processed formulations with RSV.

The effective concentration (EC_{50}) represents the minimum required concentration of the antioxidant allowing the inhibition of DPPH free radical activity by 50 %. According to the method described by Alexander et al. [158], some considerations were taken for its application: 1) that the highest response point obtained corresponds to 100 % of the inhibition; 2) that the two real recorded responses, where the 50 % maximal response is inserted, must form a straight line.

The EC_{50} values obtained in the tests with RSV are summarized in Table 3.7. A lower EC_{50} value indicates a higher free radical scavenging activity of the antioxidant compound. All the DPFs showed a higher EC_{50} value compared to the raw RSV, except the formulation with 7.5 %w/v of solids and 70 %v/v of ethanol (RSV/7.5/70), which presents a EC_{50} value of 110.36 µg/mL, thus with an antioxidant activity higher than the pure compound. One reason for this may be the fact that the compound loading in the DPF sample used could be higher than the expected value, therefore bringing a greater antioxidant effect. The fact that formulations with a higher concentration of solids and a high volume of ethanol originate smaller particle sizes, as previously seen by SEM images, may have an influence on the expression of the antioxidant activity of DPFs. Smaller particles increase the effective surface area, increasing the contact surface with the reaction medium [141].

Other causes may be due to errors associated with the replicates performed in each test. On the other hand, the formulation with the lowest solids content (RSV/5.0/45) presents the higher EC_{50} value, thus corresponding to the powder with the lowest antioxidant potential.

Table 3.7 – EC_{50} values of unprocessed and SASD processed RSV.

Sample	EC_{50}	
	(µM)	**(µg/mL)**
raw RSV	528.99	120.74
DPF RSV/5.0/45	807.96	184.41
DPF RSV/7.5/20	672.43	153.47
DPF RSV/7.5/70	483.51	110.36

Observing Figure 3.17, the same color changes occur after 30 minutes for the formulations of HPC/GA. However, this discoloration proceeds at lower concentrations, which in itself is already indicative of a greater antioxidant activity by the GA.

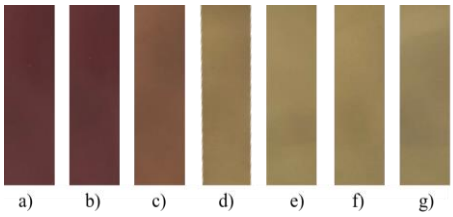

Figure 3.17 – Color of the reaction solution after 30 minutes, at different GA concentrations: a) 50, b) 120, c) 190, d) 260, e) 330, f) 400 and g) 470 µM.

Figure 3.18 shows that the two DPFs with higher solids content (GA/7.5/20 and GA/7.5/70) present a greater antioxidant activity up to about 1300 µM. in relation to raw GA. The DPF with lower solids content (GA/5.0/45) always demonstrates a curve with lower antioxidant activity when compared to the others. This is due to the fact that there is a lower phenolic loading in the formulation. However, the curve describes a more irregular behavior due to the greater associated error since the last point suggests an increase in activity similar to other formulations. After 1250 µM, a stabilization of the curves begins to be noticed for all samples, which can correspond to the almost complete conversion of the DPPH radical.

The EC_{50} values (Table 3.8) of DPPH free radical scavenging activity by GA ranged between 19 and 28 µm/mL. As it happens with RSV, the EC_{50} value for pure GA corresponds to a lower antioxidant activity than the two formulations with higher solids content.

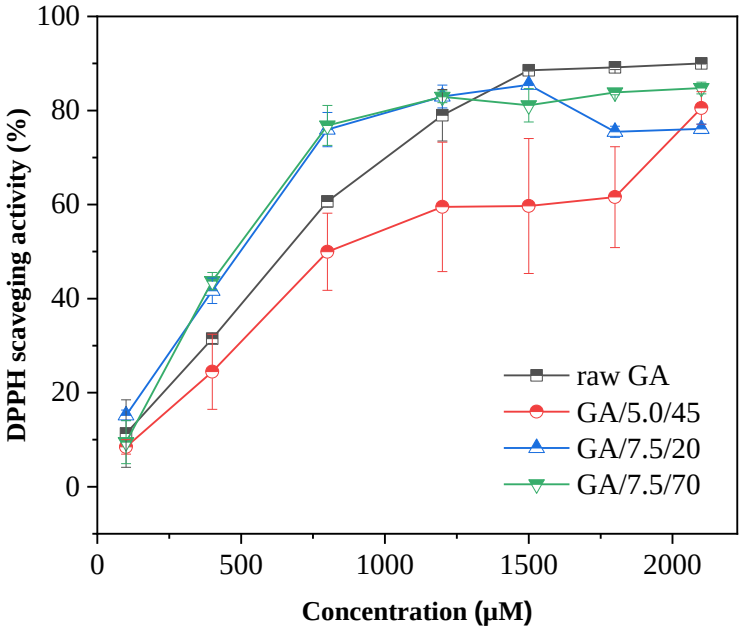

Figure 3.18 – Antioxidant activity of unprocessed GA and SASD processed formulations with GA.

Table 3.8 – EC_{50} values of unprocessed and SASD processed GA.

Sample	EC_{50}	
	(µM)	(µg/mL)
raw GA	125.55	21.36
DPF GA/5.0/45	163.40	27.80
DPF GA/7.5/20	122.16	20.78
DPF GA/7.5/70	117.28	19.95

The high temperatures to which these bioactive compounds can be subjected during SASD processing is one of the main factors that could affect their antioxidant activity. However, by comparing the antioxidant activities of the DPFs and pure compound, temperatures around 80 ºC in the SM and around 60 ºC in the cyclone do not significantly affect their antioxidant activity. This can also be a good indication that the excipient used provides an efficient protection for the bioactive compounds and that the RSV remains in its active form (*trans*-). The bioactivity losses that may have existed were probably not associated with the atomization stage. During this stage, the particles are exposed to these temperatures only for short periods of time (milliseconds). Instead, the bioactivity of DPFs can be compromised when exposed to still relatively high temperatures at the cyclone (T_{out}), since it is necessary a cool down of the installation to recover the final powder.

Comparing both phenolic compounds, it can be stated that powders containing GA have the highest scavenging activity to eliminate 50 % of the initial DPPH radical. That is, at lower concentrations of GA there is a greater antioxidant response than for RSV. The reason may be related to the higher number of active hydroxyl groups in the structure of GA when compared to the number of active hydroxyl groups in the structure of RSV. The hydroxyl groups can establish hydrogen bonds with DPPH free radical, stabilizing it [177].

The EC_{50} values obtained in the antioxidant activity tests were relatively higher than what is found in the literature, for powders produced by supercritical fluid techniques. Dal Magro et al. [141] also tested the antioxidant activity of RSV/PHBV coprecipitated particles using SESD. The EC_{50} values for these powders are in the range of 10–29 µg/mL, higher than the antioxidant activity observed for the raw RSV (28 µg/mL). Aguiar et al. [178] also studied the antioxidant activity of micronized RSV by the SEDS technique (without any excipient) and obtained EC_{50} values in the range of 26–37 µg/mL compared to 28 µg/mL of the raw RSV.

The data for the representation of the DPPH radical scavenging activity as a function of concentration is given in Appendix B.

3.5. *In vitro* Aerodynamic Performance

The tests using the Andersen Cascade Impactor (ACI) were performed to evaluate the aerodynamic behavior of the DPFs stored at different humidity conditions (20 and 45 %RH). The studied DPFs were processed in SASD with the same solid contents (7.5 %w/v), varying only the ethanol volume percentages.

According to Figure 3.19, the respirable fraction (FPF) that is most likely to deposit in the deep lung does not exceed 50 and 40 % for HPC/RSV and HPC/GA microparticles, respectively. This may be due mainly to the presence of a large amount of aggregates, which causes the retention of a significant part of the powder in the upper airways. The highest FPF values obtained were for DPFs prepared with an ethanol volume in the solution to be atomized of at least 45% %v/v, which may indicate that the powder is looser. Moreover, there was no influence of HR conditions in the aerodynamic performance of the powders.

The FPF values were below those obtained for powder formulations produced by this SASD apparatus (58–86 %) [147–149]. In these formulations, other excipients were used, having demonstrated a better aerodynamic performance for delivery to the lung.

The representations of the mass of powder distributed in each stage of the ACI are reported in Appendix D.

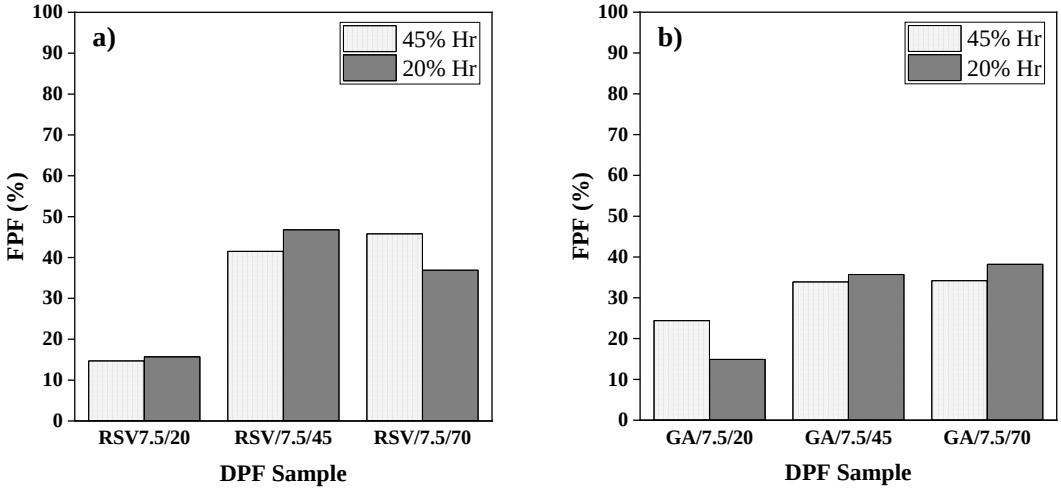

Figure 3.19 – Fine particle fraction (FPF) for 7.5 %w/v DPFs stored at different %RH, varying the ethanol volume in the formulation from 20 to 70 %v/v: a) HPC/RSV b) HPC/GA.

The MMAD of the particles represented in Figure 3.20, indicate aerodynamic diameters within the range of allowable values (0.5–5 μm) that enable particles to reach the deep lung. Above these values, the particles will be trapped in the upper airways and below these are exhaled, and fail to deposit [179].

Higher values of MMAD are obtained for RSV-DPF and GA-DPFs prepared from smaller volumes of ethanol in the solution to be atomized, due to the formation of a larger number of aggregates in these conditions, as seen previously.

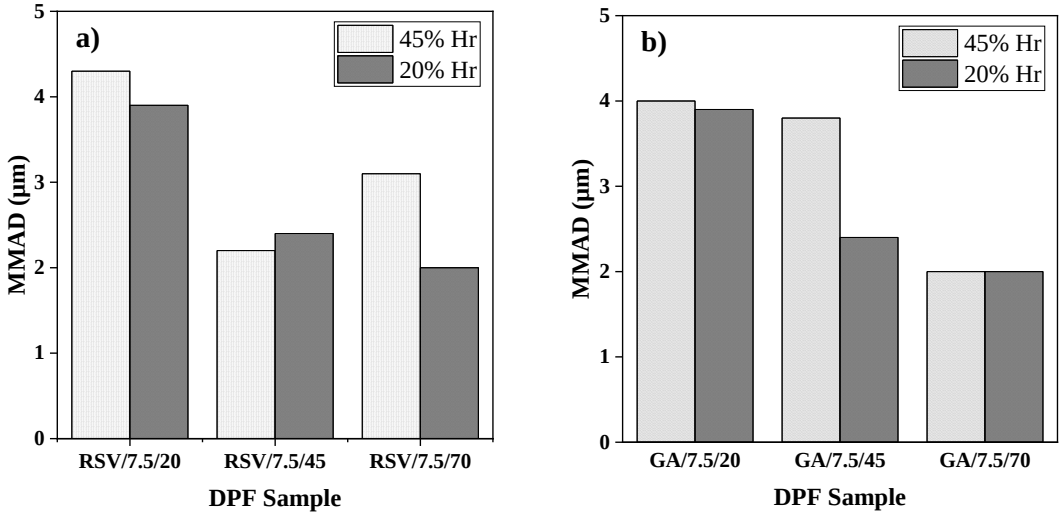

Figure 3.20 – Mass median aerodynamic diameter (MMAD) for 7.5 %w/v DPFs stored at different %RH, varying the ethanol volume in the formulation from 20 to 70 %v/v: a) HPC/RSV b) HPC/GA.

3.6. *In vitro* Phenolic Release

3.6.1. Release Profiles: 24 hours

The release profile is another key evidence that can confirm that the co-atomization was successful and can improve the bioavailability of the phenolic compounds. This study aimed to evaluate the *in vitro* phenolic release from the DPFs in an aqueous medium at pH 5.5 and 32.0 ± 0.1 ºC. These conditions were chosen to mimic an *in vitro* skin absorption experiment, as the skin surface must be maintained at a temperature of 32 ± 1 ºC and a pH between 4.5–5.5 to correspond to the physiological condition of an adult healthy skin [180].

The two selected DPFs used in the experiments were produced under the same liquid feed conditions (5.0 %w/v solids, 45 %v/v EtOH) with 1017 and 880 micrograms of phenolic per 100 milligrams of RSV-DPF and GA-DPF samples, respectively, previously determined by HPLC.

Figure 3.21 shows the percentage of phenolic released over the 24 hours, normalized for the maximum amount of RSV and GA quantified.

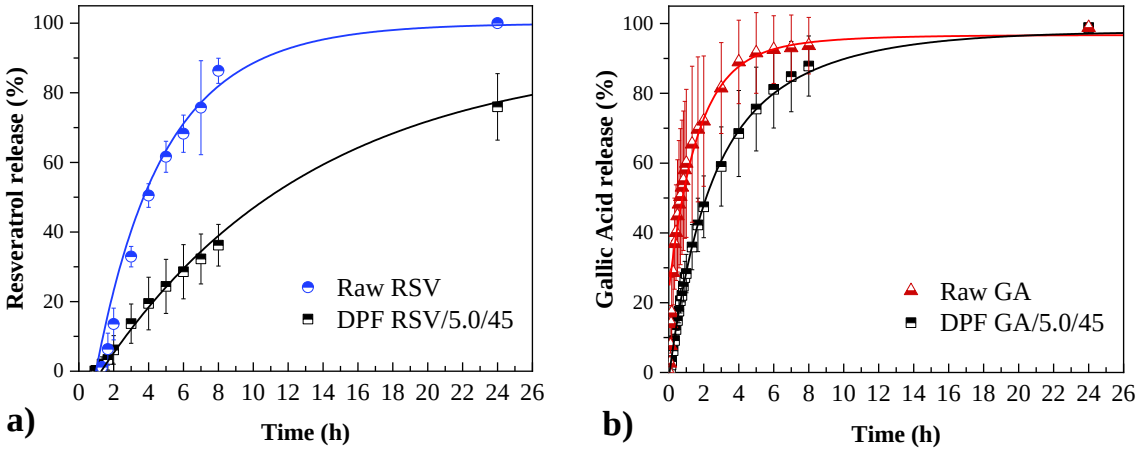

Figure 3.21 – *In vitro* phenolic release profiles in pH 5.5 PBS at 32 ºC for 24 hours of a) raw RSV and DPF RSV/5.0/45 samples and b) raw GA and DPF GA/5.0/45 samples, normalized to the maximum concentration released.

RSV only starts to be quantified after the first hour of assay, whereas GA is immediately detected within the first few minutes. As it is noted by the release profile slopes in both graphs, the release rate of the free compounds is higher than the encapsulated compounds, reaching the maximum amount released more quickly.

The slope of the RSV-DPF release profile represents a controlled release over time of the RSV present in the polymeric matrix. However, while the free RSV maximum released is reached

after 24 hours, the maximum release of RSV-DPF is only achieved after 48 hours (see Appendix G). Although the release profile slope of the encapsulated GA is very similar to the release profile slope of the free GA, its release from the polymeric matrix showed a slight delay during the assay.

Figure 3.22 shows the concentration profile in the *in vitro* release assay of each sample during the first 24 hours.

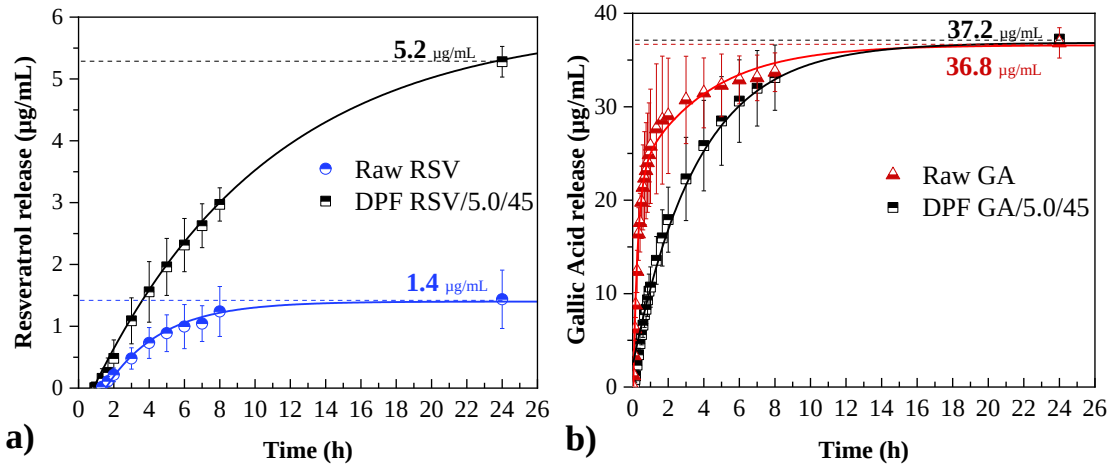

Figure 3.22 – *In vitro* phenolic release profiles in pH 5.5 PBS at 32 ºC for 24 hours from a) raw RSV and DPF RSV/5.0/45 samples and b) raw GA and DPF GA/5.0/45 samples, expressed in µg of phenolic per mL of solution.

For RSV (Figure 3.22a), the release profiles decrease gradually until reaching a maximum concentration. However, the maximum release of the pure compound stabilizes at lower concentrations and earlier than the RSV released from the polymeric matrix. Only 4 ± 1 % of the input mass of RSV was released from the raw RSV sample, while approximately 21 ± 3 % was released from DPF (Appendix G). There was a dissolution of RSV in the solution from the DPF almost 4 times greater than the RSV from the raw sample. The increased release of RSV-DPF compared to the free RSV could be attributed to the increased specific surface area (from 2.19 m^2/g of raw RSV to 4.20 m^2/g of RSV-DPF) [181]. Due to the amorphous nature of the encapsulated RSV, a higher solubility rate to this is observed when compared to the free RSV, whose nature is crystalline, thus providing a faster dissolution [152]. It is observed a decrease in the release rate over time for both samples. Although the solubility of RSV is difficult to predict at different pH's, in acidic media it varies between 64 µg/mL at pH 1.2 and 61 µg/mL at pH 6.8 [182]. HPC, being a hydrophilic polymer soluble at all pH conditions [67], may also have given advantage to the dissolution of RSV from the DPF.

For GA (Figure 3.22b), the maximum concentration of both raw and GA-DPF samples is achieved practically after the same period. About 90 ± 2 % and 93.4 ± 0.9 % of GA were released

from the raw GA and GA-DPF samples, respectively (Appendix G). The only difference is that the release profile of GA-DPF is slightly more controlled as already seen before. The release of GA from the polymeric matrix starts to stabilize after 8 hours, meaning that the release rate decreases with time. An analogous result was reported by Robert et al. [183] who stated that the rapid release of GA from GA-starch and GA-inulin microparticles in water at 25 °C is a result of the "burst effect", corresponding to the release of the superficial GA.

For times longer than 24 hours (Appendix G), a decrease in the concentration of RSV in the solutions begins to be noticed. Two reasons can justify such decreases: on the one hand, if the compounds have reached maximum solubility, the sampling and replacement of fresh solution may be causing a dilution effect; on the other hand, could be a sign of the start of its degradation after 24 hours. RSV is relatively stable in acidic medium up to pH 6, with losses below 30 % compared to its initial concentration after 8 days, while it quickly degrades at basic pH's [184]. Under pH 5.5, hydroxyl groups of RSV will be almost completely protonated. This probably reflects a minimal degradation by oxidation of the conjugated base [182]. The impact of temperature on degradation is also minimal when faced with acidic media. It is unlikely that photodegradation occurred as the tests were carried out on amber flasks, protecting the compounds from light.

Different results of *in vitro* release tests for RSV under similar conditions to those performed in this work were found in the literature. Zhang et al. [181] performed a dissolution study of resveratrol nanoparticles (produced by antisolvent precipitation and spray-drying) in a pH 6.8 solution at 37 ºC. Their results revealed a complete dissolution of RSV/HPMC nanoparticles in 45 min (30 µg/mL), whereas free RSV only reaches the maximum dissolution after 120 min (22.5 µg/mL). Dimer et al.[185] reported a release of over 80 % of free RSV in aqueous medium at 37 ºC after 30 min, while RSV/poly(ε-caprolactone) spray-dried microparticles had a controlled release, reaching 80 % release after 8 hours. In another work, Ha et al. [60] reported a maximum concentration of *trans*-RSV/HPMC nanoparticles (by SAS) released in distilled water at 37 ºC of 150 µg/mL after 24h. Cardoso et al. [104] performed the release of RSV from arabic gum microparticles produced (by spray-drying) in coconut oil at 37 ºC, reaching a maximum concentration released after 15 min.

The experimental data obtained in the *in vitro* release tests can be found in Appendix I1.

3.6.2. Quantification Tests

A new quantification test was done with the samples used in the previous *in vitro* release tests. First of all, it was quantified the total amount of phenolic dissolved in ethanol to prove that the results obtained from HPLC in the determination of the EE. Secondly, what was expected to be present in the pH 5.5 PBS solution if the DPF was placed to dissolve directly in the medium.

With these quantification tests (Figure 3.23), the total amount of RSV and GA dispersed in the ethanolic medium (1043 ± 19 and 826 ± 18 µg/100 mg DPF, respectively) is practically equivalent to the amount of RSV and GA quantified in the EE (1020 and 880 µg/100 mg DPF, respectively). Thus, the EE of at least each one of the DPF used in this release tests can be corroborated.

The maximum concentration released in the previous *in vitro* release profiles can be confirmed, with relatively coincident values for both DPFs. However, in terms of the total amount of RSV present in the solution, only about 30 % of the initial input amount is dissolved. For GA, the total amount released was about 97 %, practically with a complete dissolution of the input mass.

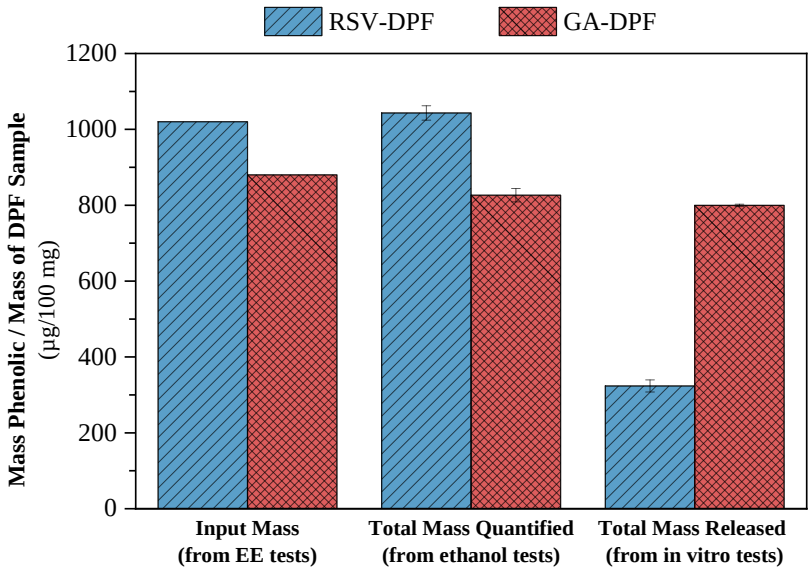

Figure 3.23 – Input (by EE tests), total quantified (in ethanol tests) and total released (in pH 5.5 PBS) masses of RSV and GA, expressed in µg of phenolic per 100 mg of total DPF sample.

The HPLC chromatograms (Appendix I3) for the processed HPC samples (without any of the phenolic compounds) did not showed any peak area of the polymer at the wavelengths related to the detection of each phenolic compound. This confirms that the polymer did not "masked" the results of the RSV-DPF and GA-DPF samples in the quantification of the *in vitro* test performed by HPLC.

All the quantification tests data is present in the Appendix I2.

3.6.3. Kinetic Models

The kinetic models Higuchi and Korsmeyer-Peppas were used to adjust the release experimental data. This study helps understanding the release behavior of phenolic compounds, when in aqueous systems, from within cellulosic structures of the DPFs. The kinetic parameters obtained for each fitted model are presented in Table 3.9.

Table 3.9 – Kinetic parameters of the Higuchi and Korsmeyer-Peppas mathematical models obtained to the release profile of RSV and GA from within the HPC matrix in pH 5.5 PBS at 32 ºC.

System	Higuchi		Korsmeyer-Peppas		
	k ($min^{-0.5}$)	**R^2**	**k (min^{-n})**	**n**	**R^2**
RSV-DPF	0.0055 †	0.9975 †	0.0001 ‡	1.1518 ‡	0.9932 ‡
GA-DPF	0.0507	0.9950	0.0051	0.9870	0.9948

† Fitted up to 16.4 % of RSV release
‡ Fitted up to 21.2 % of RSV release

In both Higuchi and Korsmeyer-Peppas models, the values of the correlation coefficients were close to 1. In accordance with the first model, a good correlation showed that the release mechanism is described by a Fickian diffusion [186]. However, in the Korsmeyer-Peppas model, diffusional release exponent (n) values obtained are well above 0.85 in both RSV-DPF and GA-DPF, which clearly suggests that the release of the phenolic compounds was governed by a Case-II transport. In this context, the release of the molecules is explained by the relaxation of the chains of the polymeric matrix when in contact in the aqueous medium. Due to the high concentration gradients at the polymer/water interface, the cellulosic structure of the HPC swells and the water is imbibed into the matrix [162].

The release rate constant (k) values obtained were higher for the GA-DPF, indicating a faster released rate of the GA when compared to the RSV release rate. This corroborates the release rates results observed in the *in vitro* release profiles. However, the determined k-values were different when comparing different models for the same DPF.

The fittings made with the kinetic models and the respective experimental data can be found in the Appendix I4.

4. Conclusions and Future Work

With the amount of residues produced by viticulture activities, the valorization of these poorly exploited by-products deserves more attention. As it is possible to state, these have a high potential to give rise to add-value products with therapeutic and cosmetic applications.

The Supercritical CO_2-Assisted Spray Drying (SASD) lab-scale apparatus has proved to be an effective technique to produce dry powders of resveratrol (RSV-DPFs) and gallic acid (GA-DPFs) with process yields above 50 % and phenolic loadings up to 100 %. However, the various problems during the experiments may indicate that the process is not yet optimized for this specific system. The phase behavior of the system is complex and governs the process with direct impact in the particle formation.

The XRD and DSC analyzes confirmed the amorphous nature of the DPFs obtained by SASD. According to the ATR-FTIR analysis, the presence of bands corresponding to some functional groups of the phenolic compounds is only noticed in both physical mixtures (PM-RSV e PM-GA), although with very low intensity peaks. The low concentration of RSV and GA in the prepared formulations did not allowed to identify accurately its main functional groups, with the peaks of the HPC groups being more intense. Besides, most of the bands of the phenolic compounds overlap the bands of the HPC, also interfering with its identification.

Design of Experiments (DoE) is a commonly used tool to predict the best combination of the process conditions. The statistical analysis that studied the content of solids (C_solids) and the ethanol volume (V_ethanol) in the solution to be atomized appears to be inconclusive for the yield response. This was influenced by the unexpected problems of nozzle blockage or O-ring breakage while the process was running. For encapsulation efficiency (EE), the results appear to be consistent for both RSV-DPF and GA-DPFs. The phenolic loading of the microparticles is higher for the level 0 and +1 of both parameters. The statistical results regarding the volumetric diameter of the microparticles of either RSV or GA-DPFs, showed an unexpected trend, with smaller particle sizes for larger solids concentrations in the atomized solution. The repetition of tests may be a way to ensure the reproducibility of these results. Finally, for span, only the V_ethanol variable affects the results clearly and consistently in the quadratic component for both RSV-DPF and GA-DPFs. More homogeneous size distributions are obtained for the low and high level of the variable V_ethanol in both cases, although, this does not make the span a decisive parameter when choosing the best combination of these parameters, since its values were, overall, below 2. It can be concluded that it would be interesting to consider only the EE response with the best

combination of factor levels when it comes to the selection of the DPF to use in the antioxidant and *in vitro* release tests.

In terms of aerodynamic performance, the co-atomization of HPC with the phenolic compounds seems to have improved the FPF of the powders, from percentages between 15–18 % with processed HPC without any bioactive compound, to percentages between 34–38% for GA-DPFs and 37–47% for RSV-DPFs. These were maximum percentage intervals obtained for DPFs prepared from ethanol volumes of 45 and 70 %v/v in the atomized solution. However, these results are still not considered the best if it is intended to administer these via inhalation, since a large amount of powder is retained in the induction port in all ACI tests.

Nevertheless, SASD has shown to be a suitable technique for thermosensitive compounds using a cellulose derivative as an excipient. The process conditions applied during the atomization step were able to preserve their antioxidant activity. Average EC_{50} values of 30.6 µg/mL for GA-DPFs and 149.4 µg/mL for RSV-DPFs coincide with the antioxidant power of the phenolic compound in its pure form. However, it would also be important to test the bioactivity of DPFs 1 month after the first tests have been performed to assess the stability of the antioxidant power, under controlled storage conditions.

Regarding the *in vitro* release in an aqueous medium at pH 5.5 and 32 ºC, different behaviors can be noted for each phenolic. From the DPF matrix, GA had a much faster release over time, whereas RSV had a more controlled release. However, the most noticeable difference was in the amount released from each phenolic. While for GA there was an almost complete release of the initial mass (93.4 ± 0.9 %), for RSV it was almost the opposite (21 ± 3 %), due also to its insufficient solubility in aqueous media. The different solubilities and release behaviors of each compound lead to the possibility of adapting the dissolution medium. The addition of small volumes of ethanol in the dissolution medium or even a surfactant may improve the RSV solubility in aqueous media. However, the second option is preferable since it is pretended avoiding the use of ethanol. Furthermore, it would also have been important to perform bioactivity tests at each sampling point, to study whether the antioxidant activity was preserved throughout the release, especially when the maximum released concentrations are reached. Through the application of the Higuchi and Korsmeyer-Peppas kinetic models, it was concluded that both models presented a good fit, with regression coefficients (R^2) values of almost 1. Diffusional release exponent (n) values above 0.85 indicated that the GA and RSV release mechanism is associated with the relaxation of the polymeric structure of the HPC (Case-II transport). Moreover, the release rate constant (k) values obtained in both models indicate that GA had a faster release.

From the point of view of feasibility for therapeutic and cosmetic purposes, it would be interesting to perform thermal and chemical stability tests on the bioactive DPFs. Assess the presence of natural/UV-light at different conditions of the human body (temperature and pH) in the powder's stability. However, this was not possible due to the small amounts of sample available and the time required to carry out the tests in proper conditions.

While there are several studies focused on the encapsulation of grape pomace extracts (including skins, stems and seeds) using mainly conventional methods, there is none focused on the encapsulation of vine shoot extracts, either by conventional or SCF-based methods. Thus, the encapsulation of antioxidant phenolic compounds using SASD has been reported for the first time in this work. The effectiveness in encapsulating these bioactive compounds can be of a high interest in order to assess the use of aqueous extracts of vine shoot residues as liquid feed for the SASD.

With this work it becomes obvious the worthwhile and interest in developing processes for the recovery of natural active compounds, since they play an important role in favor of a circular bioeconomy. Integrating residues and wastes from agri-food industries into new production chains enables an optimized and efficient use of biomass, extending its value over time.

References

[1] F.O. Obi, B.O. Ugwuishiwu, J.N. Nwakaire, Agricultural Waste Concept, Generation, Utilization and Management, Nigerian Journal of Technology. 35 (2016) 957–964. https://doi.org/10.4314/njt.v35i4.34.

[2] R. Sánchez-Gómez, G.L. Alonso, M.R. Salinas, A. Zalacain, Reuse of Vine-Shoots Wastes for Agricultural Purposes, in: Handbook of Grape Processing By-Products: Sustainable Solutions, Elsevier Inc., 2017: pp. 79–104. https://doi.org/10.1016/B978-0-12-809870-7.00004-1.

[3] The European Parliament and Council of the European Union, Directive 2008/98/EC of the European Parliament and of the Council of 19 November 2008 on waste and repealing certain directives, Official Journal of the European Union. (2008) 3–30. https://doi.org/2008/98/EC.; 32008L0098.

[4] P. Stegmann, M. Londo, M. Junginger, The circular bioeconomy: Its elements and role in European bioeconomy clusters, Resour. Conserv. Recycl. X. 6 (2020) 100029. https://doi.org/10.1016/j.rcrx.2019.100029.

[5] European Commission, Communication from the Commission to the European Parliament, the Council, the European Economic and Social Committee and the Committee of the Regions. Closing the loop – An EU action plan for the Circular Economy, Brussels, 2015. https://ec.europa.eu/transparency/regdoc/rep/1/2015/EN/1-2015-614-EN-F1-1.PDF.

[6] M. Carus, L. Dammer, The "Circular Bioeconomy" - Concepts, Opportunities and Limitations, Ind. Biotechnol. 14 (2018) 83–91. https://doi.org/10.1089/ind.2018.29121.mca.

[7] R.G. Maroun, H.N. Rajha, E. Vorobiev, N. Louka, Emerging Technologies for the Recovery of Valuable Compounds From Grape Processing By-Products, Elsevier Inc., 2017. https://doi.org/10.1016/B978-0-12-809870-7.00007-7.

[8] OIV, 2019 Statistical Report on World Vitiviniculture, 2019.

[9] M.M. Moreira, M.F. Barroso, J. Vasconcellos, M.J. Ramalhosa, Š. Jaroslava, L. Estevinho, S. Morais, C. Delerue-Matos, Potential of Portuguese vine shoot wastes as natural resources of bioactive compounds, Science of the Total Environment. 634 (2018) 831–842. https://doi.org/10.1016/j.scitotenv.2018.04.035.

[10] M.A. Nunes, F. Rodrigues, M.B.P.P. Oliveira, Chapter 11 - Grape Processing By-Products as Active Ingredients for Cosmetic Proposes, in: Handb. Grape Process. By-Products, Elsevier Inc., 2017: pp. 1–35. https://doi.org/10.1016/B978-0-12-809870-7/00011-9.

[11] OIV, Focus OIV 2017: Distribution variétale du vignoble dans le monde, 2017. www.oiv.int.

[12] The vegetative cycle of the Vitis Vinifera - The grapevine and its vegetative cycle - Wine Growing - Wine Grower's Guide - Wine & Grape Encyclopedia - Sogrape Vinhos, (n.d.). https://eng.sograpevinhos.com/enciclopedia/guia_vinha/ciclo (accessed April 9, 2020).

[13] Life cycle of a grapevine, Torres Wines. (2017). https://www.torres.es/en/blog/wine-planet/life-cycle-grapevine# (accessed April 14, 2020).

[14] M.S. Jesus, A. Romaní, Z. Genisheva, J.A. Teixeira, L. Domingues, Integral valorization of vine pruning residue by sequential autohydrolysis stages, Journal of Cleaner

Production. 168 (2017) 74–86. https://doi.org/10.1016/j.jclepro.2017.08.230.

[15] C. Cebrián, R. Sánchez-Gómez, M.R. Salinas, G.L. Alonso, A. Zalacain, Effect of post-pruning vine-shoots storage on the evolution of high-value compounds, Industrial Crops and Products. 109 (2017) 730–736. https://doi.org/10.1016/j.indcrop.2017.09.037.

[16] A. Sánchez, F. Ysunza, M.J. Beltran-García, M. Esqueda, Biodegradation of viticulture wastes by Pleurotus: A source of microbial and human food and its potential use in animal feeding, Journal of Agricultural and Food Chemistry. 50 (2002) 2537–2542. https://doi.org/10.1021/jf011308s.

[17] Ibero Massa Florestal, Estudo do impacto na economia local/regional autárquica pelo aproveitamento e valorização energética e económica das podas, 2014.

[18] Z. Mahmood, M. Yameen, M. Jahangeer, M. Riaz, A. Ghaffar, I. Javid, Chapter 8 - Lignin as Natural Antioxidant Capacity, in: Lignin: Trends Ans Applications, IntechOpen, 2018: pp. 181–206. https://doi.org/10.1016/j.colsurfa.2011.12.014.

[19] J.M. Luque-Rodríguez, P. Pérez-Juan, M.D. Luque De Castro, Extraction of polyphenols from vine shoots of Vitis vinifera by superheated ethanol-water mixtures, Journal of Agricultural and Food Chemistry. 54 (2006) 8775–8781. https://doi.org/10.1021/jf061855j.

[20] P. Oliver, A. Villem, Phenolic Compounds: Structures, Uses and Health Benefits, Nova Science Publishers Inc., New York, 2017.

[21] T. Cardoso, Microencapsulation of Resveratrol with applicability in food industry, Faculdade de Engenharia da Universidade do Porto, 2017.

[22] N.F. Santos-Sánchez, R. Salas-Coronado, B. Hernández-Carlos, C. Villanueva-Cañongo, Shikimic Acid Pathway in Biosynthesis of Phenolic Compounds, Plant Physiological Aspects of Phenolic Compounds. (2016). https://doi.org/http://dx.doi.org/10.5772/57353.

[23] A. Teixeira, N. Baenas, R. Domínguez-Perles, A. Barros, E. Rosa, Natural Bioactive Compounds from Winery By-Products as Health Promoters: A Review, International Journal of Molecular Sciences. 15 (2014) 15638–15678. https://doi.org/10.3390/ijms150915638.

[24] M.L. Soto, E. Falqué, H. Domínguez, Relevance of natural phenolics from grape and derivative products in the formulation of cosmetics, Cosmetics. 2 (2015) 259–276. https://doi.org/10.3390/cosmetics2030259.

[25] A. Barros, A. Gironés-Vilaplana, A. Teixeira, J. Collado-González, D.A. Moreno, A. Gil-Izquierdo, E. Rosa, R. Domínguez-Perles, Evaluation of grape (Vitis vinifera L.) stems from Portuguese varieties as a resource of (poly)phenolic compounds: A comparative study, Food Res. Int. 65 (2014) 375–384. https://doi.org/10.1016/j.foodres.2014.07.021.

[26] H. El Gharras, Polyphenols: food sources, properties and applications - a review, Int. J. Food Sci. Technol. 44 (2009) 2512–2518. https://doi.org/10.1111/j.1365-2621.2009.02077.x.

[27] R. Sánchez-Gómez, A. Zalacain, G.L. Alonso, M.R. Salinas, Vine-shoot waste aqueous extracts for re-use in agriculture obtained by different extraction techniques: Phenolic, volatile, and mineral compounds, Journal of Agricultural and Food Chemistry. 62 (2014) 10861–10872. https://doi.org/10.1021/jf503929v.

[28] O. Dorosh, M.M. Moreira, F. Rodrigues, A.F. Peixoto, C. Freire, S. Morais, C. Delerue-Matos, Vine-Canes Valorisation: Ultrasound-Assisted Extraction from Lab to Pilot Scale, Molecules. 25 (2020). https://doi.org/10.3390/molecules25071739.

[29] M.S. Jesus, Z. Genisheva, A. Romaní, R.N. Pereira, J.A. Teixeira, L. Domingues,

Bioactive compounds recovery optimization from vine pruning residues using conventional heating and microwave-assisted extraction methods, Industrial Crops and Products. 132 (2019) 99–110. https://doi.org/10.1016/j.indcrop.2019.01.070.

[30] B. Gullón, G. Eibes, M.T. Moreira, I. Dávila, J. Labidi, P. Gullón, Antioxidant and antimicrobial activities of extracts obtained from the refining of autohydrolysis liquors of vine shoots, Industrial Crops and Products. 107 (2017) 105–113. https://doi.org/10.1016/j.indcrop.2017.05.034.

[31] Z. Piñeiro, A. Marrufo-Curtido, M.J. Serrano, M. Palma, Ultrasound-Assisted Extraction of Stilbenes from Grape Canes, Molecules. 21 (2016) 1–13. https://doi.org/10.3390/molecules21060784.

[32] J. Garrido, F. Borges, Wine and grape polyphenols — A chemical perspective, Food Res. Int. 54 (2013) 1844–1858. https://doi.org/10.1016/j.foodres.2013.08.002.

[33] R. Flamini, M. De Rosso, F. De Marchi, A. Dalla Vedova, A. Panighel, M. Gardiman, I. Maoz, L. Bavaresco, An innovative approach to grape metabolomics: stilbene profiling by suspect screening analysis, Metabolomics. 9 (2013) 1243–1253. https://doi.org/10.1007/s11306-013-0530-0.

[34] L. Alexandru, A. Binello, S. Mantegna, L. Boffa, F. Chemat, G. Cravotto, Efficient green extraction of polyphenols from post-harvested agro-industry vegetal sources in Piedmont, Comptes Rendus Chim. 17 (2014) 212–217. https://doi.org/10.1016/j.crci.2013.09.012.

[35] M.P. Delgado-Torre, C. Ferreiro-Vera, F. Priego-Capote, P.M. Pérez-Juan, M.D. Luque De Castro, Comparison of accelerated methods for the extraction of phenolic compounds from different vine-shoot cultivars, Journal of Agricultural and Food Chemistry. 60 (2012) 3051–3060. https://doi.org/10.1021/jf205078k.

[36] J.M. Max, B., Salgado, J. M., Cortés, S., Domínguez, Extraction of Phenolic Acids by Alkaline Hydrolysis from the Solid Residue Obtained after Prehydrolysis of Trimming Vine Shoots, Journal of Agricultural and Food Chemistry. 58 (2010) 1909–1917. https://doi.org/10.1021/jf903441d.

[37] I. Soural, N. Vrchotová, J. Tříska, J. Balík, Š. Horník, P. Cuřínová, J. Sýkora, Various extraction methods for obtaining stilbenes from grape cane of Vitis vinifera L., Molecules. 20 (2015) 6093–6112. https://doi.org/10.3390/molecules20046093.

[38] B. Houillé, S. Besseau, V. Courdavault, A. Oudin, G. Glévarec, G. Delanoue, L. Guérin, A.J. Simkin, N. Papon, M. Clastre, N. Giglioli-Guivarch, A. Lanoue, Biosynthetic Origin of E-Resveratrol Accumulation in Grape Canes during Postharvest Storage, Journal of Agricultural and Food Chemistry. 63 (2015) 1631–1638. https://doi.org/10.1021/jf505316a.

[39] M. Zwingelstein, M. Draye, J.L. Besombes, C. Piot, G. Chatel, Trans-Resveratrol and trans-ϵ-Viniferin in Grape Canes and Stocks Originating from Savoie Mont Blanc Vineyard Region: Pre-extraction Parameters for Improved Recovery, ACS Sustain. Chem. Eng. 7 (2019) 8310–8316. https://doi.org/10.1021/acssuschemeng.8b06723.

[40] T. Gorena, V. Saez, C. Mardones, C. Vergara, P. Winterhalter, D. Von Baer, Influence of post-pruning storage on stilbenoid levels in Vitis vinifera L. canes, Food Chemistry. 155 (2014) 256–263. https://doi.org/10.1016/j.foodchem.2014.01.073.

[41] J. Lachman, Z. Kotikova, A. Hejtmankova, V. Pivec, O. Psenienaja, M. Sulc, R. Stoalkova, M. Didina, Resveratrol and piceid isomers concentrations in grapevine shoots, leaves, and tendrils, Hortic. Sci. 43 (2016) 25–32. https://doi.org/10.17221/258/2014-HORTSCI.

[42] G. Németh, O. Hegyi, A. Dunai, L. Kocsis, Two different organs of Vitis vinifera cv. Merlot grafted on TK5BB rootstock, Oeno One. 51 (2017) 309–322. https://doi.org/10.20870/oeno-one.2017.51.4.1861.

[43] C. Liu, L. Wang, J. Wang, B. Wu, W. Liu, P. Fan, Z. Liang, S. Li, Resveratrols in Vitis berry skins and leaves: Their extraction and analysis by HPLC, Food Chemistry. 136 (2013) 643–649. https://doi.org/10.1016/j.foodchem.2012.08.017.

[44] B. Tian, J. Liu, Resveratrol: a review of plant sources, synthesis, stability, modification and food application, J. Sci. Food Agric. 100 (2019) 1392–1404. https://doi.org/10.1002/jsfa.10152.

[45] C. Counet, D. Callemien, S. Collin, Chocolate and cocoa: New sources of trans-resveratrol and trans-piceid, Food Chemistry. 98 (2006) 649–657. https://doi.org/10.1016/j.foodchem.2005.06.030.

[46] G. Davidov-Pardo, D.J. McClements, Resveratrol encapsulation: Designing delivery systems to overcome solubility, stability and bioavailability issues, Trends in Food Science and Technology. 38 (2014) 88–103. https://doi.org/10.1016/j.tifs.2014.05.003.

[47] X. Meng, J. Zhou, C.N. Zhao, R.Y. Gan, H. Bin Li, Health Benefits and Molecular Mechanisms of Resveratrol: A Narrative Review, Foods. 9 (2020) 1–27. https://doi.org/10.3390/foods9030340.

[48] D. Perrone, M.P.I.A. Fuggetta, F. Ardito, A. Cottarelli, A. de Filippis, G. Ravagnan, S. de Maria, L. lo Muzio, Resveratrol (3,5,4'-trihydroxystilbene) and its properties in oral diseases (Review), Exp. Ther. Med. 14 (2017) 3–9. https://doi.org/10.3892/etm.2017.4472.

[49] M.A. Nunes, F. Rodrigues, M.B.P.P. Oliveira, Grape Processing By-Products as Active Ingredients for Cosmetic Proposes, in: Handbook of Grape Processing By-Products: Sustainable Solutions, Elsevier Inc., 2017: pp. 267–292. https://doi.org/10.1016/B978-0-12-809870-7/00011-9.

[50] A. Sharif, N. Akhtar, M.S. Khan, A. Menaa, B. V., B.A. Khan, F. Menaa, Formulation and evaluation on human skin of a water-in-oil emulsion containing Muscat hamburg black grape seed extract, Int. J. Cosmet. Sci. 37 (2015) 253–258. https://doi.org/10.1111/ics.12184.

[51] M. Karamać, A. Kosinska, R.B. Pegg, Content of Gallic Acid in Selected Plant Extracts, Polish J. Food Nutr. Sci. 15/56 (2016) 55–58.

[52] M.M. Vuolo, V.S. Lima, M.R. Maróstica Junior, Chapter 2 - Phenolic Compounds: Structure, Classification, and Antioxidant Power, in: Bioact. Compd. Heal. Benefits Potential Appl., Elsevier Inc., 2019: pp. 33–50. https://doi.org/10.1016/B978-0-12-814774-0.00002-5.

[53] J. Gao, J. Hu, D. Hu, X. Yang, A Role of Gallic Acid in Oxidative Damage Diseases: A Comprehensive Review, Nat. Prod. Commun. (2019) 1–9. https://doi.org/10.1177/1934578X19874174.

[54] B.A. Khan, T. Mahmood, F. Menaa, Y. Shahzad, A.M. Yousaf, T. Hussain, S.D. Ray, New Perspectives on the Efficacy of Gallic Acid in Cosmetics & Nanocosmeceuticals, Curr. Pharm. Des. 24 (2018) 1–7. https://doi.org/10.2174/1381612825666190118150614.

[55] G. Davidov-Pardo, I. Arozarena, M.R. Marín-Arroyo, Stability of polyphenolic extracts from grape seeds after thermal treatments, Eur. Food Res. Technol. 232 (2011) 211–220. https://doi.org/10.1007/s00217-010-1377-5.

[56] M. Friedman, H.S. Jürgens, Effect of pH on the Stability of Plant Phenolic Compounds,

Journal of Agricultural and Food Chemistry. 48 (2000) 2101–2110. https://doi.org/10.1021/jf990489j.

[57] I. Volf, I. Ignat, M. Neamtu, V.I. Popa, Thermal stability, antioxidant activity, and photo-oxidation of natural polyphenols, Chem. Pap. 68 (2014) 121–129. https://doi.org/10.2478/s11696-013-0417-6.

[58] A. Munin, F. Edwards-Lévy, Encapsulation of Natural Polyphenolic Compounds; a Review, Pharmaceutics. 3 (2011) 793–829. https://doi.org/10.3390/pharmaceutics3040793.

[59] F. Casanova, L. Santos, Encapsulation of cosmetic active ingredients for topical application – a review, Journal of Microencapsulation. 33 (2015).

[60] E.-S. Ha, W.-Y. Sim, S.-K. Lee, J.-S. Jeong, J.-S. Kim, I. Baek, D.H. Choi, H. Park, S.-J. Hwang, M.-S. Kim, Preparation and evaluation of resveratrol-loaded composite nanoparticles using a supercritical fluid technology for enhanced oral and skin delivery, Antioxidants. 8 (2019). https://doi.org/10.3390/antiox8110554.

[61] A. Amri, J.C. Chaumeil, S. Sfar, C. Charrueau, Administration of resveratrol: What formulation solutions to bioavailability limitations?, J. Control. Release. 158 (2012) 182–193. https://doi.org/10.1016/j.jconrel.2011.09.083.

[62] G.L. Amidon, H. Lennernäs, V.P. Shah, J.R. Crison, A Theoretical Basis for a Biopharmaceutic Drug Classification The Correlation of in Vitro Drug Product Dissolution and in Vivo Bioavailability, Pharm. Res. 12 (1995).

[63] W. Tangsongcharoen, P. Punyamoonwongsa, P. Chaiyasat, High performance biocompatible cellulose-based microcapsules encapsulating gallic acid prepared by inverse microsuspension polymerization, Polym. Int. 68 (2019) 714–723. https://doi.org/10.1002/pi.5757.

[64] S.K. Ghosh, Functional Coatings by Polymer Microencapsulation, 2006. https://doi.org/10.1002/3527608478.

[65] M. Arenas-Jal, J.M. Suñé-Negre, E. García-Montoya, An overview of microencapsulation in the food industry: opportunities, challenges, and innovations, Eur. Food Res. Technol. (2020). https://doi.org/10.1007/s00217-020-03496-x.

[66] Z. Fang, B. Bhandari, Encapsulation of polyphenols - a review, Trends in Food Science and Technology. 21 (2010) 510–523. https://doi.org/10.1016/j.tifs.2010.08.003.

[67] P. Narayan, W.W. Porter III, M. Brackhagen, C. Tucker, Polymers and Surfactants, in: A. Newman (Ed.), Pharm. Amorph. Solid Dispersions, Wiley, 2015: pp. 42–84. https://doi.org/10.16309/j.cnki.issn.1007-1776.2003.03.004.

[68] N. Shah, H. Sandhu, D.S. Choi, H. Chokshi, A.W. Malick, Advances in Delivery Science and Technology: Amorphous Solid Dispersions, Springer, 2014. https://doi.org/10.1007/978-1-4939-1598-9.

[69] R.B. Chavan, S. Rathi, V.G.S.S. Jyothi, N.R. Shastri, Cellulose based polymers in development of amorphous solid dispersions, Asian J. Pharm. Sci. 14 (2019) 248–264. https://doi.org/10.1016/j.ajps.2018.09.003.

[70] C. Leuner, J. Dressman, Improving drug solubility for oral delivery using solid dispersions, Eur. J. Pharm. Biopharm. 50 (2000) 47–60. https://doi.org/10.1016/S0939-6411(00)00076-X.

[71] P. Sharma, S.R. Modi, A.K. Bansal, Co-processing as a tool to improve aqueous dispersibility of cellulose ethers, Drug Dev. Ind. Pharm. 41 (2015) 1–14. https://doi.org/10.3109/03639045.2015.1058814.

[72] A. Gómez-Carracedo, C. Alvarez-Lorenzo, J. Gómez-Amoza, A. Concheiro, Chemical structure and glass transition temperature of non-ionic cellulose ethers, J. Therm. Anal. Calorim. 73 (2003) 587–596. https://doi.org/10.1023/A:1025434314396.

[73] FDA, Inactive Ingredient Database, (n.d.). https://www.fda.gov/ (accessed August 17, 2020).

[74] P.J. Sheskey, W.G. Cook, C.G. Cable, Handbook of Pharmaceutical Excipients, Eighth edi, Pharmaceutical Press and the American Pharmacists Association, 2017.

[75] S.A. Vshivkov, E. V. Rusinova, Phase diagrams of a hydroxypropyl cellulose-water system under static conditions and in the shear field, Polym. Sci. - Ser. B. 49 (2007) 209–212. https://doi.org/10.1134/S1560090407070093.

[76] A. Sarode, P. Wang, C. Cote, D.R. Worthen, Low-viscosity Hydroxypropylcellulose (HPC) Grades SL and SSL: Versatile Pharmaceutical Polymers for Dissolution Enhancement, Controlled Release, and Pharmaceutical Processing, AAPS PharmSciTech. 14 (2013) 151–159. https://doi.org/10.1208/s12249-012-9897-x.

[77] K.M. Picker, S.W. Hoag, Characterization of the thermal properties of microcrystalline cellulose by modulated temperature differential scanning calorimetry, J. Pharm. Sci. 91 (2002) 342–349. https://doi.org/10.1002/jps.10018.

[78] S.A. Vshivkov, L. V. Adamova, E. V. Rusinova, A.P. Safronov, V.E. Dreval', A.G. Galyas, Thermodynamics of liquid-crystalline solutions of hydroxypropyl cellulose in water and ethanol, Polym. Sci. - Ser. A. 49 (2007) 578–583. https://doi.org/10.1134/S0965545X07050124.

[79] L. Yan, Q. Zhu, P.U. Kenkare, Lower critical solution temperature of linear PNIPA obtained from a Yukawa potential of polymer chains, J. Appl. Polym. Sci. 78 (2000) 1971–1976. https://doi.org/10.1002/1097-4628(20001209)78:11<1971::AID-APP170>3.0.CO;2-P.

[80] A. Penhasi, Microencapsulation of probiotic bacteria using thermo-sensitive sol-gel polymers for powdered infant formula, Journal of Microencapsulation. 32 (2015) 372–380. https://doi.org/10.3109/02652048.2015.1028497.

[81] M.R.I. Shishir, L. Xie, C. Sun, X. Zheng, W. Chen, Advances in micro and nano-encapsulation of bioactive compounds using biopolymer and lipid-based transporters, Trends in Food Science and Technology. 78 (2018) 34–60. https://doi.org/10.1016/j.tifs.2018.05.018.

[82] F. Edwards-Lévy, A. Munin-César, Chapter 36: Encapsulation of Polyphenolics, in: M. Mishra (Ed.), Handb. Encapsulation Control. Release, CRC Press, 2015: pp. 741–763. https://doi.org/10.1201/b19038-13.

[83] L.F. Ballesteros, M.J. Ramirez, C.E. Orrego, J.A. Teixeira, S.I. Mussatto, Encapsulation of antioxidant phenolic compounds extracted from spent coffee grounds by freeze-drying and spray-drying using different coating materials, Food Chemistry. 237 (2017) 623–631. https://doi.org/10.1016/j.foodchem.2017.05.142.

[84] A.H. Salama, Spray drying as an advantageous strategy for enhancing pharmaceuticals bioavailability, Drug Deliv. Transl. Res. 10 (2020) 1–12. https://doi.org/10.1007/s13346-019-00648-9.

[85] M.R.I. Shishir, W. Chen, Trends of spray drying: A critical review on drying of fruit and vegetable juices, Trends in Food Science and Technology. 65 (2017) 49–67. https://doi.org/10.1016/j.tifs.2017.05.006.

[86] V. Đorđević, B. Balanč, A. Belščak-Cvitanović, S. Lević, K. Trifković, A. Kalušević, I.

Kostić, D. Komes, B. Bugarski, V. Nedović, Trends in Encapsulation Technologies for Delivery of Food Bioactive Compounds, 2015. https://doi.org/10.1007/s12393-014-9106-7.

[87] S.P. Ishwarya, C. Anandharamakrishnan, A.G.F. Stapley, Spray-freeze-drying: A novel process for the drying of foods and bioproducts, Trends in Food Science and Technology. 41 (2015) 161–181. https://doi.org/10.1016/j.tifs.2014.10.008.

[88] A. Rezvankhah, Z. Emam-Djomeh, G. Askari, Encapsulation and delivery of bioactive compounds using spray and freeze-drying techniques: A review, Drying Technology. 38 (2020) 235–258. https://doi.org/10.1080/07373937.2019.1653906.

[89] S.L. Kosaraju, D. Labbett, M. Emin, I. Konczak, L. Lundin, Delivering polyphenols for healthy ageing, Nutr. Diet. 65 (2008) S48–S52. https://doi.org/10.1111/j.1747-0080.2008.00261.x.

[90] L. Zhang, D. Mou, Y. Du, Procyanidins: Extraction and micro-encapsulation, J. Sci. Food Agric. 87 (2007) 2192–2197. https://doi.org/10.1002/jsfa.

[91] J.A. Pérez-Serradilla, M.D. Luque de Castro, Microwave-assisted extraction of phenolic compounds from wine lees and spray-drying of the extract, Food Chemistry. 124 (2011) 1652–1659. https://doi.org/10.1016/j.foodchem.2010.07.046.

[92] T. Boonchu, N. Utama-Ang, Optimization of extraction and microencapsulation of bioactive compounds from red grape (Vitis vinifera L.) pomace, J. Food Sci. Technol. 52 (2013) 783–792. https://doi.org/10.1007/s13197-013-1079-7.

[93] G. Davidov-Pardo, I. Arozarena, M.R. Marín-Arroyo, Optimization of a Wall Material Formulation to Microencapsulate a Grape Seed Extract Using a Mixture Design of Experiments, Food Bioprocess Technol. 6 (2013) 941–951. https://doi.org/10.1007/s11947-012-0848-z.

[94] V.B. De Souza, A. Fujita, M. Thomazini, E.R. Da Silva, J.F. Lucon, M.I. Genovese, C.S. Favaro-Trindade, Functional properties and stability of spray-dried pigments from Bordo grape (Vitis labrusca) winemaking pomace, Food Chemistry. 164 (2014) 380–386. https://doi.org/10.1016/j.foodchem.2014.05.049.

[95] G. V. Mote, M.I. Talib, Optimization of extraction and microencapsulation of polyphenols from pomace of Indian grapes, Int. J. ChemTech Res. 10 (2017) 576–582.

[96] A. Tolun, Z. Altintas, N. Artik, Microencapsulation of grape polyphenols using maltodextrin and gum arabic as two alternative coating materials: Development and characterization, J. Biotechnol. 239 (2016) 23–33. https://doi.org/10.1016/j.jbiotec.2016.10.001.

[97] T. Moreno, E. de Paz, I. Navarro, S. Rodríguez-Rojo, A. Matías, C. Duarte, M. Sanz-Buenhombre, M.J. Cocero, Spray Drying Formulation of Polyphenols-Rich Grape Marc Extract: Evaluation of Operating Conditions and Different Natural Carriers, Food Bioprocess Technol. 9 (2016) 2046–2058. https://doi.org/10.1007/s11947-016-1792-0.

[98] B.R. Böger, S.R. Georgetti, L.E. Kurozawa, Microencapsulation of grape seed oil by spray drying, Food Sci. Technol. 38 (2018) 263–270. https://doi.org/10.1590/fst.04417.

[99] D. Escobar-Avello, Ja. Avendaño, S. Riquelme, C. Gómez, J. Luengo, A. Vallverdú-Queralt, R.M. Lamuela-Raventós, C. Mardones, Grape cane by-products as food additives: Changes in phenolic profile during production and microencapsulation, in: 5th Lat. Am. Congr. Biorefineries From Lab. to Ind. Pract., Concepción, Chile, 2019.

[100] A. Tolun, N. Artik, Z. Altintas, Effect of different microencapsulating materials and relative humidities on storage stability of microencapsulated grape pomace extract, Food

Chemistry. 302 (2020) 125347. https://doi.org/10.1016/j.foodchem.2019.125347.

[101] C.B. da Rocha, C.P.Z. Noreña, Microencapsulation and controlled release of bioactive compounds from grape pomace, Drying Technology. (2020) 1–15. https://doi.org/10.1080/07373937.2020.1741004.

[102] S.T. Carpes, D. Pereira, C. de Moura, A.S. dos Reis, L.D. da Silva, T.L.C. Oldoni, J.F. Almeida, M.V.S. Plata-Oviedo, Lyophilized and microencapsulated extracts of grape pomace from winemaking industry to prevent lipid oxidation in chicken pâté, Brazilian J. Food Technol. 23 (2020). https://doi.org/10.1590/1981-6723.11219.

[103] B. Li, L.A. Wegiel, L.S. Taylor, K.J. Edgar, Stability and solution concentration enhancement of resveratrol by solid dispersion in cellulose derivative matrices, Cellulose. 20 (2013) 1249–1260. https://doi.org/10.1007/s10570-013-9889-3.

[104] T. Cardoso, A. Gonçalves, B.N. Estevinho, F. Rocha, Potential food application of resveratrol microparticles: Characterization and controlled release studies, Powder Technology. 355 (2019) 593–601. https://doi.org/10.1016/j.powtec.2019.07.079.

[105] N. Theyssen, K. Scovell, M. Poliakoff, N.R. Foster, F.P. Lucien, R. Mammucari, C.M. Rayner, P.M. Rose, D.C. Barnes, Handbook of Green Chemistry, Wiley-VCH, 2010.

[106] A. Braeuer, High Pressure: Fellow and Opponent of Spectroscopic Techniques, in: Supercritical Fluid Science and Technology, 2015: pp. 1–40. https://doi.org/10.1016/B978-0-444-63422-1.00001-8.

[107] R. Smith, C. Peters, H. Inomata, Chapter 4: Historical background and applications, in: Supercritical Fluid Science and Technology, Elsevier B.V., 2013: pp. 175–273. https://doi.org/10.1016/B978-0-444-52215-3.00004-0.

[108] FDA, GRAS Substances (SCOGS) Database, (n.d.). https://www.fda.gov/food/generally-recognized-safe-gras/gras-substances-scogs-database (accessed August 28, 2020).

[109] H.A. Every, M. V. Natu, Supercritical CO2 encapsulation of cosmetic ingredients: Novel methods for tailoring ingredients for the cosmetics industry, Household and Personal Care Today. 9 (2014) 42–45.

[110] E.M. Martin Del Valle, M.A. Galan, Supercritical fluid technique for particle engineering: Drug delivery applications, Reviews in Chemical Engineering. 21 (2005) 33–69. https://doi.org/10.1515/REVCE.2005.21.1.33.

[111] A. Aguiar-Ricardo, Building Dry Powder Formulations using Supercritical CO2 Spray Drying, Current Opinion in Green and Sustainable Chemistry. 5 (2017) 12–16. https://doi.org/10.1016/j.cogsc.2017.03.005.

[112] T. Fornari, R.P. Stateva, High Pressure Fluid Technology for Green Food Processing, 2015. https://doi.org/10.1007/978-3-319-10611-3.

[113] S. Rodríguez-Rojo, Á. Martín, M.J. Cocero, Encapsulation Methods with Supercritical Carbon Dioxide: Basis and Applications, in: Encapsulation Nanotechnologies, 2013: pp. 391–424. https://doi.org/10.1002/9781118729175.ch12.

[114] C. Moura, E. Costa, A. Aguiar-Ricardo, Optimization of Supercritical-CO2 Assisted Spray Drying for the Production of Inhalable composite particles, Hovione. (2016).

[115] R. Viveiros, T. Casimiro, Impressão Molecular em CO2 Supercrítico: Uma Abordagem Verde no Desenvolvimento de Novos Materiais de Afinidade, Bol. Da Soc. Port. Química 140. (2016) 19–25.

[116] S.H. Soh, L.Y. Lee, Microencapsulation and Nanoencapsulation Using Supercritical Fluid (SCF) Techniques, Pharmaceutics. 11 (2019).

https://doi.org/10.3390/pharmaceutics11010021.

[117] M. Temtem, C. Moura, T. Casimiro, E. Costa, A. Aguiar-Ricardo, Benchmarking Supercritical CO2-assisted Spray Drying with Conventional Spray Drying for the Manufacture of Inhalation Formulations, Respir. Drug Deliv. Eur. (2017) 1–14.

[118] I. Pasquali, R. Bettini, F. Giordano, Supercritical fluid technologies: An innovative approach for manipulating the solid-state of pharmaceuticals, Advanced Drug Delivery Reviews. 60 (2008) 399–410. https://doi.org/10.1016/j.addr.2007.08.030.

[119] A. Tabernero, E.M. Martín del Valle, M.A. Galán, Supercritical fluids for pharmaceutical particle engineering: Methods, basic fundamentals and modelling, Chem. Eng. Process. Process Intensif. 60 (2012) 9–25. https://doi.org/10.1016/j.cep.2012.06.004.

[120] Y. Wang, Development of Supercritical Fluid Processes for Particle Coating/Encapsulation with Polymers, New Jersey, 2004.

[121] Á. Martín, M.J. Cocero, Micronization processes with supercritical fluids: Fundamentals and mechanisms, Advanced Drug Delivery Reviews. 60 (2008) 339–350. https://doi.org/10.1016/j.addr.2007.06.019.

[122] T.K. Fahim, I.S.M. Zaidul, A.B.M. R, U.M. Salim, M.B. Awang, F. Sahena, K.C.A. Jalal, K.M. Sharif, M.H. Sohrab, Particle formation and micronization using non-conventional techniques- review, Chem. Eng. Process. Process Intensif. 86 (2014) 47–52. https://doi.org/10.1016/j.cep.2014.10.009.

[123] A.V.M. Nunes, C.M.M. Duarte, Dense CO2 as a Solute, Co-Solute or Co-Solvent in Particle Formation Processes: A review, Materials. 4 (2011) 2017–2041. https://doi.org/10.3390/ma4112017.

[124] E. Reverchon, Process For The Production Of Micro And/Or Nano Particles., U.S. Patent 7276190B2, 2001.

[125] E. Reverchon, G. Lamberti, A. Antonacci, Supercritical fluid assisted production of HPMC composite microparticles, The Journal of Supercritical Fluids. 46 (2008) 185–196. https://doi.org/10.1016/j.supflu.2008.04.010.

[126] E. Reverchon, A. Antonacci, Cyclodextrins Micrometric Powders Obtained by Supercritical Fluid Processing, Biotechnology and Bioengineering. 94 (2006) 753–761. https://doi.org/10.1002/bit.

[127] E. Reverchon, A. Antonacci, Chitosan microparticles production by supercritical fluid processing, Industrial and Engineering Chemistry Research. 45 (2006) 5722–5728. https://doi.org/10.1021/ie060233k.

[128] C. Costa, T. Casimiro, A. Aguiar-Ricardo, Optimization of Supercritical CO2-Assisted Atomization: Phase Behavior and Design of Experiments, Journal of Chemical and Engineering Data. 63 (2018) 885–896. https://doi.org/10.1021/acs.jced.7b00820.

[129] E. Reverchon, G. Della Porta, A. Spada, Ampicillin micronization by supercritical assisted atomization, Journal of Pharmacy and Pharmacology. 55 (2003) 1465–1471. https://doi.org/10.1211/0022357022043.

[130] E. Reverchon, G. Lamberti, A. Antonacci, Supercritical fluid assisted production of HPMC composite microparticles, The Journal of Supercritical Fluids. 46 (2008) 185–196. https://doi.org/10.1016/j.supflu.2008.04.010.

[131] S. Liparoti, R. Adami, E. Reverchon, Supercritical assisted atomization: Effect of operative conditions on PVP microparticle size and morphology, The Journal of Supercritical Fluids. 97 (2015) 31–35. https://doi.org/10.1016/j.supflu.2014.10.028.

[132] O. Nuchuchua, Supercritical carbon dioxide sprat drying for the production of stable dried protein formulations, Leiden University, 2017. https://doi.org/10.1017/CBO9781107415324.004.

[133] M.A. Rodrigues, J. Li, A.J. Almeida, H.A. Matos, E.G. De Azevedo, Efficiency of Water Removal from Water/Ethanol Mixtures using Suoercritical Carbon Dioxide, Brazilian Journal of Chemical Engineering. 23 (2006) 205–212.

[134] R. Adami, S. Liparoti, E. Reverchon, A new supercritical assisted atomization configuration, for the micronization of thermolabile compounds, Chem. Eng. J. 173 (2011) 55–61. https://doi.org/10.1016/j.cej.2011.07.036.

[135] B. Aliakbarian, M. Paini, R. Adami, P. Perego, Use of Supercritical Assisted Atomization to Produce Nanoparticles from Olive Pomace Extract, Innov. Food Sci. Emerg. Technol. (2016). https://doi.org/10.1016/j.ifset.2016.09.016.

[136] A. Di Capua, A. Bejarano, R. Adami, E. Reverchon, Preparation and characterization of Chilean propolis coprecipitates using Supercritical Assisted Atomization, Chem. Eng. Res. Des. (2018). https://doi.org/10.1016/j.cherd.2018.06.037.

[137] R. Zhou, F. Wang, Z. Guo, Y.L. Zhao, Preparation and characterization of resveratrol/hydroxypropyl-β-cyclodextrin inclusion complex using supercritical antisolvent technology, Journal of Food Process Engineering. 35 (2012) 677–686. https://doi.org/10.1111/j.1745-4530.2010.00617.x.

[138] M. Salgado, S. Rodríguez-Rojo, F.M. Alves-Santos, M.J. Cocero, Encapsulation of resveratrol on lecithin and β-glucans to enhance its action against Botrytis cinerea, Journal of Food Engineering. 165 (2015) 13–21. https://doi.org/10.1016/j.jfoodeng.2015.05.002.

[139] A. Natolino, C. Da, S. Rodríguez-Rojo, T. Moreno, M.J. Cocero, Supercritical antisolvent precipitation of polyphenols from grape marc extract, The Journal of Supercritical Fluids. 118 (2016) 54–63. https://doi.org/10.1016/j.supflu.2016.07.015.

[140] N. Mezzomo, D.A. Oliveira, S.R.R. Comim, S.R.S. Ferreira, Encapsulation of extract from winery industry residue using the supercritical anti-solvent technique, Brazilian Journal of Chemical Engineering. 33 (2016) 589–598. https://doi.org/10.1590/0104-6632.20160333s20150051.

[141] C. Dal Magro, G.P.S. Aguiar, J.G. Veneral, A.E. dos Santos, L.M.P.C. de Chaves, J.V. Oliveira, M. Lanza, Co-precipitation of trans-resveratrol in PHBV using Solution Enhanced Dispersion by Supercritical Fluids technique, The Journal of Supercritical Fluids. 127 (2017) 182–190. https://doi.org/10.1016/j.supflu.2017.03.025.

[142] P. Elliott, S. Billingham, J. Bi, H. Zhang, Quality by design for biopharmaceuticals: a historical review and guide for implementation, Pharm. Bioprocess. 1 (2013) 105–122. https://doi.org/10.4155/pbp.13.6.

[143] ICH, Pharmaceutical Development Q8(R2), 2009. https://www.ich.org/page/quality-guidelines.

[144] C. Moura, Improved Particle Engineering and DPI Formulation for Optimal Pulmonary Delivery, 2016. Available in http://hdl.handle.net/10362/20779.

[145] L. Eriksson, E. Johansson, N. Kettaneh-Wold, C. Wikström, S. Wold, Design of Experiments: Principles and Applications, Third, Umetrics AB, 2008. https://www.researchgate.net/publication/260081086_Design_of_Experiments_Principles_and_Applications.

[146] F. Gaspar, J. Vicente, F. Neves, J.-R. Authelin, Spray Drying: Scale-Up and Manufacturing, in: Adv. Deliv. Sci. Technol. Amorph. Solid Dispersions, Springer, 2014:

pp. 261–302. https://doi.org/10.1007/978-1-4939-1598-9.

[147] R.P. Cabral, A.M.L. Sousa, A.S. Silva, A.I. Paninho, M. Temtem, E. Costa, T. Casimiro, A. Aguiar-Ricardo, Design of experiments approach on the preparation of dry inhaler chitosan composite formulations by supercritical CO2-assisted spray-drying, The Journal of Supercritical Fluids. 116 (2016) 26–35. https://doi.org/10.1016/j.supflu.2016.04.001.

[148] M. Tavares, R.P. Cabral, C. Costa, P. Martins, A.R. Fernandes, T. Casimiro, A. Aguiar-Ricardo, Development of PLGA dry powder microparticles by supercritical CO2-assisted spray-drying for potential vaccine delivery to the lungs, The Journal of Supercritical Fluids. (2017). https://doi.org/10.1016/j.supflu.2017.06.004.

[149] C. Moura, T. Casimiro, E. Costa, A. Aguiar-Ricardo, Optimization of supercritical CO2-assisted spray drying technology for the production of inhalable composite particles using quality-by-design principles, Powder Technology. 357 (2019) 387–397. https://doi.org/10.1016/j.powtec.2019.08.090.

[150] E.P. 7.0, Buffer solutions, in: Eur. Pharmacopoeia 7.0, 2011: pp. 489–494.

[151] C. Duarte, A. Aguiar-Ricardo, N. Ribeiro, T. Casimiro, Correlation of Vapor–Liquid Equilibrium for Carbon Dioxide + Ethanol + Water at Temperatures from 35 to 70°C, Separation Science and Technology. 35 (2000) 2187–2201.

[152] M. Rahman, S. Ahmad, J. Tarabokija, E. Bilgili, Roles of surfactant and polymer in drug release from spray-dried hybrid nanocrystal-amorphous solid dispersions (HyNASDs), Powder Technology. 361 (2020) 663–678. https://doi.org/10.1016/j.powtec.2019.11.058.

[153] M. Rahman, S. Ahmad, J. Tarabokija, N. Parker, E. Bilgili, Spray-Dried Amorphous Solid Dispersions of Griseofulvin in HPC/Soluplus/SDS: Elucidating the Multifaceted Impact of SDS as a Minor Component, Pharmaceutics. 12 (2020). https://doi.org/10.3390/pharmaceutics12030197.

[154] I. Ahmad, M. Anwar, S. Akhter, P. Thakur, R. Chawla, R.K. Sharma, A. Ali, F.J. Ahmad, Supercritical Fluid Technology-Based Trans-Resveratrol SLN for Long Circulation and Improved Radioprotection, Journal of Pharmaceutical Innovation. 11 (2016) 308–322. https://doi.org/10.1007/s12247-016-9254-9.

[155] S.I.F. Badawy, D.B. Gray, M.A. Hussain, A study on the effect of wet granulation on microcrystalline cellulose particle structure and performance, Pharm. Res. 23 (2006) 634–640. https://doi.org/10.1007/s11095-005-9555-z.

[156] Metrohm, 756/831 KF Coulometer: Instructions for Use, 8.831.1003, 2003.

[157] L. Medina-Torres, D.M. Núñez-Ramírez, F. Calderas, R.F. González-Laredo, R. Minjares-Fuentes, M.A. Valadez-García, M.J. Bernad-Bernad, O. Manero, Microencapsulation of gallic acid by spray drying with aloe vera mucilage (aloe barbadensis miller) as wall material, Industrial Crops and Products. 138 (2019). https://doi.org/10.1016/j.indcrop.2019.06.024.

[158] B. Alexander, D.J. Browse, S.J. Reading, I.S. Benjamin, A simple and accurate mathematical method for calculation of the EC50, J. Pharmacol. Toxicol. Methods. 41 (1999) 55–58. https://doi.org/10.1016/S1056-8719(98)00038-0.

[159] European Pharmacopeia 7.0, Preparations for inhalation: aerodynamic assessment of fine particles, (Counc. Eur. 2.9.18), 2010.

[160] Copley, Driving Results in Inhaler Testing, (2020) 45–49.

[161] N.A. Peppas, J.J. Sahlin, A simple equation for the description of solute release. III. Coupling of diffusion and relaxation, International Journal of Pharmaceutics. 57 (1989) 169–172. https://doi.org/10.1016/0378-5173(89)90306-2.

[162] J. Siepmann, N.A. Peppas, Modeling of drug release from delivery systems based on hydroxypropyl methylcellulose (HPMC), Advanced Drug Delivery Reviews. 48 (2001) 139–157. https://doi.org/10.1016/S0169-409X(01)00112-0.

[163] E. Reverchon, A. Antonacci, Polymer microparticles production by supercritical assisted atomization, The Journal of Supercritical Fluids. 39 (2007) 444–452. https://doi.org/10.1016/j.supflu.2006.03.005.

[164] M.K. Trivedi, Influence of Biofield Treatment on Physicochemical Properties of Hydroxyethyl Cellulose and Hydroxypropyl Cellulose, J. Mol. Pharm. Org. Process Res. 03 (2015) 0–7. https://doi.org/10.4172/2329-9053.1000126.

[165] N. Nyamweya, S.W. Hoag, Assessment of Polymer-Polymer Interactions in Blends of HPMC and Film Forming Polymers by Modulated Temperature Differential Scanning Calorimetry, Pharm. Res. 17 (2000) 625–631. https://doi.org/10.1023/A:1007585403781.

[166] N.D. Alharbi, O.W. Guirguis, Macrostructure and optical studies of hydroxypropyl cellulose in pure and Nano-composites forms, Results Phys. 15 (2019) 102637. https://doi.org/10.1016/j.rinp.2019.102637.

[167] C.M. Lin, Y.C. Chang, L.C. Cheng, C.H. Liu, S.C. Chang, T.Y. Hsien, D.M. Wang, H.J. Hsieh, Preparation of graphene-embedded hydroxypropyl cellulose/chitosan/polyethylene oxide nanofiber membranes as wound dressings with enhanced antibacterial properties, Cellulose. 27 (2020) 2651–2667. https://doi.org/10.1007/s10570-019-02940-w.

[168] N. Eguchi, K. Kawabata, H. Goto, Electrochemical Polymerization of 4,4-Dimethyl-2,2'-Bithiophene in Concentrated Polymer Liquid Crystal Solution, J. Mater. Sci. Chem. Eng. 05 (2017) 64–70. https://doi.org/10.4236/msce.2017.52007.

[169] J. Varshosaz, E. Ghassami, Enhancement of Dissolution Rate of Fenofibrate by Spray Drying Technique: Comparison of Eudragit E-100, Solutol® HS15 and Hydroxypropyl Cellulose as Carriers, Farmacia. 63 (2015) 433–445. https://apps.webofknowledge.com/full_record.do?product=WOS&search_mode=GeneralSearch&qid=45&SID=C5YFVaktuYjDqAuvWmN&page=2&doc=14&cacheurlFromRightClick=no.

[170] A.L. Sarode, S.A. Malekar, C. Cote, D.R. Worthen, Hydroxypropyl cellulose stabilizes amorphous solid dispersions of the poorly water soluble drug felodipine, Carbohydr. Polym. 112 (2014) 512–519. https://doi.org/10.1016/j.carbpol.2014.06.039.

[171] Particle Analytical, BET (Brunauer, Emmett and Teller), (n.d.). https://particle.dk/methods-analytical-laboratory/surface-area-bet-2/ (accessed November 5, 2020).

[172] M. Thommes, K. Kaneko, A. V. Neimark, J.P. Olivier, F. Rodriguez-Reinoso, J. Rouquerol, K.S.W. Sing, Physisorption of gases, with special reference to the evaluation of surface area and pore size distribution (IUPAC Technical Report), Pure Appl. Chem. 87 (2015) 1051–1069. https://doi.org/10.1515/pac-2014-1117.

[173] A. de C.S. Alves, R.M. Mainardes, N.M. Khalil, Nanoencapsulation of gallic acid and evaluation of its cytotoxicity and antioxidant activity, Mater. Sci. Eng. C. 60 (2016) 126–134. https://doi.org/10.1016/j.msec.2015.11.014.

[174] Y.P. Neo, S. Ray, J. Jin, M. Gizdavic-Nikolaidis, M.K. Nieuwoudt, D. Liu, S.Y. Quek, Encapsulation of food grade antioxidant in natural biopolymer by electrospinning technique: A physicochemical study based on zein-gallic acid system, Food Chemistry. 136 (2013) 1013–1021. https://doi.org/10.1016/j.foodchem.2012.09.010.

[175] I.C.C.M. Porto, T.G. Nascimento, J.M.S. Oliveira, P.H. Freitas, A. Haimeur, R. França,

Use of polyphenols as a strategy to prevent bond degradation in the dentin–resin interface, Eur. J. Oral Sci. 126 (2018) 146–158. https://doi.org/10.1111/eos.12403.

[176] A.S. Pessoa, G.P.S. Aguiar, J. Vladimir Oliveira, A.J. Bortoluzzi, A. Paulino, M. Lanza, Precipitation of resveratrol-isoniazid and resveratrol-nicotinamide cocrystals by gas antisolvent, The Journal of Supercritical Fluids. 145 (2019) 93–102. https://doi.org/10.1016/j.supflu.2018.11.014.

[177] Y. Zhang, Y. Shen, Y. Zhu, Z. Xu, Assessment of the correlations between reducing power, scavenging DPPH activity and anti-lipid-oxidation capability of phenolic antioxidants, LWT - Food Science and Technology. 63 (2015) 569–574. https://doi.org/10.1016/j.lwt.2015.03.047.

[178] G.P.S. Aguiar, B.D. Arcari, L.M.P.C. Chaves, C.D. Magro, D.L. Boschetto, A.L. Piato, M. Lanza, J.V. Oliveira, Micronization of trans-resveratrol by supercritical fluid: Dissolution, solubility and in vitro antioxidant activity, Industrial Crops and Products. 112 (2018) 1–5. https://doi.org/10.1016/j.indcrop.2017.11.008.

[179] M.C. Silva, A.S. Silva, J. Fernandez-Lodeiro, T. Casimiro, C. Lodeiro, A. Aguiar-Ricardo, Supercritical CO2-assisted spray drying of strawberry-like gold-coated magnetite nanocomposites in chitosan powders for inhalation, Materials. 10 (2017). https://doi.org/10.3390/ma10010074.

[180] World Health Organization, Environmental Health Criteria 235: Dermal Absorption, 2006.

[181] X.-P. Zhang, Y. Le, J.-X. Wang, H. Zhao, J.-F. Chen, Resveratrol nanodispersion with high stability and dissolution rate, LWT - Food Science and Technology. 50 (2013) 622–628. https://doi.org/10.1016/j.lwt.2012.07.041.

[182] Š. Zupančič, Z. Lavrič, J. Kristl, Stability and solubility of trans-resveratrol are strongly influenced by pH and temperature, Eur. J. Pharm. Biopharm. 93 (2015) 196–204. https://doi.org/10.1016/j.ejpb.2015.04.002.

[183] P. Robert, P. García, N. Reyes, J. Chávez, J. Santos, Acetylated starch and inulin as encapsulating agents of gallic acid and their release behaviour in a hydrophilic system, Food Chemistry. 134 (2012) 1–8. https://doi.org/10.1016/j.foodchem.2012.02.019.

[184] K. Robinson, C. Mock, D. Liang, Pre-formulation studies of resveratrol, Drug Dev. Ind. Pharm. 41 (2015) 1464–1469. https://doi.org/10.1016/j.physbeh.2017.03.040.

[185] F.A. Dimer, M. Ortiz, A.R. Pohlmann, S.S. Guterres, Inhalable resveratrol microparticles produced by vibrational atomization spray drying for treating pulmonary arterial hypertension, Journal of Drug Delivery Science and Technology. 29 (2015) 152–158. https://doi.org/10.1016/j.jddst.2015.07.008.

[186] P. García, C. Vergara, P. Robert, Release Kinetic in Yogurt from Gallic Acid Microparticles with Chemically Modified Inulin, J. Food Sci. 80 (2015) C2147–C2152. https://doi.org/10.1111/1750-3841.13001.

Appendices

Appendix A

Table A.1 – Process conditions in Batch 1 of RSV-DPFs assays.

Batch #1 RSV-DPF	F_{CO2} (mL/min)	F_{Feed} (mL/min)	RH (%)	T_{room} (ºC)	T_{in} (ºC)	Th_{CO2} (ºC)	Tc_{CO2} (ºC)	T_{SM} (ºC)	T_{out} (ºC)	P_{SM} (bar)
RSV/2.5/20	25	3.5	40	25	101 ± 4	77.0 ± 0.0	-17.4 ± 0.2	84 ± 5	67 ± 4	104 ± 3
RSV/2.5/45	25	3.5	41 ± 2	27.0 ± 0.1	97 ± 7	80.7 ± 0.5	-20.65 ± 0.02	82 ± 4	73 ± 6	102.0 ± 0.6
RSV/2.5/70	25	3.5	31.7 ± 0.5	29.3	100 ± 4	76.3 ± 0.9	-15.8 ± 0.1	88 ± 7	68 ± 4	102 ± 2
RSV/5.0/20	25	3.5	37 ± 0.0	25.7	102 ± 2	78.3 ± 0.5	-20.6 ± 0.3	86 ± 3	58 ± 4	100.2 ± 0.8
RSV/5.0/45	25	3.5	32.7 ± 0.9	30.0 ± 0.1	92 v 4	73.0 ± 0.8	-17.3 ± 0.2	84 ± 4	54 ± 2	104.6 ± 0.9
RSV/5.0/70	25	3.5	34 ± 3	28.0 ± 0.7	96 ± 5	81.3 ± 0.5	-21.827 ± 0.005	93 ± 8	70 ± 6	108 ± 4
RSV/7.5/20	25	3.5	40	26.7	103 ± 3	77.7 ± 0.5	-17.7 ± 0.2	60 ± 36	61 ± 3	100 ± 1
RSV/7.5/45	25	3.5	28 ± 1	31.2 ± 0.2	105.3 ± 0.5	74.0 ± 0.8	-16.5 ± 0.3	91 ± 4	69.6 ± 0.5	103 ± 2
RSV/7.5/70	25	3.5	28	29.3 ± 0.1	94 ± 3	73.0 ± 0.0	-15.21 ± 0.03	83 ± 4	57 ± 3	106 ± 2

Table A.2 – Process conditions in Batch 2 of RSV-DPFs assays.

Batch #2 RSV-DPF	F_{CO2} (mL/min)	F_{Feed} (mL/min)	RH (%)	T_{room} (ºC)	T_{in} (ºC)	Th_{CO2} (ºC)	Tc_{CO2} (ºC)	T_{SM} (ºC)	T_{out} (ºC)	P_{SM} (bar)
RSV/2.5/20	25	3.5	28	29.3 ± 0.1	99 ± 7	72.7 ± 0.5	-16.9 ± 0.1	85 ± 4	63 ± 2	105 ± 1
RSV/2.5/45	25	3.5	28	29.3 ± 0.1	98 ± 7	74.3 ± 0.9	-16.47 ± 0.0	81 ± 4	59 ± 4	100.3 ± 0.3
RSV/2.5/70	25	3.5	28	29.3 ± 0.1	104 ± 3	74 ± 1	-17.1 ± 0.0	87 ± 5	62 ± 4	104 ± 4
RSV/5.0/20	25	3.5	28	29.3 ± 0.1	101 ± 3	75 ± 2	-17.5 ± 0.1	90 ± 7	61 ± 2	106 ± 1
RSV/5.0/45	25	3.5	28	29.3 ± 0.1	103 ± 3	61.0 ± 0.8	-19.04 ± 0.1	84 ± 6	67.2 ± 0.7	100.6 ± 0.3
RSV/5.0/70	25	3.5	28	29.3 ± 0.1	97 ± 6	76.7 ± 0.5	-20.2 ± 0.1	85 ± 5	65 ± 4	106.8 ± 0.7
RSV/7.5/20	25	3.5	28	29.3 ± 0.1	97 ± 6	74.3 ± 0.9	-17.3 ± 0.1	87 ± 6	62 ± 4	99.9 ± 0.8
RSV/7.5/45	25	3.5	28	29.3 ± 0.1	93 ± 6	75.7 ± 0.5	-20.0 ± 0.1	85 ± 5	60 ± 2	104 ± 2
RSV/7.5/70	25	3.5	28	29.4 ± 0.0	102 ± 4	74 ± 1	-21.3 ± 0.1	92 ± 8	64 ± 1	103.4 ± 0.9

Table A.3 – Process conditions in Batch 1 of GA-DPFs assays.

Batch #1 GA-DPF	F_{CO2} (mL/min)	F_{Feed} (mL/min)	RH (%)	T_{room} (ºC)	T_{in} (ºC)	Th_{CO2} (ºC)	Tc_{CO2} (ºC)	T_{SM} (ºC)	T_{out} (ºC)	P_{SM} (bar)
GA/2.5/20	25	3.5	33	26 ± 0.1	103 ± 7	77 ± 0	-20.6 ± 0.3	83 ± 5	59 ± 3	102 ± 1
GA/2.5/45	25	3.5	47	24	93 ± 3	76.3 ± 0.5	-19.5 ± 0.3	83 ± 6	55 ± 2	100.7 ± 0.3
GA/2.5/70	25	3.5	45	26	95 ± 7	76.0 ± 0.8	-18.0 ± 0.1	81 ± 2	61 ± 3	99.8 ± 0.8
GA/5.0/20	25	3.5	36	28	98.3 ± 2.4	80 ± 2	-18 ± 1	83 ± 1	60 ± 2	102 ± 3
GA/5.0/45	25	3.5	47	26	104 ± 2	77.0 ± 0.8	-15.3 ± 0.2	89.0 ± 0.8	71 ± 4	100 ± 2
GA/5.0/70	25	3.5	44	26	97 ± 6	77.0 ± 0.8	-13.1 ± 0.1	89 ± 4	59 ± 3	99.4 ± 0.4
GA/7.5/20	25	3.5	37	26	98 ± 6	78.7 ± 0.5	-17.5 ± 0.0	86 ± 5	60 ± 3	104 ± 3
GA/7.5/45	25	3.5	45	26 ± 0.5	105 ± 2	76 ± 1	-16.6 ± 0.2	83 ± 5	63 ± 2	100.0 ± 0.1
GA/7.5/70	25	3.5	41	25	101 ± 6	76.0 ± 0.8	-18.2 ± 0.6	90 ± 7	62 ± 4	104 ± 2

Table A.4 – Process conditions in Batch 2 of GA-DPFs assays.

Batch #2 GA-DPF	F_{CO2} (mL/min)	F_{Feed} (mL/min)	RH (%)	T_{room} (ºC)	T_{in} (ºC)	Th_{CO2} (ºC)	Tc_{CO2} (ºC)	T_{SM} (ºC)	T_{out} (ºC)	P_{SM} (bar)
GA/2.5/20	25	3.5	28	29.3 ± 0.1	97 ± 8	77.3 ± 0.5	-12.91 ± 0.05	85 ± 6	49 ± 3	105 ± 3
GA/2.5/45	25	3.5	28	29.3 ± 0.1	97 ± 8	77.0 ± 0.8	-16.41 ± 0.05	84 ± 3	60 ± 5	103 ± 1
GA/2.5/70	25	3.5	28	29.3 ± 0.1	97 ± 8	78 ± 1	-15.76 ± 0.05	83 ± 5	61 ± 2	104.5 ± 0.3
GA/5.0/20	25	3.5	28	29.3 ± 0.1	99 ± 7	77 ± 1	-19.9 ± 0.1	86 ± 6	55 ± 3	104.8 ± 0.3
GA/5.0/45	25	3.5	28	29.3 ± 0.1	100 ± 6	77.0 ± 0.8	-17.7 ± 0.1	87 ± 5	56 ± 4	104 ± 2
GA/5.0/70	25	3.5	28	29.3 ± 0.1	98 ± 6	77 ± 1	-14.9 ± 0.4	86 ± 4	62 ± 3	101.8 ± 0.3
GA/7.5/20	25	3.5	28	29.3 ± 0.1	100 ± 7	77 ± 3	-20.3 ± 0.1	85 ± 6	59 ± 3	104.6 ± 0.5
GA/7.5/45	25	3.5	28	29.3 ± 0.1	96 ± 6	75.7 ± 0.5	-13.22 ± 0.02	84 ± 6	59 ± 1	100.8 ± 0.4
GA/7.5/70	25	3.5	28	29.3 ± 0.1	94 ± 6	81 ± 2	-13.5 ± 0.2	81 ± 4	60 ± 4	101.3 ± 0.2

F_{CO2} – CO_2 flow rate; **F_{Feed}** – liquid feed solution flow rate; **RH** – Relative Humidity; **T_{room}** – room temperature; **T_{in}** – inlet drying gas temperature; **Th_{CO}** – CO_2 oil bath temperature; **Tc_{CO}** – CO_2 cooling bath temperature; **T_{SM}** – saturator temperature; **T_{out}** – outlet temperature (cyclone); **P_{sat}** – saturator pressure.

Appendix B

Table B.1 – DPPH radical scavenging activity (%) of raw RSV and RSV-DPFs; C_{RSV} – concentration of RSV (µM) in the analysed solution, after 30 min.

C_{RSV} (µM)	raw RSV	RSV / 5.0 / 45	RSV / 7.5 / 20	RSV / 7.5 / 70
100	10.75 ± 0.08	7.30 ± 0.32	11.54 ± 0.34	9.79 ± 0.31
400	28.40 ± 0.75	15.22 ± 0.75	19.32 ± 1.33	22.33 ± 0.57
800	43.01 ± 0.73	24.54 ± 0.67	33.60 ± 3.36	34.90 ± 0.34
1200	48.57 ± 5.63	38.63 ± 4.29	48.27 ± 0.33	43.86 ± 0.28
1500	53.75 ± 5.74	37.25 ± 7.21	52.26 ± 1.01	47.60 ± 0.35
1800	66.22 ± 2.50	46.87 ± 0.46	55.45 ± 0.70	43.49 ± 2.81
2100	62.24 ± 1.32	49.64 ± 0.63	58.09 ± 0.50	49.92 ± 0.74

Table B.2 – DPPH radical scavenging activity (%) of raw GA and GA-DPFs. C_{GA} – concentration of GA (µM) in the analysed solution, after 30 min.

C_{GA} (µM)	raw GA	GA / 5.0 / 45	GA / 7.5 / 20	GA / 7.5 / 70
50	11.31 ± 7.18	8.47 ± 1.54	15.18 ± 1.13	9.48 ± 4.58
120	31.50 ± 1.04	24.44 ± 7.98	41.67 ± 2.72	43.72 ± 1.83
190	60.67 ± 1.15	49.96 ± 8.20	75.95 ± 3.64	76.82 ± 4.25
260	79.00 ± 5.48	59.51 ± 13.75	82.97 ± 2.42	82.92 ± 1.25
330	88.54 ± 0.15	59.69 ± 14.34	85.46 ± 0.16	81.12 ± 3.55
400	89.17 ± 0.46	61.58 ± 10.72	75.47 ± 1.18	83.86 ± 0.52
470	90.00 ± 0.12	80.53 ± 3.46	76.10 ± 1.01	84.79 ± 1.25

Appendix C

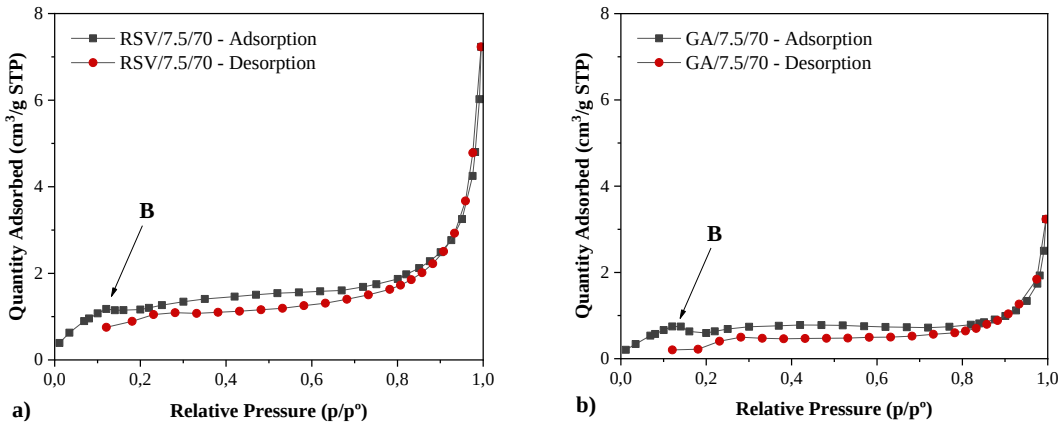

Figure C.1 – Isotherms for a) RSV-DPF (RSV/7.5/70) and b) GA-DPF (GA/7.5/70) microparticles.

Appendix D

- **HPC Preliminary Studies**

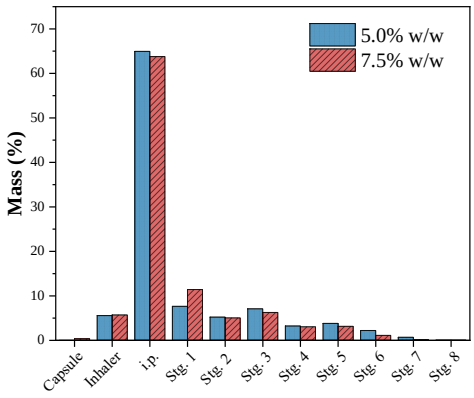

Figure D.1 – Powder mass entrapment distribution from ACI tests with processed HPC powder, formulated with 5.0 and 7.5 %w/v of solids, stored in RH conditions of 45 %.

- **RSV-DPF and GA-DPFs**

Table D.1 – Fine particle fraction (FPF) and mass median aerodynamic diameter (MMAD) values of RSV-DPF and GA-DPFs from ACI tests.

	FPF (%)		MMAD (µm)	
%HR	**45 %**	**20 %**	**45 %**	**20 %**
RSV/7.5/20	14.7	15.7	4.3	4.1
RSV/7.5/45	41.5	46.8	2.2	4.0
RSV/7.5/70	45.8	36.9	3.1	1.9
GA/7.5/20	24.4	14.9	4.0	3.9
GA/7.5/45	33.9	35.7	3.8	2.4
GA/7.5/70	34.2	38.2	2.0	2.0

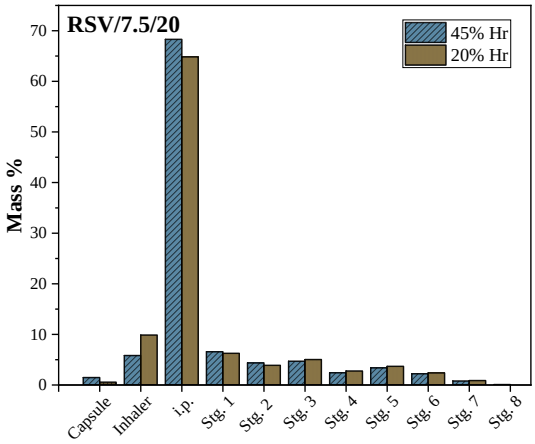

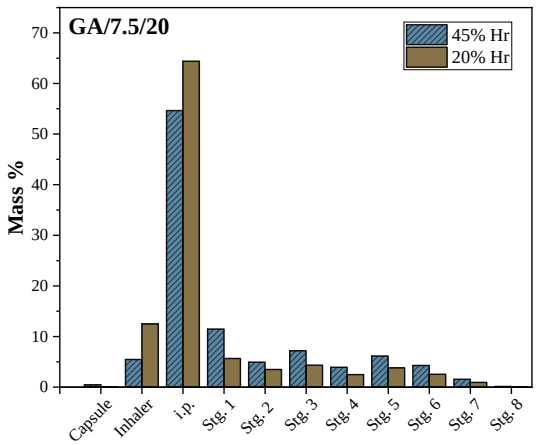

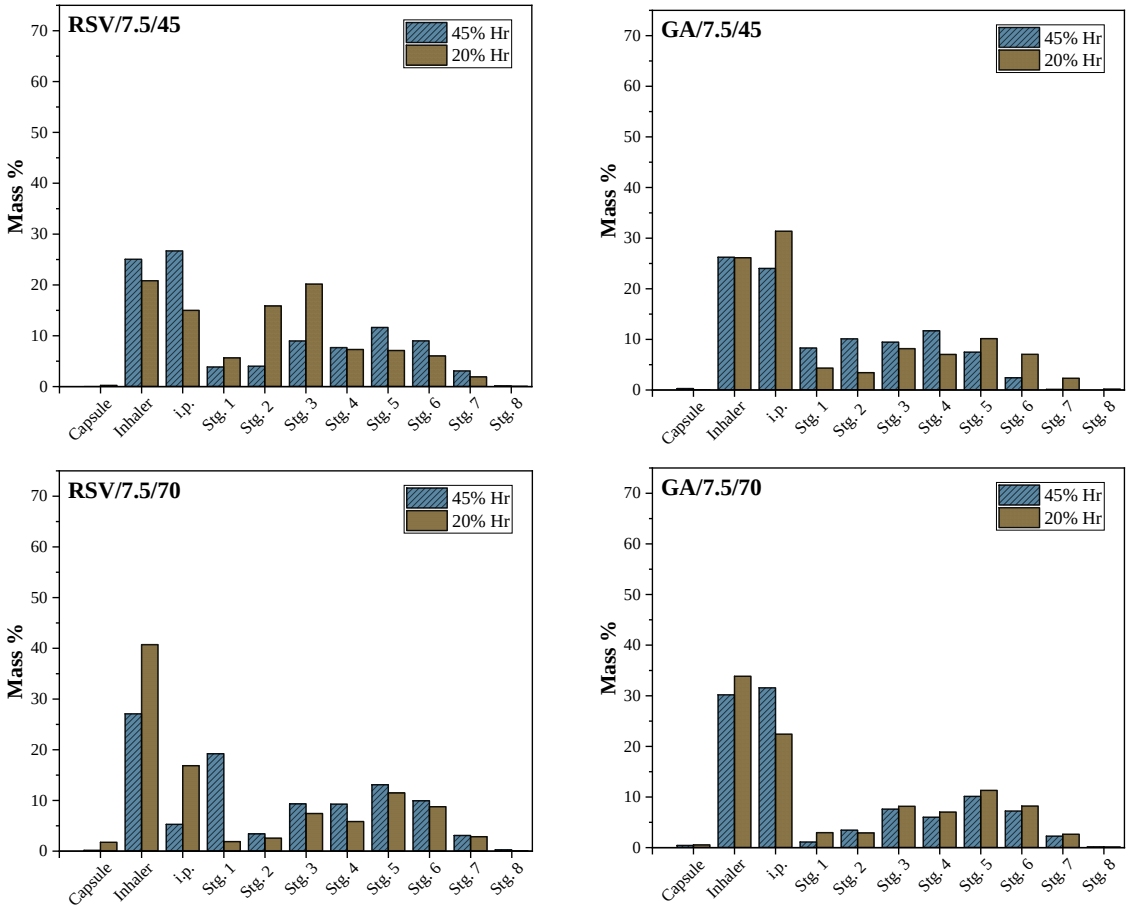

Figure D.2 – Powder mass distribution from ACI tests with the RSV-DPF and GA-DPF with 7.5 %w/v solids, varying the ethanol volume from 20 to 70 %v/v, stored at different %RH (20 and 45 %RH).

Appendix E

- **RSV-DPFs**

Table E.1 – ANOVA for variable EE (RSV-DPFs).

Factor	SS	g.l.	MS	F	*p*
(1)C_Solids (L)	363.0	1	363.0	1.25	0.2924
C_Solids (Q)	160.4	1	160.4	0.55	0.4762
(2)V_Ethanol (L)	3.0	1	3.0	0.01	0.9212
V_Ethanol (Q)	32.1	1	32.1	0.11	0.7471
1L by 2L	66.1	1	66.1	0.22	0.6446
1L by 2Q	18.4	1	18.4	0.06	0.8070
1Q by 2L	459.4	1	459.4	1.58	0.2401
1Q by 2Q	369.0	1	369.0	1.27	0.2887
Error	2613.5	9	290.4		
Total SS	4084.9	17			

Table E.2 – ANOVA for variable EE (RSV-DPFs).

Factor	SS	g.l.	MS	F	*p*
(1)C_Solids (L)	468.2	1	468.2	7.80	0.0209
C_Solids (Q)	9.7	1	9.7	0.16	0.6964
(2)V_Ethanol (L)	871.3	1	871.3	14.52	0.0041
V_Ethanol (Q)	141.2	1	141.2	2.35	0.1595
1L by 2L	7.9	1	7.9	0.13	0.7247
1L by 2Q	38.3	1	38.3	0.64	0.4448
1Q by 2L	88.1	1	88.1	1.46	0.2564
1Q by 2Q	78.9	1	78.9	1.32	0.2809
Error	2613.5	9	60.0		
Total SS	540.2	9	60.0		

Table E.3 – ANOVA for variable $D_{v,50}$ (RSV-DPFs).

Factor	SS	g.l.	MS	F	*p*
(1)C_Solids (L)	165.5	1	165.5	11.53	0.0079
C_Solids (Q)	15.1	1	15.1	1.05	0.3324
(2)V_Ethanol (L)	1.6	1	1.6	0.11	0.7441
V_Ethanol (Q)	39.6	1	39.6	2.76	0.1310
1L by 2L	37.9	1	37.9	2.64	0.1388
1L by 2Q	5.0	1	5.0	0.35	0.5712
1Q by 2L	0.8	1	0.8	0.05	0.8232
1Q by 2Q	4.0	1	4.0	0.28	0.6125
Error	129.3	9	14.4		
Total SS	398.7	17			

Table E.4 – ANOVA for variable span (RSV-DPFs).

Factor	SS	g.l.	MS	F	*p*
(1)C_Solids (L)	0.319	1	0.319	2.55	0.1450
C_Solids (Q)	0.042	1	0.042	0.34	0.5748
(2)V_Ethanol (L)	1.516	1	1.516	12.12	0.0069
V_Ethanol (Q)	0.773	1	0.773	6.18	0.0347
1L by 2L	0.850	1	0.850	6.79	0.0284
1L by 2Q	0.447	1	0.447	3.57	0.0914
1Q by 2L	0.118	1	0.118	0.95	0.3561
1Q by 2Q	0.129	1	0.129	1.03	0.3361
Error	1.126	9	0.125		
Total SS	5.322	17			

- **GA-DPFs**

Table E.5 – ANOVA for variable Yield (GA-DPFs).

Factor	SS	g.l.	MS	F	*p*
(1)C_Solids (L)	752.1	1	752.1	10.89	0.0092
C_Solids (Q)	30.3	1	30.3	0.44	0.5246
(2)V_Ethanol (L)	290.1	1	290.1	4.20	0.0707
V_Ethanol (Q)	812.3	1	812.3	11.76	0.0075
1L by 2L	15.1	1	15.1	0.22	0.6509
1L by 2Q	672.0	1	672.0	9.73	0.0123
1Q by 2L	70.0	1	70.0	1.01	0.3402
1Q by 2Q	3.1	1	3.1	0.05	0.8363
Error	621.5	9	69.1	10.89	
Total SS	3266.5	17			

Table E.6 – ANOVA for variable EE (GA-DPFs).

Factor	SS	g.l.	MS	F	*p*
(1)C_Solids (L)	683.6	1	683.6	8.36	0.0178
C_Solids (Q)	26.1	1	26.1	0.32	0.5857
(2)V_Ethanol (L)	2833.9	1	2833.9	34.66	0.0002
V_Ethanol (Q)	987.1	1	987.1	12.07	0.0070
1L by 2L	272.1	1	272.1	3.33	0.1014
1L by 2Q	69.6	1	69.6	0.85	0.3804
1Q by 2L	22.3	1	22.3	0.27	0.6141
1Q by 2Q	47.1	1	47.1	0.58	0.4671
Error	735.9	9	81.8		
Total SS	5677.9	17			

Table E.7 – ANOVA for variable $D_{v,50}$ (GA-DPFs).

Factor	SS	g.l.	MS	F	*p*
(1)C_Solids (L)	238.3	1	238.3	8.71	0.0162
C_Solids (Q)	0.1	1	0.1	0.01	0.9427
(2)V_Ethanol (L)	9.4	1	9.4	0.34	0.5722
V_Ethanol (Q)	38.2	1	38.2	1.39	0.2679
1L by 2L	88.4	1	88.4	3.23	0.1057
1L by 2Q	23.6	1	23.6	0.86	0.3772
1Q by 2L	0.8	1	0.8	0.03	0.8645
1Q by 2Q	2.2	1	2.2	0.08	0.7846
Error	246.2	9	27.4		
Total SS	647.3	17			

Table E.8 – ANOVA for variable span (GA-DPFs).*

Factor	SS	g.l.	MS	F	*p*
(1)C_Solids (L)	0.061	1	0.061	0.19	0.6735
C_Solids (Q)	0.062	1	0.062	0.19	0.6704
(2)V_Ethanol (L)	0.643	1	0.643	2.00	0.1911
V_Ethanol (Q)	1.153	1	1.153	3.58	0.0909
1L by 2L	0.019	1	0.019	0.06	0.8144
1L by 2Q	0.035	1	0.035	0.11	0.7499
1Q by 2L	0.002	1	0.002	0.01	0.9405
1Q by 2Q	0.004	1	0.004	0.01	0.9086
Error	2.896	9	0.322		
Total SS	4.876	17			

***NOTE**: In the main ANOVA (Table E.8) there was no significant effect, but when ANOVA is condensed for the lowest *p*-value (Table E.9), it was found that the quadratic component of V_ethanol variable can be considered significant ($p < 0.05$) for this response.

Table E.9 – Condensed ANOVA for variable span (GA-DPFs).*

Factor	**SS**	**g.l.**	**MS**	**F**	***p***
V_Ethanol (Q)	1.153	1	1.153	4.96	0.0407
Error	3.722	16	0.232		
Total SS	4.876	17			

- **Validation of the Assumptions**

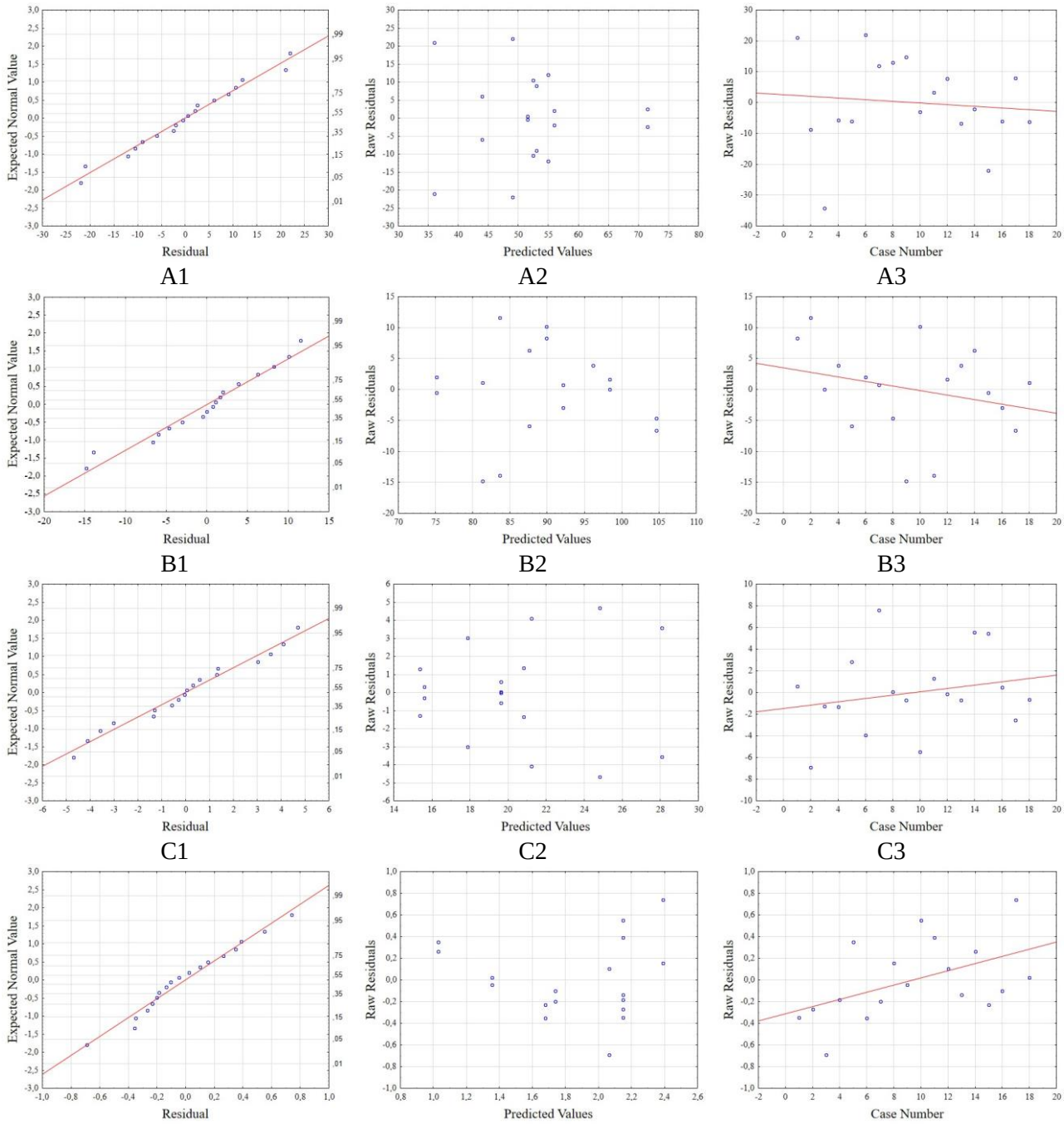

Figure E.1 – Validation of the assumptions for the RSV-DPFs. Variables: A - Yield; B - EE; C - $D_{v,50}$; D – Span. Assumptions: 1 - Normality of the residues; 2 - Homogeneity of the variance; 3 - Independence of the residues.

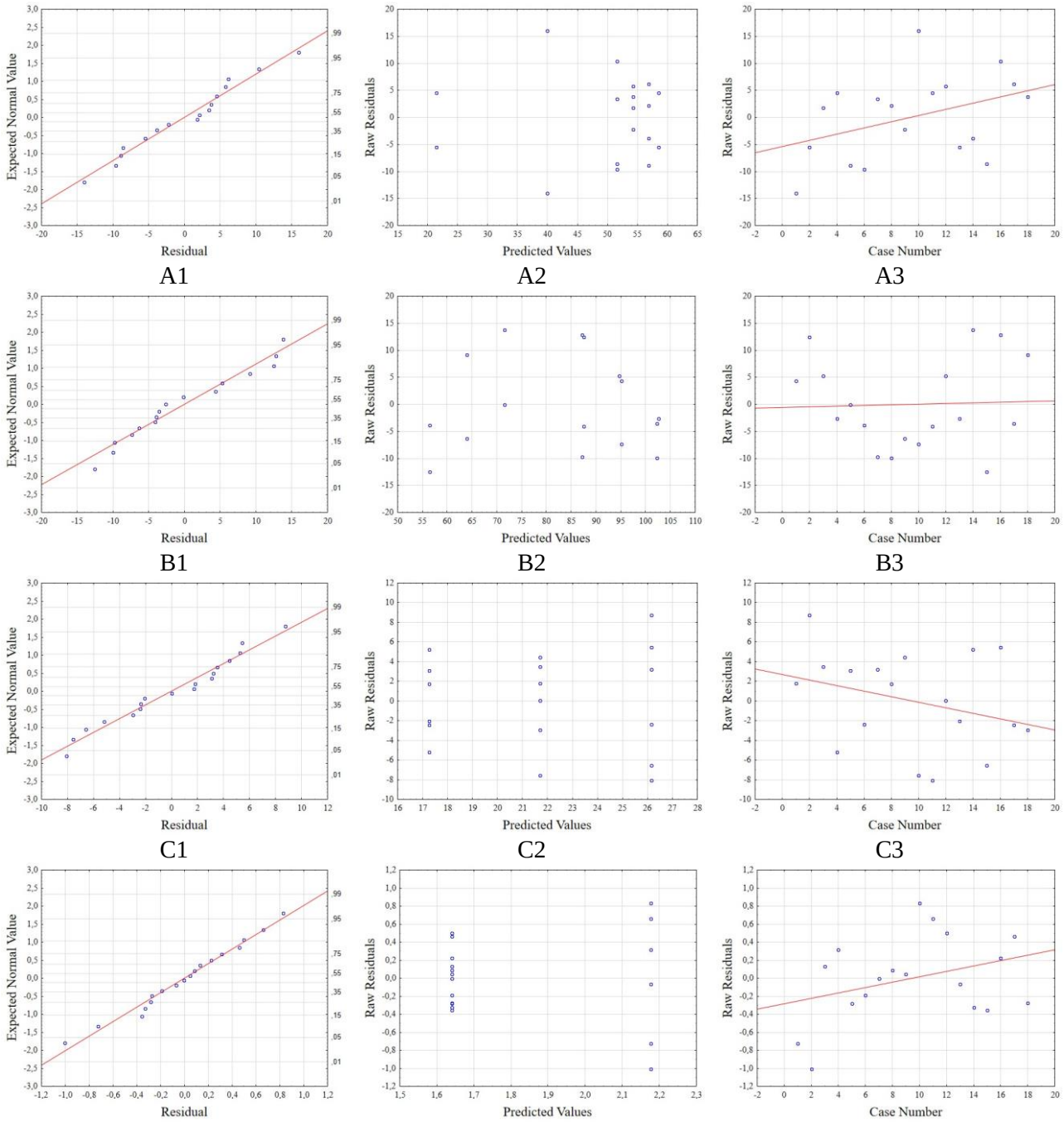

Figure E.2 – Validation of the assumptions for the GA-DPFs. Variables: A - Yield; B - EE; C - $D_{v,50}$; D – Span. Assumptions: 1 - Normality of the residues; 2 - Homogeneity of the variance; 3 - Independence of the residues.

Appendix F

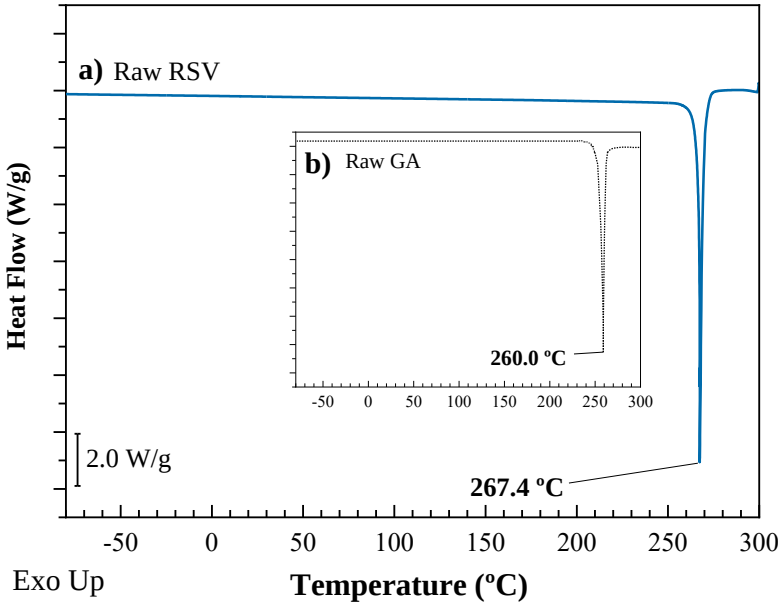

Figure F.1 – DSC thermogram of a) raw RSV (obtained by DSC) and b) raw GA (adapted according to Neo et al. [174]).

Appendix G

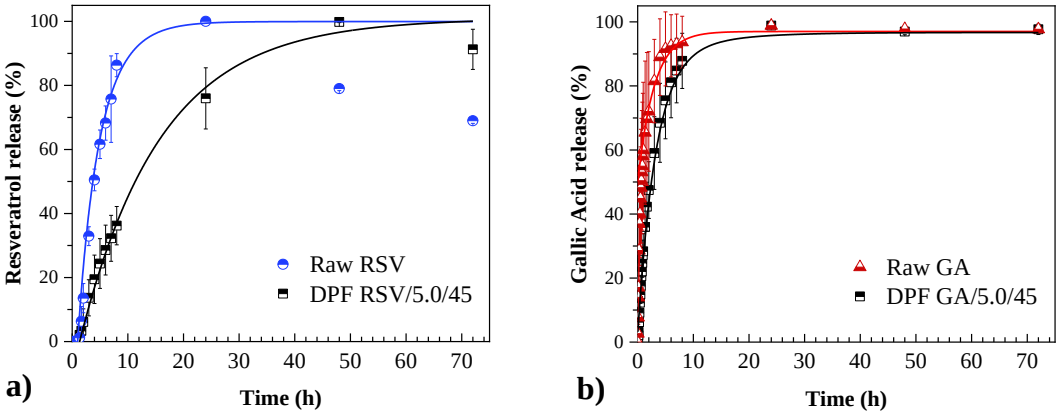

Figure G.1 – *In vitro* release profiles for 72 hours of a) raw RSV and HPC/RSV DPF (RSV/5.0/45) and b) raw GA and HPC/GA DPF (GA/5.0/45).

Table G.1 – Input amount (M_{Input}) and maximum amount quantified ($M_{Released}$) of each phenolic compound, expressed in µg, after 72 h of the *in vitro* release tests.

	Raw RSV	**Raw GA**	**RSV-DPF** (RSV/5.0/45)	**GA-DPF** (GA/5.0/45)
M_{Input} (µg $_{phenolic}$)	1023 ± 5	1035 ± 15	1017.9 ± 0.3	1008.9 ± 0.9
$M_{Released}$ (µg $_{phenolic}$)	36 ± 12	928 ± 34	201 ± 33	942 ± 9
Total Released (%)	4 ± 1	90 ± 2	21 ± 3	93.4 ± 0.9

Appendix H

- **Calibration Curve:** Encapsulation Effiency

Table H.1 – Standard values used in the calibration curves of a) RSV and b) GA.

a)

Standard No.	Concentration (mg/L)	Area (mAU.s)
1	51.5	45936
2	41.2	3575.5
3	30.9	2724.3
4	206	1813.1
5	10.3	862.2
6	5.2	446.5
7	1.0	824
8	0.5	43.2

b)

Standard No.	Concentration (mg/L)	Area (mAU.s)
1	52.1	1727.8
2	41.7	1360.3
3	31.3	1042.0
4	20.8	697.4
5	10.4	329.4
6	5.2	171.0
7	1.0	32.1
8	0.5	16.6

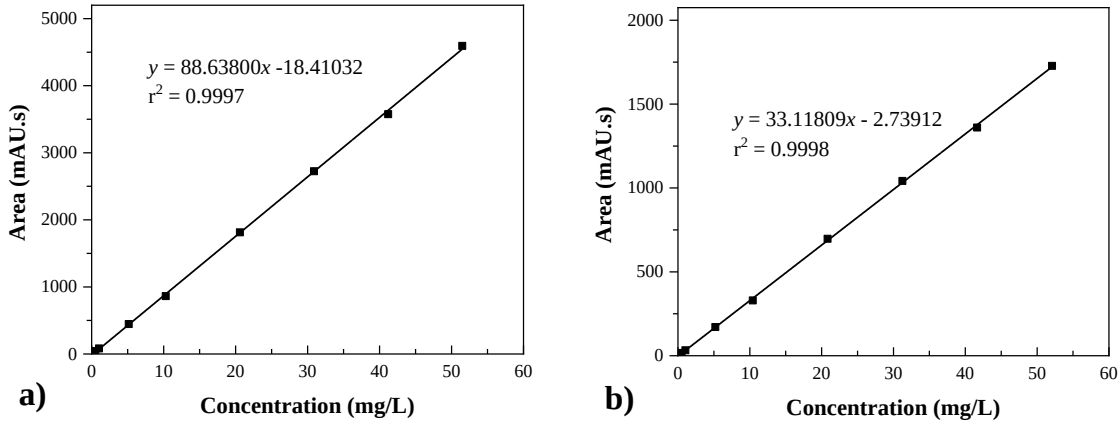

Figure H.1 – Standard calibration curves for a) RSV and b) GA.

- **Calibration Curve:** *In vitro* Release Studies and Quantification Tests.

Table H.2 – Standard values used in the calibration curves of a) RSV and b) GA.

a)

Standard No.	Concentration (mg/L)	Area (mAU.s)
1	57.5	5000.9
2	46.0	3992.4
3	34.5	3012.4
4	23.0	2026.6
5	11.5	998.6
6	5.8	520.5
7	0.6	107.0
8	0.3	52.2
9	0.1	27.5

b)

Standard No.	Concentration (mg/L)	Area (mAU.s)
1	51.1	1602.7
2	40.8	1307.6
3	30.6	977.9
4	20.4	638.6
5	10.2	332.3
6	5.1	167.2
7	0.5	30.6
8	0.3	14.6
9	0.1	2.2

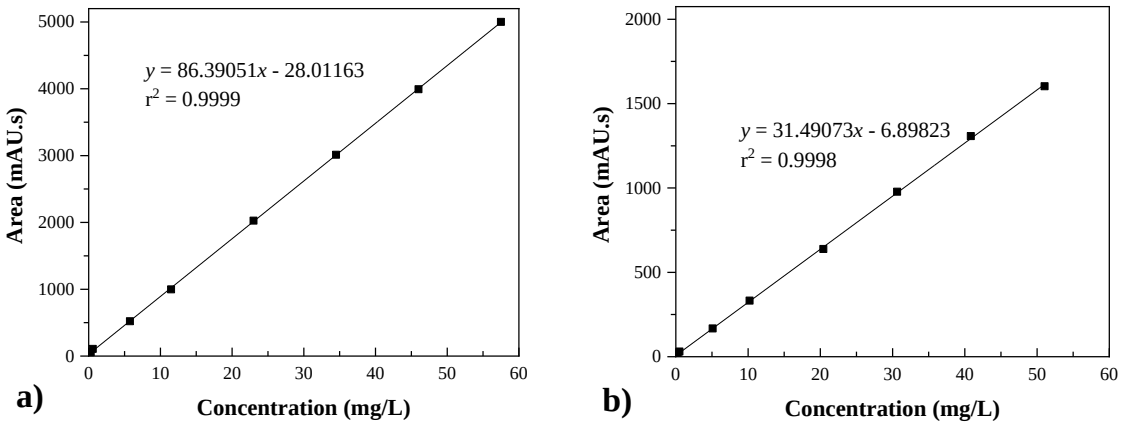

Figure H.2 – Standard calibration curves for a) RSV and b) GA.

- **Calibration Curve:** Quantification Tests in Ethanol

Table H.3 – Standard values used in the calibration curves of a) RSV and b) GA using ethanol as eluent.

* The signal in the chromatogram was "dragged" and lost intensity, and it was not possible to see the signal from the lowest concentrations.

a)

Standard No.	Concentration (mg/L)	Area (mAU.s)
1	50.1	4413.1
2	40.0	3465.3
3	30.0	2679.3
4	20.0	1765.3
5	10.0	900.3
6	5.0	425.8
7	1.0	95.4
8	0.5	15.3
9	0.1	0.0
10	0.0	0.0

b)

Standard No.	Concentration (mg/L)	Area (mAU.s)
1	51.0	1528.1
2	40.8	1150.2
3	30.6	921.6
4	20.4	541.0
5	10.2	295.9
6	5.1	128.5
7	1.0	0.0
8	0.5	0.0
9	0.1	0.0
10	0.0	0.0

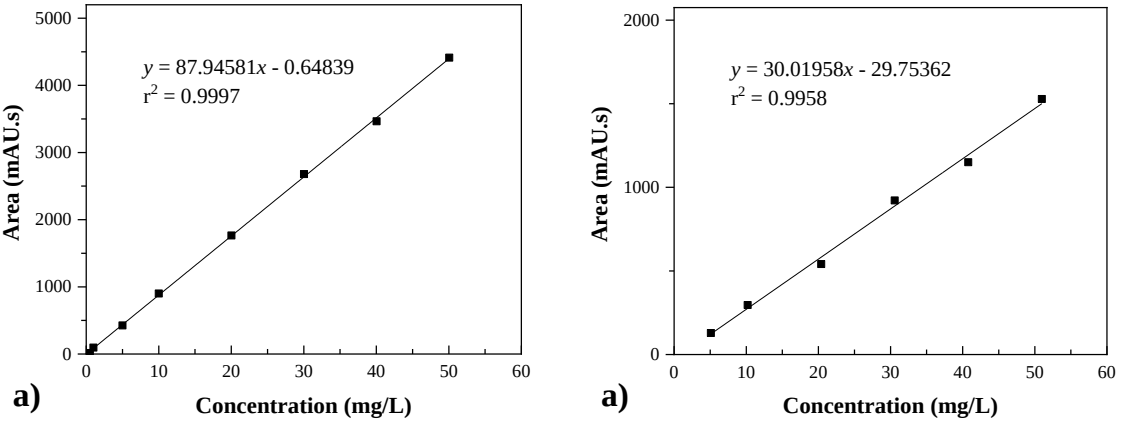

Figure H.3 – Standard calibration curves for a) RSV and b) GA with ethanol as eluent.

Appendix I1

Table I.1.1 – Experimental data of the *in vitro* release profiles in 72 h for each replica of the raw RSV sample; C_{RSV}: concentration of RSV detected expressed in µg of RSV per mL of eluent; $\%_{rel}$: released percentage of RSV normalized for the maximum amount detected; o.r.: out of range in the calibration curve.

Time (h)	Raw RSV												
	Replica A			Replica B			Replica C			Average value (µg/mL)	Std. Dev. (µg/mL)	Average value (%)	Std. Dev. (%)
	Area (mAU.s)	C_{RSV} (µg/mL)	% release	Area (mAU.s)	C_{RSV} (µg/mL)	% release	Area (mAU.s)	C_{RSV} (µg/mL)	% release				
0.03	–	–	–	–	–	–	–	–	–	–	–	–	–
0.07	–	–	–	–	–	–	–	–	–	–	–	–	–
0.10	–	–	–	–	–	–	–	–	–	–	–	–	–
0.13	–	–	–	–	–	–	2.81	o.r.	o.r.	–	–	–	–
0.17	–	–	–	–	–	–	3.75	o.r.	o.r.	–	–	–	–
0.25	–	–	–	–	–	–	3.01	o.r.	o.r.	–	–	–	–
0.33	–	–	–	3.00	o.r.	o.r.	3.33	o.r.	o.r.	–	–	–	–
0.42	3.10	o.r.	o.r.	4.05	o.r.	o.r.	4.66	o.r.	o.r.	–	–	–	–
0.50	5.05	o.r.	o.r.	6.08	o.r.	o.r.	4.43	o.r.	o.r.	–	–	–	–
0.58	8.59	o.r.	o.r.	8.04	o.r.	o.r.	6.89	o.r.	o.r.	–	–	–	–
0.67	9.60	o.r.	o.r.	11.07	o.r.	o.r.	7.68	o.r.	o.r.	–	–	–	–
0.75	11.31	o.r.	o.r.	12.03	o.r.	o.r.	10.91	o.r.	o.r.	–	–	–	–
0.83	13.24	o.r.	o.r.	16.69	o.r.	o.r.	11.64	o.r.	o.r.	–	–	–	–
0.92	16.16	o.r.	o.r.	18.21	o.r.	o.r.	12.87	o.r.	o.r.	–	–	–	–
1.00	18.88	o.r.	o.r.	20.67	o.r.	o.r.	13.86	o.r.	o.r.	–	–	–	–
1.33	28.05	0.0004	0.0	32.88	0.0564	3.5	6.77	0.0000	0.0	0.0190	0.0265	1.2	1.6
1.67	41.33	0.1542	8.1	43.09	0.1768	10.8	26.09	0.0000	0.0	0.1103	0.0786	6.3	4.6
2.00	52.14	0.2855	15.1	52.88	0.2971	18.2	33.01	0.0579	7.4	0.2135	0.1101	13.6	4.6
3.00	78.30	0.5994	31.6	78.28	0.6026	37.0	48.27	0.2368	30.1	0.4796	0.1717	32.9	2.9
4.00	103.21	0.9111	48.1	102.03	0.9008	55.3	59.68	0.3782	48.1	0.7300	0.2488	50.5	3.4
5.00	115.62	1.0895	57.5	116.76	1.1056	67.8	66.18	0.4681	59.5	0.8877	0.2968	61.6	4.5
6.00	127.35	1.2659	66.8	123.82	1.2285	75.4	66.69	0.4917	62.5	0.9954	0.3564	68.2	5.3
7.00	106.70	1.0729	56.6	133.32	1.3827	84.8	80.90	0.6742	85.7	1.0433	0.2900	75.7	13.5
8.00	145.92	1.5633	82.5	138.02	1.4859	91.2	78.47	0.6705	85.3	1.2399	0.4039	86.3	3.6
24.00	169.79	1.8942	**100.0**	146.05	1.6298	**100.0**	86.48	0.7865	**100.0**	1.4368	0.4723	100.0	0.0
48.00	128.75	1.4848	78.4	112.96	1.3014	79.9	69.71	0.6196	78.8	1.1353	0.3723	79.0	0.6
72.00	107.56	1.2861	67.9	95.49	1.1385	69.9	61.46	0.5434	69.1	0.9893	0.3210	68.9	0.8

Table I.1.2 – Experimental data of the *in vitro* release profiles in 72 h for each replica of the RSV-DPF sample; C_{RSV}: concentration of RSV detected expressed in μg of RSV per mL of eluent; $\%_{rel}$: released percentage of RSV normalized for the maximum amount detected; o.r.: out of range in the calibration curve.

Time (h)	DPF RSV/5.0/45												
	Replica A			Replica B			Replica C			Average value (μg/mL)	Std. Dev. (μg/mL)	Average value (%)	Std. Dev. (%)
	Area (mAU.s)	C_{RSV} (μg/mL)	% release	Area (mAU.s)	C_{RSV} (μg/mL)	% release	Area (mAU.s)	C_{RSV} (μg/mL)	% release				
0.03	–	–	–	–	–	–	–	–	–	–	–	–	–
0.07	–	–	–	–	–	–	–	–	–	–	–	–	–
0.10	–	–	–	–	–	–	–	–	–	–	–	–	–
0.13	–	–	–	–	–	–	–	–	–	–	–	–	–
0.17	–	–	–	–	–	–	–	–	–	–	–	–	–
0.25	–	–	–	–	–	–	–	–	–	–	–	–	–
0.33	2.54	o.r	0.0	1.58	o.r	o.r.	1.74	o.r	o.r.	–	–	–	–
0.42	3.78	o.r	0.0	3.93	o.r	o.r.	5.34	o.r	o.r.	–	–	–	–
0.50	6.29	o.r	0.0	5.31	o.r	o.r.	7.92	o.r	o.r.	–	–	–	–
0.58	5.61	o.r	0.0	8.56	o.r	o.r.	13.38	o.r	o.r.	–	–	–	–
0.67	8.55	o.r	0.0	9.49	o.r	o.r.	17.81	o.r	o.r.	–	–	–	–
0.75	11.99	o.r	0.0	14.39	o.r	o.r.	20.45	o.r	o.r.	–	–	–	–
0.83	11.77	o.r	0.0	17.23	o.r	o.r.	26.40	o.r	o.r.	–	–	–	–
0.92	13.80	o.r	0.0	17.69	o.r	o.r.	29.68	0.0193	0.3	0.0064	0.0091	0.1	0.1
1.00	14.28	o.r	0.0	22.90	o.r	o.r.	32.86	0.0561	0.7	0.0187	0.0264	0.2	0.3
1.33	25.40	o.r	0.0	37.14	0.1057	1.4	59.98	0.3701	4.8	0.1586	0.1556	2.1	2.0
1.67	27.39	o.r	0.0	45.39	0.2054	2.7	76.44	0.5605	7.3	0.2553	0.2316	3.4	3.0
2.00	43.62	0.1807	1.8	58.96	0.3705	4.9	104.86	0.8895	11.6	0.4802	0.2996	6.1	4.1
3.00	82.76	0.6409	6.5	118.56	1.0747	14.2	161.92	1.5501	20.3	1.0886	0.3713	13.7	5.6
4.00	112.16	1.0066	10.2	148.85	1.4672	19.4	217.67	2.1954	28.8	1.5564	0.4894	19.5	7.6
5.00	143.12	1.4039	14.3	185.22	1.9442	25.7	246.82	2.5327	33.2	1.9603	0.4610	24.4	7.8
6.00	176.40	1.8425	18.7	202.19	2.2135	29.2	277.14	2.8838	37.8	2.3133	0.4309	28.6	7.8
7.00	209.37	2.2928	23.3	217.28	2.4688	32.6	297.39	3.1182	40.8	2.6266	0.3550	32.3	7.2
8.00	251.44	2.8637	29.1	230.23	2.7063	35.8	316.64	3.3409	43.8	2.9703	0.2698	36.2	6.0
24.00	751.71	8.7580	89.0	423.00	5.0313	66.5	505.50	5.5271	72.4	6.4388	1.6524	76.0	9.5
48.00	816.11	9.8386	**100.0**	623.37	7.5336	99.5	687.62	7.6352	**100.0**	8.3358	1.0635	99.8	0.2
72.00	661.59	8.4148	85.5	602.64	7.5693	**100.0**	610.53	6.7428	88.3	7.5756	0.6826	91.3	6.3

Table I.1.3 – Experimental data of the *in vitro* release profiles in 72 h for each replica of the raw GA sample; C_{GA}: concentration of GA detected expressed in µg of GA per mL of eluent; $\%_{rel}$: released percentage of GA normalized for the maximum amount detected; o.r.: out of range in the calibration curve.

Time (h)	Raw GA												
	Replica A			Replica B			Replica C			Average value (µg/mL)	Std. Dev. (µg/mL)	Average value (%)	Std. Dev. (%)
	Area (mAU.s)	C_{GA} (µg/mL)	% release	Area (mAU.s)	C_{GA} (µg/mL)	% release	Area (mAU.s)	C_{GA} (µg/mL)	% release				
0.03	4.75	o.r	o.r	–	–	–	4.07	o.r	o.r	–	–	–	–
0.07	53.82	1.4900	3.9	35.71	0.9151	2.6	40.92	1.0803	1.5	1.1618	0.2417	2.7	1.0
0.10	101.21	3.0545	7.9	120.46	3.6428	10.2	117.07	3.5417	5.0	3.4130	0.2569	7.7	2.1
0.13	157.66	4.9670	12.9	235.87	7.4521	20.8	183.16	5.7804	8.1	6.0665	1.0345	14.0	5.2
0.17	229.56	7.4416	19.3	310.32	10.1068	28.3	74.55	2.5552	3.6	6.7012	3.1271	17.1	10.2
0.25	304.80	10.1138	26.3	440.67	14.6318	40.9	409.32	13.2719	18.7	12.6725	1.8925	28.6	9.2
0.33	401.23	13.5542	35.2	566.99	19.1939	53.7	464.55	15.5371	21.8	16.0951	2.3360	36.9	13.0
0.42	413.86	14.4561	37.6	593.09	20.7342	58.0	510.70	17.5837	24.7	17.5914	2.5630	40.1	13.7
0.50	443.00	15.8984	41.3	661.34	23.6460	66.1	545.88	19.3409	27.2	19.6284	3.1695	44.9	16.1
0.58	454.52	16.8183	43.7	706.59	25.9143	72.5	552.97	20.2506	28.5	20.9944	3.7505	48.2	18.2
0.67	454.61	17.3896	45.2	723.17	27.3295	76.4	555.47	21.0237	29.5	21.9143	4.1066	50.4	19.5
0.75	456.28	18.0113	46.8	724.97	28.2965	79.1	617.08	23.6771	33.3	23.3283	4.2062	53.1	19.2
0.83	459.95	18.6989	48.6	728.19	29.3109	82.0	614.60	24.3734	34.3	24.1277	4.3358	54.9	20.0
0.92	461.46	19.3222	50.2	734.10	30.4149	85.0	694.81	27.6924	38.9	25.8098	4.7202	58.1	19.6
1.00	453.75	19.6547	51.1	751.33	31.8858	89.2	680.35	28.1069	39.5	26.5492	5.1134	59.9	21.2
1.33	468.04	20.6760	53.8	806.60	34.5865	96.7	794.25	32.5793	45.8	29.2806	6.1393	65.4	22.4
1.67	482.55	21.7227	56.5	800.59	35.4112	99.0	936.63	38.1006	53.5	31.7448	7.1712	69.7	20.8
2.00	499.23	22.8566	59.4	762.19	35.2001	98.4	1004.60	41.4400	58.2	33.1656	7.7219	72.0	18.7
3.00	580.17	26.0522	67.7	738.43	35.4049	99.0	1402.83	55.3534	77.8	38.9368	12.2201	81.5	13.0
4.00	610.32	27.7377	72.1	703.53	35.2258	98.5	1762.80	68.5576	96.4	43.8404	17.7430	89.0	12.0
5.00	623.82	28.9329	75.2	688.84	35.6443	99.7	1770.68	71.0380	99.8	45.2051	18.4710	91.6	11.6
6.00	642.60	30.3128	78.8	654.96	35.4345	99.1	1697.37	70.9505	99.7	45.5660	18.0710	92.5	9.7
7.00	627.91	30.6538	79.7	632.00	35.5286	99.3	1636.14	71.1533	**100.0**	45.7786	18.0527	93.0	9.4
8.00	633.75	31.6282	82.2	614.41	35.7643	**100.0**	1542.51	70.2495	98.7	45.8807	17.3139	93.7	8.1
24.00	823.86	38.4614	**100.0**	572.57	35.2071	98.4	1465.58	69.7573	98.0	47.8086	15.5768	98.8	0.8
48.00	772.11	37.8558	98.4	538.37	34.8395	97.4	1395.78	69.3936	97.5	47.3630	15.6266	97.8	0.5
72.00	725.86	37.3591	97.1	533.44	35.3582	98.9	1330.57	69.0868	97.1	47.2680	15.4498	97.7	0.8

Table I.1.4 – Experimental data of the *in vitro* release profiles in 72 h for each replica of the GA-DPF sample; C_{GA}: concentration of GA detected expressed in µg of GA per mL of eluent; $\%_{rel}$: released percentage of GA normalized for the maximum amount detected. o.r.: out of range in the calibration curve.

Time (h)	DPF GA/5.0/45												
	Replica A			Replica B			Replica C			Average value (µg/mL)	Std. Dev. (µg/mL)	Average value (%)	Std. Dev. (%)
	Area (mAU.s)	C_{GA} (µg/mL)	% release	Area (mAU.s)	C_{GA} (µg/mL)	% release	Area (mAU.s)	C_{GA} (µg/mL)	% release				
0.03	–	–	–	–	–	–	–	–	–	–	–	–	–
0.07	9.59	0.0855	0.2	3.89	o.r.	o.r.	–	–	–	0.0285	0.0403	0.1	0.1
0.10	27.13	0.6458	1.7	19.32	0.3946	1.1	8.71	0.0574	0.2	0.3659	0.2411	1.0	0.6
0.13	44.38	1.2195	3.2	31.79	0.8063	2.2	18.95	0.3850	1.0	0.8036	0.3407	2.1	0.9
0.17	54.86	1.5996	4.2	41.49	1.1460	3.1	33.02	0.8470	2.2	1.1975	0.3094	3.2	0.8
0.25	98.61	3.0501	8.0	75.42	2.2673	6.1	59.70	1.7276	4.6	2.3483	0.5430	6.2	1.4
0.33	136.93	4.3833	11.5	105.10	3.2968	8.8	87.00	2.6616	7.1	3.4472	0.7109	9.1	1.8
0.42	182.17	5.9851	15.7	126.90	4.1137	11.0	120.46	3.8259	10.1	4.6416	0.9572	12.3	2.5
0.50	212.10	7.1582	18.8	149.88	4.9960	13.4	143.22	4.6928	12.4	5.6157	1.0977	14.9	2.8
0.58	244.27	8.4403	22.2	172.89	5.9082	15.8	163.66	5.5150	14.6	6.6212	1.2963	17.6	3.3
0.67	271.69	9.6125	25.3	209.59	7.2845	19.5	184.02	6.3606	16.9	7.7525	1.3682	20.6	3.5
0.75	288.54	10.4842	27.6	208.11	7.4951	20.1	196.55	6.9836	18.5	8.3210	1.5438	22.1	3.9
0.83	318.92	11.8066	31.0	218.40	8.0774	21.7	223.53	8.0814	21.4	9.3218	1.7570	24.7	4.5
0.92	339.19	12.8464	33.8	239.34	9.0110	24.2	241.08	8.9138	23.6	10.2571	1.8314	27.2	4.7
1.00	353.51	13.7233	36.1	225.39	8.8633	23.8	250.36	9.5058	25.2	10.6975	2.1556	28.4	5.5
1.33	447.68	17.1540	45.1	299.64	11.4987	30.8	319.86	12.0222	31.9	13.5583	2.5515	35.9	6.5
1.67	522.45	20.0882	52.8	335.00	12.9934	34.8	394.41	14.7871	39.2	15.9563	3.0121	42.3	7.7
2.00	584.84	22.7245	59.8	372.73	14.6083	39.2	430.17	16.4147	43.5	17.9158	3.4793	47.5	8.9
3.00	739.97	28.3848	74.6	461.89	17.9041	48.0	542.74	20.5270	54.5	22.2720	4.4531	59.0	11.3
4.00	843.42	32.6009	85.7	555.62	21.4586	57.5	613.74	23.4625	62.2	25.8407	4.8497	68.5	12.3
5.00	889.32	35.1210	92.3	625.28	24.3675	65.3	667.72	25.9474	68.8	28.4786	4.7409	75.5	12.0
6.00	907.57	36.8215	96.8	684.02	27.0186	72.4	705.17	27.9761	74.2	30.6054	4.4128	81.2	11.1
7.00	897.57	37.6479	99.0	704.97	28.5439	76.5	732.86	29.7424	78.9	31.9780	4.0389	84.8	10.1
8.00	874.05	38.0324	**100.0**	732.56	30.3066	81.3	743.41	30.9995	82.2	33.1128	3.4901	87.8	8.6
24.00	820.68	37.4391	98.4	923.76	37.3000	**100.0**	902.16	36.9762	98.1	37.2384	0.1939	98.8	0.8
48.00	768.24	36.8076	96.8	866.68	36.6519	98.3	840.01	36.1396	95.9	36.5330	0.2854	97.0	1.0
72.00	735.58	36.7374	96.6	811.45	35.9902	96.5	855.73	37.6972	**100.0**	36.8083	0.6987	97.7	1.6

Appendix I2

Table I.2.1 – Mass of samples used for the quantification test in ethanol (P) and pH 5.5 PBS (P) dissolution media.

Sample's Solvent	DPF Sample	Weighted DPF mass (mg)	Input Mass of Phenolic (µg)	µg $_{phenolic}$/ 100 mg sample
Ethanol (E)	HPC	100.15	n.d.	n.d.
	HPC/RSV	100.06	1020.61	1220.00
	HPC/GA	114.99	1011.91	880.00
pH 5.5 PBS (P)	HPC	100.56	n.d.	n.d
	HPC/RSV	100.02	1020.20	1220.00
	HPC/GA	115.02	1012.18	880.00

Table I.2.2 – Mass of phenolic quantified from the HPC, RSV and GA-DPFs in the ethanol dissolution medium.

Sample Code	Area (mAU.s)	C $_{phenolic}$ (µg/mL)	Mass of Phenolic Released (µg)	µg $_{phenolic}$/ 100 mg sample	µg $_{phenolic}$/100 mg sample (Average value ± Std. Dev.)
E1 HPC-DPF	n.d.	n.d.	n.d.	n.d.	n.d.
E2 HPC-DPF	n.d.	n.d.	n.d.	n.d.	n.d.
E3 HPC-DPF	n.d.	n.d.	n.d.	n.d.	n.d.
E4 RSV-DPF	3726.40	42.36	1059.10	1058.47	
E5 RSV-DPF	3579.11	40.69	1017.23	1016.62	1043 ± 19
E6 RSV-DPF	3713.45	42.22	1055.42	1054.79	
E7 GA-DPF	1104.77	37.79	944.82	821.65	
E8 GA-DPF	1144.06	39.10	977.54	850.11	826 ± 18
E9 GA-DPF	1085.54	37.15	928.81	807.73	

*n.d. - not detected

Table I.2.3 – Mass of phenolic quantified from the HPC, RSV and GA-DPFs in the pH 5.5 PBS dissolution medium.

Sample Code	Area (mAU.s)	C $_{phenolic}$ (µg/mL)	Mass of Phenolic Released (µg)	µg $_{phenolic}$/ 100 mg sample	µg $_{phenolic}$/100 mg sample (Average value ± Std. Dev.)
P1 HPC-DPF	n.d.	n.d.	n.d.	n.d.	n.d.
P2 HPC-DPF	n.d.	n.d.	n.d.	n.d.	n.d.
P3 HPC-DPF	n.d.	n.d.	n.d.	n.d.	n.d.
P4 RSV-DPF	1228.07	13.34	333.52	333.45	
P5 RSV-DPF	1068.24	11.57	289.28	289.22	315 ± 18
P6 RSV-DPF	1189.56	12.91	322.86	322.79	
P7 GA-DPF	1243.92	36.91	922.65	802.16	
P8 GA-DPF	1242.22	36.86	921.38	801.06	800 ± 3
P9 GA-DPF	1234.14	36.61	915.36	795.82	

*n.d. - not detected

Appendix I3

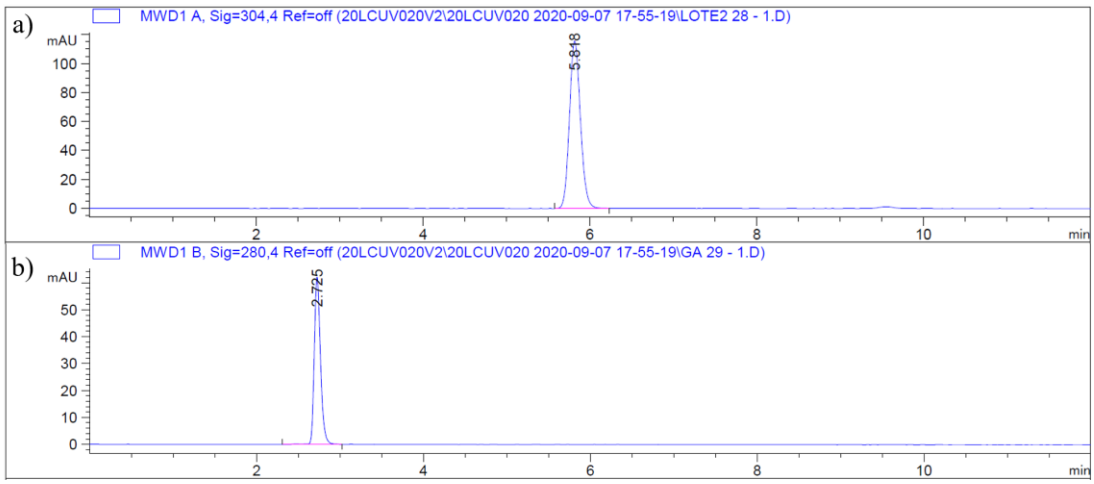

Figure I.3.1 – HPLC chromatograms example for the a) RSV-DPFs (304 nm) and a) GA-DPFs (280 nm).

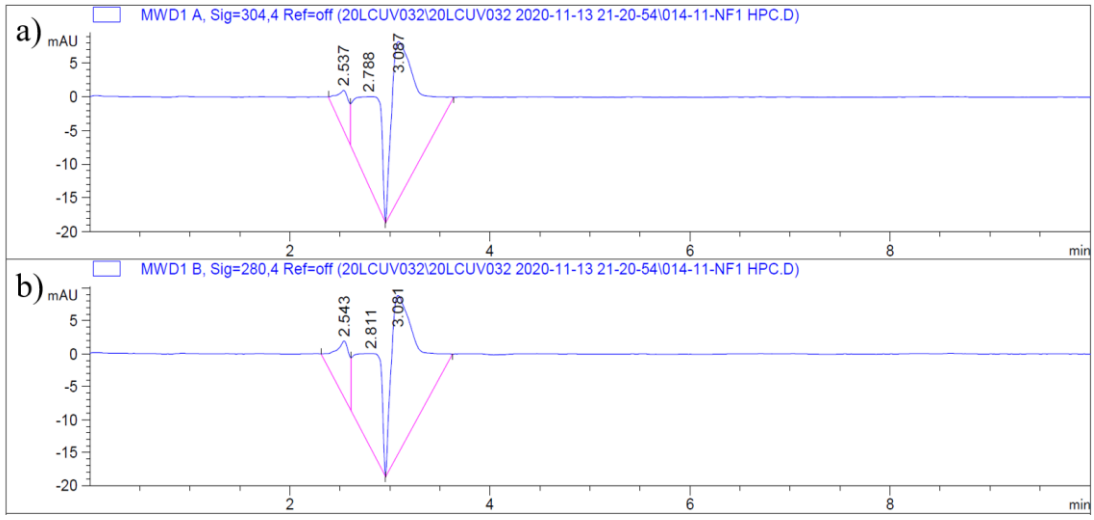

Figure I.3.2 – HPLC chromatograms example for the processed HPC sample (HPC-DPF) at a) 304 and b) 280 nm.

Appendix I4

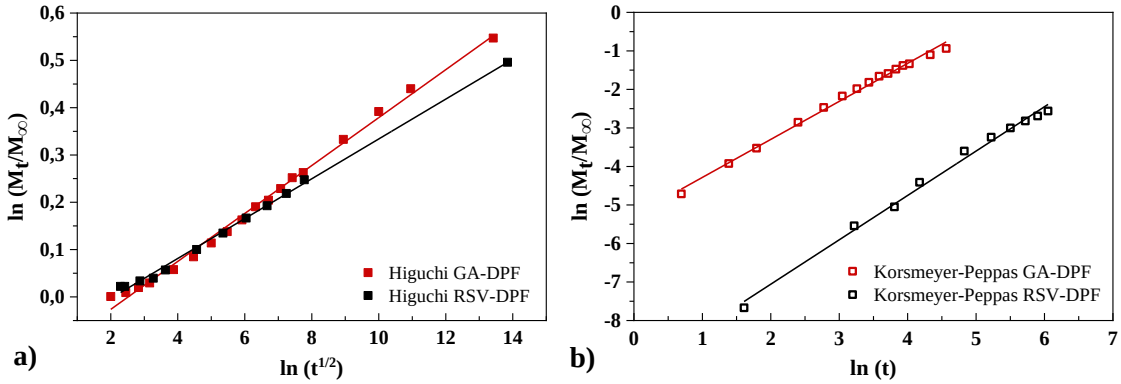

Figure I.4.1 – Mechanism of RSV and GA release profile from RSV/HPC and GA/HPC microparticles by a) Higuchi and b) Korsmeyer-Peppas mathematical models.

Table I.4.1 – Experimental data used in the application of the Higuchi and Korsmeyer-Peppas models.

t (min)	$t^{1/2}$ ($min^{1/2}$)	ln (t)	RSV			GA		
			% released	Mt/M∞	ln (Mt/M∞)	% released	Mt/M∞	ln (Mt/M∞)
2	1.41		n.d.	n.d.	n.d.	n.d.	n.d.	n.d.
4	2.00	1.39	n.d.	n.d.	n.d.	0.07	0.00	-7.26
6	2.45	1.79	n.d.	n.d.	n.d.	0.90	0.01	-4.71
8	2.83	2.08	n.d.	n.d.	n.d.	1.97	0.02	-3.93
10	3.16	2.30	n.d.	n.d.	n.d.	2.94	0.03	-3.53
15	3.87	2.71	n.d.	n.d.	n.d.	5.77	0.06	-2.85
20	4.47	3.00	n.d.	n.d.	n.d.	8.47	0.08	-2.47
25	5.00	3.22	n.d.	n.d.	n.d.	11.40	0.11	-2.17
30	5.48	3.40	n.d.	n.d.	n.d.	13.79	0.14	-1.98
35	5.92	3.56	n.d.	n.d.	n.d.	16.26	0.16	-1.82
40	6.32	3.69	n.d.	n.d.	n.d.	19.04	0.19	-1.66
45	6.71	3.81	n.d.	n.d.	n.d.	20.44	0.20	-1.59
50	7.07	3.91	n.d.	n.d.	n.d.	22.90	0.23	-1.47
55	7.42	4.01	0.02	0.00	-8.75	25.19	0.25	-1.38
60	7.75	4.09	0.05	0.00	-7.67	26.27	0.26	-1.34
80	8.94	4.38	0.39	0.00	-5.54	33.30	0.33	-1.10
100	10.00	4.61	0.64	0.01	-5.05	39.19	0.39	-0.94
120	10.95	4.79	1.21	0.01	-4.41	44.00	0.44	-0.82
180	13.42	5.19	2.74	0.03	-3.60	54.70	0.55	-0.60
240	15.49	5.48	3.94	0.04	-3.24	63.47	0.63	-0.45
300	17.32	5.70	5.00	0.05	-3.00	69.95	0.70	-0.36
360	18.97	5.89	5.95	0.06	-2.82	75.17	0.75	-0.29
420	20.49	6.04	6.81	0.07	-2.69	78.54	0.79	-0.24
480	21.91	6.17	7.76	0.08	-2.56	81.33	0.81	-0.21
1440	37.95	7.27	16.39	0.16	-1.81	91.46	0.91	-0.09
2880	53.67	7.97	21.23	0.21	-1.55	89.73	0.90	-0.11
4320	65.73	8.37	19.61	0.20	-1.63	90.41	0.90	-0.10

*n.d. - not detected